Title
Characterization of IE2 Autoregulation and its Impact on Viral Fitness in Human Cytomegalovirus /

Permalink
https://escholarship.org/uc/item/1d43g7sc

Author
Teng, Melissa W.

Publication Date
2013

Peer reviewed|Thesis/dissertation

UNIVERSITY OF CALIFORNIA, SAN DIEGO

Characterization of IE2 Autoregulation and

its Impact on Viral Fitness in Human Cytomegalovirus

A dissertation submitted in partial satisfaction of the requirements for the degree

Doctor of Philosophy

in

Chemistry

by

Melissa W. Teng

Committee in charge:

> Professor Leor Weinberger, Chair
> Professor Alexander Hoffmann, Co-Chair
> Professor Pieter Dorrestein
> Professor Judy Kim
> Professor Elizabeth Komives
> Professor William McGinnis

2013

The Dissertation of Melissa W. Teng is approved, and it is acceptable in quality and form for publication on microfilm and electronically:

_____

_____

_____

_____

_____
Co-Chair
_____
Chair

University of California, San Diego

2013

TABLE OF CONTENTS

5Aza-C – 5' Azacytidine
7-AAD – 7-Aminoactinomycin D
AIDS – Acquired immunodeficiency syndrome
BAC –Bacterial artificial chromosome
BP – Base pair
BRDU - Bromodeoxyuridine
CMV – Cytomegalovirus
CREB – cAMP response element-binding protein
CRS – *Cis* repression sequence
DMEM – Dulbecco's modified essential media
DNA – deoxyribonucleic acid
DTT - Dithiothreitol
EDTA – Ethylenediamenetetracetic acid
EGFP – Enhanced green fluorescent protein
EM – Electron microscopy
EMSA – Electrophoretic mobility shift assay
EYFP – Enhanced yellow fluorescent protein
FACS – Fluorescence-activated cell sorting
FBS – Fetal bovine serum
FCS – Fetal calf serum
FRAP – Fluorescence recovery after photobleaching
FRET – Forster Resonance Energy Transfer
GBW – Gain and bandwidth
GFP – Green fluorescent protein
HDAC – Histone deacetylase
HFF – Human foreskin fibroblasts
HHV-5 – Human herpesvirus 5
H.P.I. – Hours post infection
HSV-1 – Herpes simplex virus-1
IE1 – Immediate-early 1
IE2 – Immediate-early 2
IPTG – Isopropyl β-D-1-thiogalactopyranoside
IRES – Internal ribosome entry site
KB - Kilobases
LB – Luria broth
MBP – Maltose-binding protein
MIE – Major Immediate-early
MIEP – Major Immediate-early promoter
MOI – Multiplicity of infection
mRNA – Messenger ribonucleic acid
ND10 – Nuclear domain 10

NF-κB – Nuclear Factor kappaB
ODE – Ordinary differential equation
PBS – Phosphate buffered saline
PCR – Polymerase chain reaction
PML – Promyelocytic leukemia protein
PMSF – Phenylmethylsulfonyl fluoride
RNA – Ribonucleic acid
SDS-PAGE – sodium dodecyl sulfate polyacrylamide gel electrophoresis
SP1 – Specificity protein 1
SV40 – Simian virus 40
TAF – TBP-associated factors
TBP – TATA-binding protein
TCID$_{50}$ – Median tissue culture infective dose
TFIIB – Transcription Factor II B
TNF-α – Tumor Necrosis Factor Alpha
TSA – Trichostatin A
VPA – Valproic Acid
YFP – Yellow fluorescent protein

LIST OF FIGURES

LIST OF TABLES

ACKNOWLEGEMENTS

I have been blessed with the support of many people throughout graduate school over the past 6 years. I would like to thank my advisor, Leor Weinberger, for his guidance and support during my graduate school career. Before joining his lab, I had never heard of systems biology nor did I understand the value of mathematical modeling of biological systems. I am grateful to him for introducing me to a highly interdisciplinary way of thinking about virology. Without him, this dissertation would not have been possible.

I thank the members of my committee: Alex Hoffmann, Pieter Dorrestein, Judy Kim, Betsy Komives, and Bill McGinnis for their feedback and insight on my thesis work. I have been impressed with how highly they value students and their jobs as educators.

I thank the members of the Weinberger lab for their unwavering support and scientific insight. They made even the most mundane days in the lab fun. To Cynthia, I thank you for your herpes expertise but also for always encouraging me, reminding me not to take life too seriously, and standing up for me. To Winnie, thank you for always rooting for me and for joining the lab so soon after I joined! I appreciate your scientific insight, and your unflappable nature is refreshing. To Brandon, thank you for your honesty, for being a sounding board, and for your uncanny knack for knowing the right way to handle difficult situations. To the rest of the lab past and present, especially Roy, Tim, Jeff, Lisa, Jac, and Grayson, thank you for all of the amazing memories and for all

your technical and emotional support. I will miss scheming ways to find out what the

"S" in Leor S. Weinberger stands for.

Last but not least, I thank my family: Mom, Dad, Katherine, and Dan for allowing

me to pursue any career I desired, even when it did not make sense to them. Dan, thank

you for driving down to San Diego from Los Angeles to visit me, even when you had to

spend half of the weekend waiting for me to finish an experiment. I appreciate all the big

and little ways you have cared for me during my time in graduate school: from taking

our dog Roscoe out to fixing dinner to cleaning the apartment. I am especially grateful

for the way you left your life in Los Angeles behind to move to San Francisco when the

Weinberger lab moved to The Gladstone Institutes.

Chapters 2 and 3, in full, are modified reprints of work published in An

Endogenous Accelerator for Viral Gene Expression Confers a Fitness Advantage. Teng

MW, Bolovan-Fritts C, Dar RD, Womack A, Simpson ML, Shenk T, Weinberger LS.

Cell. 2012 Dec 21; 151(7):1569-1580. The dissertation author was the co-primary

researcher and author of this work.

Chapter 4 is based on unpublished work, for which I was the primary researcher,

and Cynthia Bolovan-Fritts, Jac Luna, Renee Ram, Brian Linhares, Leor Weinberger, Ya

(Maggie) Nang, Sam Li, David Agard, and JJ Miranda critically contributed to the work.

VITA

2003   Bachelor of Science, Biochemistry, University of California, Los Angeles

2009   Master of Science, Chemistry, University of California, San Diego

2013   Doctor of Philosophy, Chemistry, University of California, San Diego

PUBLICATIONS

Pilpa RM, Fadeev EA, Villareal VA, **Wong ML#**, Phillips M, Clubb RT.   Solution structure of the NEAT (NEAr Transporter) domain from IsdH/HarA: the human hemoglobin receptor in *Staphylococcus aureus*. *Journal of Molecular Biology*.   2006; 360(2):435-7.

Pilpa RM, Robson SA, Villareal VA, **Wong ML#**, Phillips M, Clubb RT. The IsdC protein from *Staphylococcus aureus* uses a flexible binding pocket to capture heme. *Journal of Biological Chemistry*. 2009; 284(2):1166-76.

Gardner TJ, Bolovan-Fritts C, **Teng MW**, Redmann V, Kraus TA, Sperling R, Moran T, Britt W, Weinberger LS, Tortorella D. Development of a high-throughput assay to measure the neutralization capability of anti-cytomegalovirus antibodies. *Clin Vaccine Immunol.* 2013; 20(4):540-50.

Teng MW*, Bolovan-Fritts C*, Dar RD, Womack A, Simpson ML, Shenk T, Weinberger LS. An endogenous accelerator for viral gene expression confers a fitness advantage. *Cell.* 2012; 151(7):1569-80.

#Maiden name

*These authors contributed equally to this work.

ABSTRACT OF THE DISSERTATION

Characterization of IE2 Autoregulation

and its Impact on Viral Fitness in Human Cytomegalovirus

by

Melissa W. Teng

Doctor of Philosophy in Chemistry

University of California, San Diego, 2013

Professor Leor Weinberger, Chair
Professor Alexander Hoffmann, Co-Chair

Systems biology is an emergent field in the biological sciences that has enabled biologists to quantitatively study gene circuits and networks by integrating mathematical modeling, bioinformatics, and biological approaches. Here, we use mathematical modeling and single-cell fluorescence microscopy to reveal a novel gene circuitry in CMV, a global pathogen and major health concern in infants and immunocompromised individuals.   This gene circuitry produces acceleration while limiting amplification of output protein levels in the presence of transactivators. IE2 (Immediate-Early 2), CMV's essential viral transactivator, drives this accelerator circuit by autoregulating itself via

cooperative binding to the *cis repression sequence (crs)*, a 12 base-pair (bp) sequence located just upstream of the Major Immediate-Early promoter (MIEP)'s Initiator site. IE2 acceleration produces a viral replication fitness advantage, and mutation of the *crs* sequence eliminates IE2 acceleration and produces amplification of IE2 protein in response to transactivators, severely limiting CMV's replication ability. The Δ*crs* mutant virus exhibits lowered transcriptional strength due to its inability to efficiently localize to sub-nuclear PML bodies, where CMV immediate-early transcription typically occurs. The low transcriptional strength in the Δ*crs* mutant virus results in slower IE2 expression and a severe fitness cost.

To further understand the mechanism behind the IE2 accelerator circuit, IE2's interaction with the *crs* sequence was studied using gel filtration chromatography and electron microscopy. IE2 self-multimerizes into a ring-like structure in the presence of *crs* DNA, using multiple IE2 subunits. IE2 multimerization only occurs in the presence of the *crs* sequence and does not occur in the presence of a mutated *crs* sequence.

Chapter 1:

Introduction

Human cytomegalovirus

Human cytomegalovirus (CMV), or human herpesvirus 5 (HHV-5), is the leading cause of birth defects and presents significant health complications in immuno-compromised individuals such as AIDS patients or organ transplant recipients.   In undeveloped countries, CMV seroprevalence is close to 100% while some areas in developed and affluent countries have seroprevalence rates below 50% (Shenk and Stinski, 2008). Because of CMV's ability to undergo latency and later reactivate, CMV has been difficult to therapeutically target in immuno-compromised individuals. Congential CMV infection, however, has been the focus of clinical research due to the devastating complications that may arise in infants born to mothers who are undergoing primary infection during pregnancy. CMV infections in newborns can result in mental retardation, hearing loss, or even death (Britt, 2008; Fields et al., 2007).

CMV is a double-stranded, linear DNA virus and betaherpesvirus. Betaherpesviruses, a subset of herpesviruses, are characterized by their large genome size, ability to undergo latency in leukocytes, and their slow replication cycle (Fields et al., 2007; Murphy and Shenk, 2008). The CMV virion particle is approximately 200-300 nm in diameter. The CMV genome is approximately 235 kb and is enclosed in an icosahedral capsid with tegument proteins immediately surrounding the outside (Fig. 1.1). The capsid and tegument are surrounded by an amorphous tegument layer and an outer lipid envelope (Chen et al., 1999). CMV enters the human cell via these glycoproteins. In fibroblasts, the virus enters through fusion to the cell membrane. In epithelial and endothelial cells, CMV enters via pH-mediated endocytosis (Bodaghi et al., 1999; Ryckman et al., 2006).
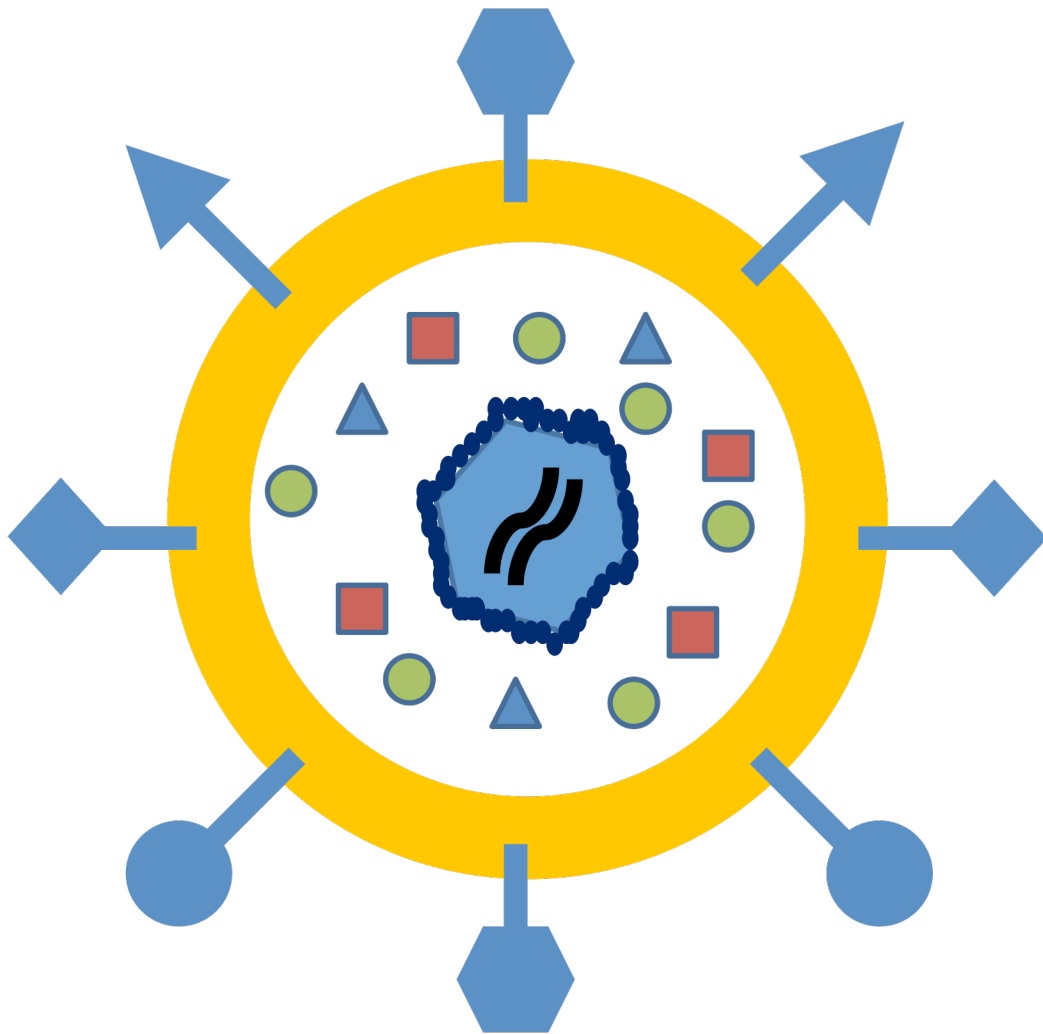
Figure 1.1: The CMV virion structure. The CMV virion particle has a diameter of 200-300 nm. At its core lies a 125 nm icosahedral capsid (blue hexagon) containing a linear double-stranded DNA genome (black). Tegument proteins (dark blue circles) are attached to the outside of the capsid, and a larger amorphous tegument layer (red squares, green circles, and blue triangles) surrounds the capsid and attached tegument proteins. The outer most layer of the virion particle is a lipid envelope (yellow) with glycoproteins (blue) attached to the outside surface.

CMV has the ability to infect a range of cell types (e.g., fibroblasts, monocytes, dendritic cells, epithelial cells, endothelial cells and CD34+ progenitor cells). Cell culture models have been mostly unsuccessful in recapitulating infection in the human host because CMV loses its tropism after several passages in fibroblasts, which are the preferred cell type for virus propagation due to fibroblasts' high yield of cell-free virus. AD169, an attenuated lab strain, is the primary strain of CMV studied. It is only able to infect fibroblasts due to its loss of the ULb' region in the CMV genome. This region of the genome is necessary for infection in epithelial cells, endothelial cells, dendritic cells, and monocytes (Gerna et al., 2003; Wang and Shenk, 2005a, b). Because of AD169's attenuation, ability to be produced in high titers, and release of cell-free virus, it is a favored strain for study in the lab. Clinical isolates such as TB40-E are able to infect a wider range of cell types and thus more closely resemble infection in humans(Sinzger et al., 2008). However, it is technically challenging to harvest and purify high titers of virus from propagation of these isolates.

CMV's viral lifecycle is controlled through a coordinated cascade of gene expression with three stages: immediate-early, early, and late (Fields et al., 2007). Once the virus enters the cell, the Major Immediate-Early (MIE) circuit, CMV's master transcriptional circuit, begins transcribing the Immediate-Early (IE) gene products. It remains unclear how the CMV genome reaches the cell's nucleus. Once in the nucleus, the genome localizes next to ND10 domains which contain ND10-associated proteins such as PML and Sp100 (Ishov et al., 1997). These proteins have been implicated in the interferon response and antiviral defense mechanisms (Maul, 1998).

By 12 hours post infection, the early proteins can be detected in the nucleus. By 24 hours post infection, DNA replication is initiated by IE2 transactivation of the UL84 promoter. Late genes begin expression 24-36 hours post infection, and release of progeny peaks at 72-96 hours post infection (Fields et al., 2007).

The Major Immediate-early Circuit and the Immediate-early Proteins

IE transcripts begin accumulating at or near ND10 domains, or PML oncogenic domains (PODs) soon after infection, suggesting that ND10 domains are sites of IE transcription. The pp71 tegument protein activates the MIE circuit by relieving Daxx-dependent HDAC repression of the MIEP.   Other tegument proteins have been shown to be involved in MIEP activation at the beginning of infection but pp71 appears to be the main driver of MIEP activation (Bresnahan and Shenk, 2000). The Major Immediate-Early promoter/enhancer (MIEP) drives expression of the Immediate-early genes (Fig. 1.2) (Stinski and Isomura, 2008; Stinski and Petrik, 2008). The MIEP is an exceptionally strong promoter that contains multiple transcription sites such as Nf-kb, Sp1, CREB, etc (Stinski and Isomura, 2008). The IE mRNA transcripts yield two major alternative splice variants: IE1 and IE2 (Stinski and Petrik, 2008). IE1 is a 72 kDa protein with a diverse set of functions during the CMV lifecycle but is non-essential for viral replication at high MOI. The protein contains exons 2-4 of the MIE mRNA pre-spliced RNA and upregulates IE gene expression by antagonizing HDAC deacetylases. However, IE1's most studied function has been its interaction with cellular defense proteins. After the first few hours of IE transcript accumulation, IE1 protein disperses ND10 proteins throughout the nucleus via an unknown mechanism and allows for IE2 protein to begin

CMV genome

MIEP → IE1 | IE2

•Autoregulation of IE expression
•Cellular and viral promoter activation
•Cell cycle regulation

•HDAC inhibition
•Cellular defense antagonism
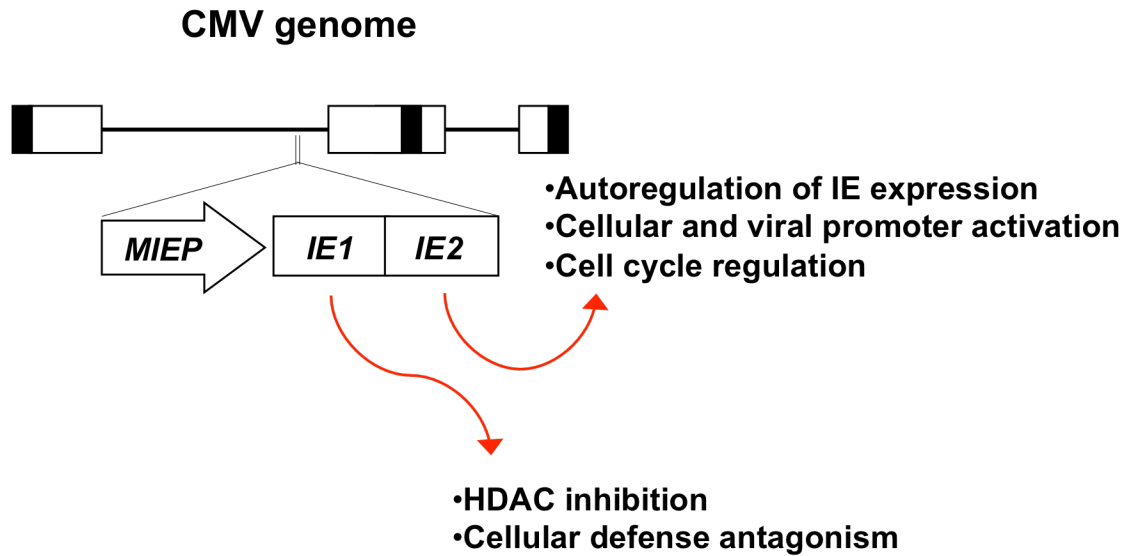
Figure 1.2: The Major Immediate-early circuit. The CMV genome is ~235 bp and contains a number of terminal and internal repeats (white boxes) and untranslated regions (black boxes). The Major Immediate-early (MIE) circuit is the first gene circuit activated upon infection and includes the Major Immediate-early promoter-enhancer (MIEP) driving the expression of IE1 and IE2. IE1 and IE2 are alternative splice variants. IE1 protein inhibits histone deacetylases (HDACs) to promote activation of viral promoters and antagonizes cellular defense mechanisms such as ND10. IE2 protein autoregulates IE gene expression by binding to the MIEP, transactivates cellular and viral promoters, and arrests cell cycle progression.

accumulating at the ND10 domains where IE transcripts are located (Ishov et al., 1997).

IE2 colocalization with ND10 domains have been shown to coincide with

transcription factor (e.g., TBP, TFIIB) accumulation in domains adjacent to ND10,

suggesting that IE2 is responsible for recruitment of pretranscription complexes (Ahn et

al., 1999).

IE2 is an 86 kDa protein containing exons 2,3, and 5 and is the essential major

transactivator that initiates activation of the CMV early and late genes.   IE2 also

negatively regulates itself and IE1 by binding to the *cis*-repression sequence (*crs*), a 13

bp palindromic sequence just upstream of the initiator site in the MIEP (Stinski and

Petrik, 2008). IE2's carboxyl terminal end contains a dimerization domain and a DNA-

binding domain that includes a zinc finger motif and encompasses and overlaps with a

large part of the dimerization domain (Chiou et al., 1993; Shenk and Stinski, 2008).

IE2's other important functions involve its ability to transactivate viral and

cellular promoters.   It is a promiscuous transactivator that is able to activate homologous

and heterologous promoters through both direct binding to promoters and recruitment of

transcription factors. IE2 tranactivates early viral promoters containing TATA boxes by

associating with basal transcription machinery, such as TBP and TFIIB. Cellular

transcription factors, such as CREB, Nf-kB or SP1, also interact with IE2 to transactivate

viral and cellular promoters. Similarly to IE1, IE2 can recruit histone acetylases to

upregulate viral promoters (Stinski and Petrik, 2008).

IE2 transactivation can induce cell progression and initiate cell cycle arrest to set

up an advantageous environment for CMV replicaton. IE2 can bind to UL84 and form

the IE2:UL84 complex, which is necessary for DNA replication. UL84 is an early gene

that counteracts IE2's transcriptional activation of early genes (Xu et al., 2004).   In

addition to UL84, IE2 also binds to other early gene promoters such as the UL112 and

UL4 promoters (Petrik et al., 2007).

Autoregulation in gene circuits

Negative feedback and autoregulatory circuits are prevalent in signal transduction

circuits and have thus been examined extensively theoretically and experimentally.

Negative autoregulation in biological systems was first extensively mathematically

modeled and analyzed by Michael Savageau in the 1970's (Savageau, 1970, 1974, 1975;

Savageau, 1976). In the early 2000's, Uri Alon extended Savageau's work by

experimentally testing much of his theoretical work in synthetic and endogenous

biological circuits in *E. coli* and yeast (Alon, 2007a; Milo et al., 2002; Rosenfeld et al.,

2002; Shen-Orr et al., 2002)

A simple gene circuit includes a gene driven by a promoter. RNA polymerase

transcribes the gene into mRNA, and the mRNA is translated into protein. The promoter

can be activated or repressed by transcription factors.

A simple gene circuit without any regulatory feedback can be described by a one-

equation ordinary differential equation model: $dx/dt = \beta - \delta \cdot x$ where β is the basal

promoter activation rate and δ is the decay rate of the protein x. Autoregulatory circuits

employ the Hill function $f(x) = \dfrac{\beta}{k + (x/\gamma)^H}$ where k is the Michaelis constant, γ is the

dissociation constant of x, and H is the Hill coefficient. Typically, k is set to 1 in most

simple autoregulatory circuit models. The one-equation model for an autoregulatory

circuit is $f(x) = \dfrac{\beta}{k + (x/\gamma)^H} - \delta \cdot x$. These simple models assume mRNA to be at a quasi-

steady-state due to the short half-life of mRNA (Alon, 2007a).

In 1974, Michael Savageau compared the response time of no-feedback circuits to autoregulatory circuits. He found that autoregulatory circuits exhibit a faster response time when the steady-state solutions of both circuits are equivalent (Fig. 1.3) (Savageau, 1974). Rosenfeld et al. followed Savageau's work almost thirty years later by expounding upon and validating Savageau's theoretical work *in silico* and in synthetic *E. coli* gene circuits. For a strongly autoregulated circuit, they found that the response time of a negatively autoregulated circuit is about 1/5 the response time of an equivalent simple circuit with no regulation in *E. coli,* in which the cell doubling time is faster than protein degradation (Rosenfeld et al., 2002).

Cooperativity in autoregulation further decreases the response time compared to an autoregulatory circuit with no cooperativity. The higher the Hill coefficient, the shorter the response time is due to the increased strength in negative feedback from the increased cooperativity (Alon, 2007a).

The work discussed in the dissertation will expound upon previous literature on highly cooperative autoregulation and its impact on response time by exploring the effect of increased transcriptional activation of a highly cooperative autoregulatory circuit. In a simple gene circuit with no feedback, increasing levels of transcriptional activation will amplify steady-state protein levels proportionally (Fig. 1.4). However, a negative feedback circuit in which transcriptional activation is increased produces dampened

No feedback

Autoregulation

$$X = \beta - \partial X$$

$$X = \frac{\beta}{k + (X/\gamma)^H} - \partial X$$
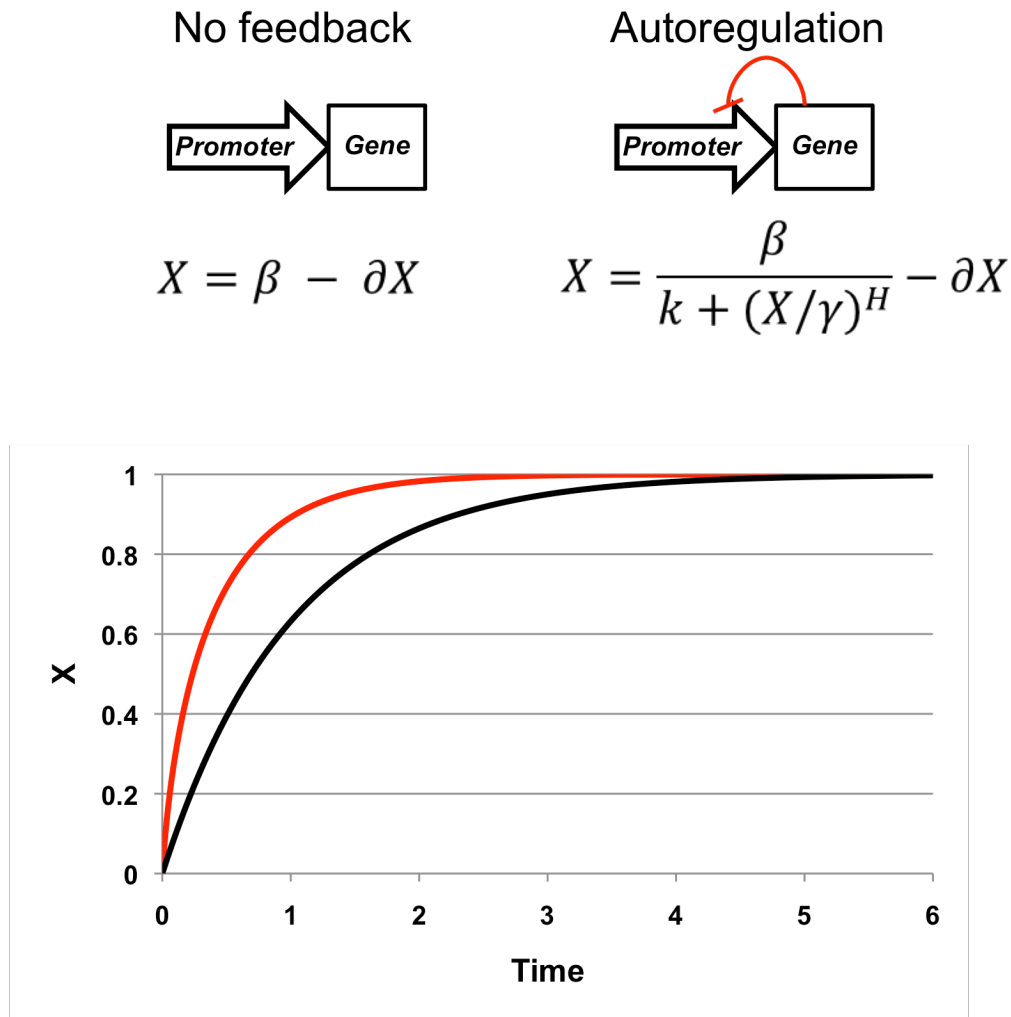
Figure 1.3: **Negative feedback speeds response time.** The expression of a gene, X, over time is plotted for a simple gene circuit with no feedback (black) and an autoregulatory gene circuit (red). Curves were generated using ordinary differential equations (left: no feedback circuit, right: autoregulation circuit). The steady-state solutions of both equations are the same, but the negative feedback circuit reaches its steady state faster than the no feedback circuit.
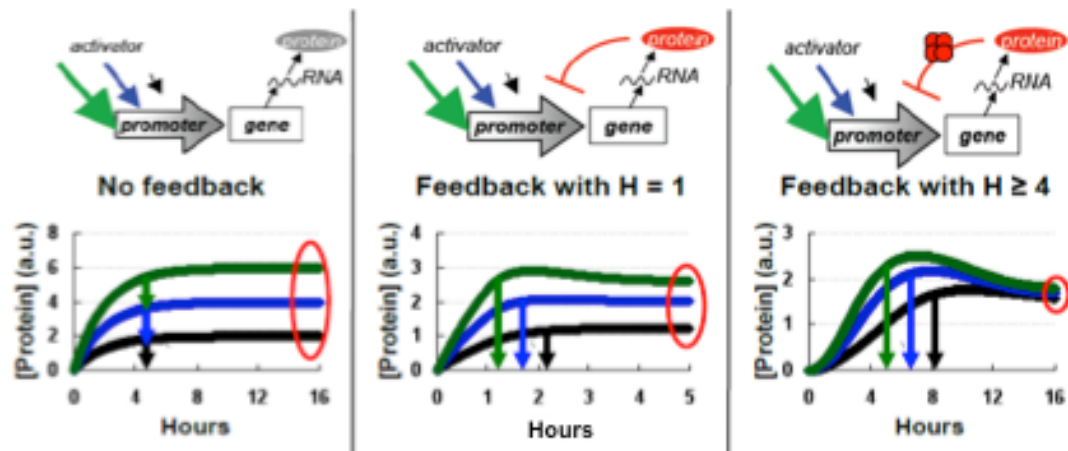
Figure 1.4: Highly cooperative negative feedback entirely dampens amplification of protein output by transcriptional activators. Numerical solutions are plotted for a minimal model of gene expression for differing values of basal promoter strength and the Hill coefficient. Left panel: unregulated/no-feedback circuit ($H = 0$); middle panel: circuit encoding "non-cooperative" negative feedback ($H = 1$); right panel: circuit encoding self-cooperative negative feedback with $H = 4$. Each circuit simulated after induction by a transcriptional activator that increases basal promoter activity 2-fold (blue) or 3-fold (green). When $H = 0$ (i.e. unregulated circuit), expression rate is accelerated by activators but the final steady-state level is also linearly amplified. When $H = 1$, expression is accelerated by activators but steady-state level is still significantly amplified (sub-linearly). When $H = 4$, expression rate is accelerated by activators and steady-state level remains non-amplified.

amplification of steady-state protein levels due to the presence of negative feedback. When the negative feedback is highly cooperative and the delay from transcriptional activation to protein output is sufficiently large, increasing levels of transcriptional activation generate almost equivalent steady-state levels despite the increasing transcriptional rate.

Chapter 2:

The CMV IE2 accelerator circuit converts signaling inputs into faster rates of expression

ABSTRACT

Many signaling circuits face a fundamental tradeoff between accelerating their response speed while maintaining final levels below a cytotoxic threshold. Here, we describe a transcriptional circuitry that dynamically converts signaling inputs into faster rates without amplifying final equilibrium levels. Using time-lapse microscopy, we find that transcriptional activators accelerate human cytomegalovirus (CMV) gene expression in single cells without amplifying steady-state expression levels, and this acceleration generates a significant replication advantage. We map the accelerator to a highly self-cooperative transcriptional negative-feedback loop (Hill coefficient ~ 7) generated by homo-multimerization of the virus's essential transactivator protein IE2 at nuclear PML bodies. In general, accelerators may provide a mechanism for signal-transduction circuits to respond quickly to external signals without increasing steady-state levels of potentially cytotoxic molecules.

INTRODUCTION

Biological signaling circuits, like electrical circuits, face a fundamental tradeoff between speed and amplitude (Alon, 2007; Savageau, 1976). That is, a faster rate of initial increase is typically obtained at the cost of a higher steady-state level. This tradeoff creates an evolutionary pressure when quick turn-on of a signaling molecule is essential but the signaling molecule is cytotoxic at high levels, as with inflammatory cytokines (Cauwels and Brouckaert, 2007), many viral systems (Dwarakanath et al., 2001), and even the fever response (Roth et al., 2006). For example, herpesviruses must quickly express viral genes that modulate the host-cell environment into a replication-

favorable state, but these genes often yield cytotoxic products when expressed at high levels and can prematurely damage the cell before an optimal number of viral progeny are produced. Here, we investigate mechanisms that may optimize this "rate-versus-level" tradeoff to generate a functional advantage.

We utilize the human herpesvirus cytomegalovirus (CMV), since many of the viral processes that alter the host-cell environment have been well characterized (Mocarski et al., 2006). CMV infects a majority of the world's population and is a leading cause of birth defects and is a leading cause of morbidity and mortality in the immunocompromised population. The virus initiates an infectious program within the cell by expressing its 86-kDa viral transactivator protein Immediate-Early 2 (IE2), which is a promiscuous transactivator of viral promoters and is essential for viral replication (Stinski and Petrik, 2008), but also highly cytotoxic (Dwarakanath et al., 2001; Sanders et al., 2008). CMV must quickly express IE2 to establish a replication-favorable environment but also limit IE2 levels to avoid prematurely compromising the cell's ability to produce viral progeny. IE2, along with IE1, is encoded by a precursor mRNA expressed from the CMV Major Immediate-Early (MIE) promoter, which directs all subsequent viral gene expression and is considered to be the chief regulator of the lytic cycle (Stinski and Petrik, 2008). The MIE promoter (MIEP) is exceptionally strong and encodes multiple transcription factor–binding sites within its ~500-nucleotide enhancer (Stinski and Isomura, 2008). The MIEP is also auto-repressed by IE2 via direct DNA binding to a 12-nucleotide *cis repression sequence* (*crs*) located between positions -13 and +1 relative to the transcriptional start site (Macias and Stinski, 1993). The impact of IE2 autoregulation upon the virus life cycle is largely unknown.

Using an integrated approach that couples mathematical modeling with quantitative time-lapse microscopy, we show that IE2 negative feedback is highly cooperative, which allows the virus to overcome the rate-versus-level tradeoff (Fig. 2.1) by accelerating IE2 gene expression without any measureable increase in the steady-state expression level. To simplify comparison of level and rate, we introduce the "response vector", which maps time-lapse trajectories into points on a two-dimensional plane in terms of time to reach steady state and level of expression. Circuits that respond upward (or upward and to the right) in response-vector space are amplifiers, while circuits that respond in a horizontal leftward direction, like the IE2 circuit, are accelerators (Fig. 2.1). Strikingly, the IE2 circuit appears to be a "pure" accelerator circuit that exhibits an almost perfectly horizontal response vector. This finding may lead to other examples where tuning the expression rate, rather than the expression level, enhances fitness.

MATERIALS AND METHODS

Cloning of recombinant viruses

The CMV IE2-YFP virus was constructed in the CMV AD169 background (Bankier et al., 1991) by inserting EYFP (Clontech) to the 3' end of IE2 exon 5 in the parent AD169 bacterial artificial chromosome (BAC) as previously described (Moorman et al., 2008; Yu et al., 2002). The following IE2 targeting primers were used (sequences in capitals are the homology arms to IE2 sequence:

5'CTGAGCCTGGCCATCGAGGCAGCCATCCAGGACCTGAGGAACAAGTCTCA
Ggccggaagaagatggaaaaag3' (forward);
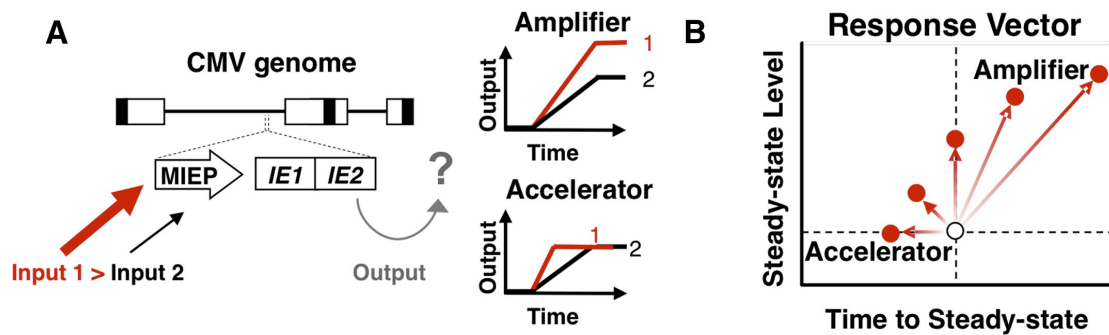
Figure 2.1: **Mapping protein output characteristics on the "response-vector" can determine whether the CMV MIE circuit is an amplifier or an accelerator circuit.** **A,** Schematic of the CMV genome (~230 kb), with the MIE regulatory circuit (~5 kb) magnified. Increased inputs (transcriptional activation) to the MIE promoter could result in either increased output of protein levels (amplifier) or acceleration of gene expression without amplification of level (accelerator). **B,** The "response-vector" allows convenient comparison between output time-lapse trajectories (i.e. white versus red points) in terms of steady-state level versus the time to steady state. Circuits that act as amplifiers respond to increased input by shifting vertically or diagonally to the upper right, while circuits that act as 'accelerators' respond by shifting horizontally left.

5'ACGGGGAATCACTATGTACAAGAGTCCATGTCTCTCTTTCCAGTTTTTCACcg tcgtggaatgccttcg3' (reverse).

The CMV GFP control virus (Yu et al., 2003)(Yu et al., 2003)(Yu et al., 2003) encodes an SV40 promoter–EGFP cassette. To propagate and purify virus, BAC DNA was electroporated (Yu et al., 2002) into MRC5 cells (American Type Culture Collection) using a GenePulser Xcell Electroporation System (Bio-Rad). Upon infection reaching 100% viral cytopathic effect or 100% GFP, the culture supernatant was collected and filtered with a 0.45 μm filter (Corning Inc.). Viral stocks were titered by TCID$_{50}$ (Nevels et al., 2004).

Cell-culture conditions and drug perturbations

MRC5 fibroblasts and life-extended human foreskin fibroblasts (HFFs) (Bresnahan and Shenk, 2000) were maintained in Dulbecco's Modified Eagle's Medium (DMEM) supplemented with 10% fetal bovine serum (FBS) and 50 U/ml penicillin-streptomycin at 37ºC and 5% CO$_2$ in a humidified incubator. ARPE-19 cells were maintained in a 1:1 mixture of DMEM/F-12 (Mediatech Inc.) with 10% FBS (HyClone) and 50 U/ml Penicillin-Streptomycin (Mediatech Inc.). Cells were treated with a final concentration of 400nM TSA (Sigma-Aldrich) resuspended in dimethylsulfoxide, for 20-24 hours, a final concentration of 10 ng/mL TNF-α (Sigma-Aldrich) resuspended in PBS, or a final concentration of 1 mM VPA (Calbiochem) for approximately 24 hours before imaging.

Quantitative Western blot analysis

MRC5s at ~60% confluency were infected at MOI = 1. To synchronize viral

entry, adsorption was done at 4°C for 30 min., cells washed once in PBS (Mediatech,

Inc.), fresh media added, and cells placed in a 37°C in a humidified CO_2 incubator.

Time points were collected every 1-2 hrs for 20-24 hrs as indicated. Sample collection,

protein transfer, and blot preparation were as previously described (Bolovan-Fritts et al.,

2004) and samples were loaded and separated on precast SDS PAGE 10% or 7.5%

bisacrylamide gels (BioRad).

For quantitative IE2 detection in Fig. 2.2 and Appendix Fig. 2.1, the 1° antibody

MAB810 (Millipore) was used at 1:100 and 2° antibody 926-32212 (LI-COR™) was

used at a dilution of 1:20,000. For normalization, anti-beta tubulin antibody 26-42211

(LI-COR™) used at a dilution of 1:2000 followed by 2' antibody 926-68073 (LI-COR™)

at a dilution of 1:20,000. Blots were scanned and quantified on a LI-COR™ Odyssey™

according to manufacturer's protocols.

For all other Western blots, the blot was incubated with chemiluminescence

substrate from the Western Lightning ECL detection kit (NEN/Perkin-Elmer) according

to the manufacturer's instructions.   Protein bands were detected using a Typhoon

PhosphoImager (GE Healthcare). The following antibodies and dilutions were used

where indicated: primary mouse monoclonal anti-IE2 (clone 3A9) at 1:100 (Cuevas-

Bennett and Shenk, 2008), a primary mouse monoclonal antibody against a shared

epitope present in IE1 and IE2 at 1:100 (MAB810, Millipore), primary goat polyclonal

anti-human actin at 1:2000 (sc-1615, Santa Cruz Biotechology, Inc.), secondary goat

anti-mouse IgG conjugated to horse radish peroxidase (HRP) at 1:500 (sc-2005, Santa

Cruz Biotechnology, Inc.), and secondary donkey anti-goat IgG-HRP at 1:1000 (sc-2020, Santa Cruz Biotechnology, Inc.).

Time-lapse fluorescence microscopy measurements

Cells were passed onto a 35 mm glass-bottom dish (MatTek Corp.) or a 96-well glass-bottom plate (Thermo Fisher Scientific) and grown to confluency for several days in order to hold cells in the G0 phase. Cells were synchronously infected on ice at 4ºC for 30 minutes or at room temperature for 30 minutes with virus at a MOI of 1. Live cells were imaged using a 20X oil objective on a spinning disk confocal microscope (Olympus DSU, Olympus America, Inc.) equipped with a 37°C, humidified, 5% CO_2 live-cell chamber. Image collection began when YFP signal was first detected and frames were subsequently captured every 10 minutes for 16-24 hours using an exposure time between 200 and 800 msec. Images were acquired with Slidebook^{TM} 4.2 software (Imaging Innovations, Inc.). Single-cell tracking and segmentation were performed with custom-written code in MatLab^{TM} (Mathworks) as previously described (Weinberger et al., 2008). Code is available upon request. Homo-FRET imaging was performed as previously described (Weinberger and Shenk, 2007). FRAP imaging was performed on a FluoView 1000 confocal laser microscope (Olympus America, Inc.). At 12 hours post infection (h.p.i) (CMV IE2-YFP) or 24 h.p.i. (CMV Δ*crs* IE2-YFP), an initial snapshot was imaged and then a fixed pixel area within the nucleus (corresponding to ~1/4 to ~1/3 of the nucleus) was photobleached down to ~50% of its original intensity. The nuclei chosen for bleaching were roughly equivalent in size. An image was collected 30 sec post-bleach and then every minute for 25 minutes. Each image capture took 1000 msec.

Analysis of Homo-FRET Data

The theoretical formula: $r_n = r_1 \dfrac{1 \cdot (R_0/R)^6}{1 + N(R_0/R)^6} + r_{et} \dfrac{(N-1)(R_0R)^6}{1 + N(R_0R)^6}$ (obtained from

(Runnels and Scarlata, 1995)) was solved for N (the number of IE2-YFP monomers

bound together) for a range of possible r_n (the anisotropy value experimentally measured

by homo-FRET) and R (the distance in Angstroms between any two IE2-YFP monomers

in the homo-multimer).   The range of r_n represented in Fig. 2.6 are the range of

anisotropy values determined from our IE2-YFP homo-FRET experiments. r_{et} is defined

as the anisotropy contribution from the 1st acceptor in the N-mer and assumed to be very

small for large N-mers, making the 2nd term on the right hand side of the formula equal to

0. r_1 is the anisotropy value for a single IE2-YFP monomer randomly tumbling in space

and is equal to 0.5, determined from our experimental homo-FRET results using CMV

GFP virus. The calculated R_0, Förster distance, for an YFP-YFP interaction is 51.1

Angstroms (Patterson et al., 2000).

Mathematical modeling to estimate H from time-lapse microscopy data and closed-loop

analysis to measure H from flow cytometry data

Numerical simulations and fitting of an ODE model (Appendix) were performed

in Berkeley Madonna^{TM} (www.berkeleymadonna.com).

Mathematica^{TM} (Wolfram Research) was used for closed-loop analysis. Standard

lentiviral cloning was used to create minimal MIE circuits (Dull et al., 1998). The

minimal MIEP-IE2-GFP and MIEP-GFP circuits are driven by a full-length ~2.5kb MIE

promoter-enhancer (MIEP) that spans the sequence from the MIEP modulator at the 5'

edge to the junction of IE exons 1 and 2. The MIEP was PCR-cloned from AD169 into pLEIGW (a gift from Ihor Lemishka) in place of the EF1a promoter. This full-length MIEP drives an IE2-IRES-GFP or mCherry-IRES-GFP cassette. IE2 was cloned from pRSV-IE86 (a gift from Jay Nelson). ARPE-19 cells were infected and FACS sorted for GFP to create stably expressing cell lines (Fig. 2.9). Cells were treated with TSA for 17 hours, and GFP expression was quantified by flow cytometry. Live cells were gated by forward-versus-side scattering on a FacsCalibur[TM] cytometer (BD Biosciences) and mean fluorescence intensity recorded. At least 20,000 live cells were recorded for each experiment and data was analyzed in FlowJo[TM] (Treestar Inc.).

Replication Kinetics

Confluent MRC5 monolayers at $\sim5 \times 10^4$ cells per well were infected at indicated MOIs using 0.45μm pre-filtered virus inoculum stocks diluted in culture media. Inoculums were calculated based on plaque-assay titrations (Bolovan-Fritts and Wiedeman, 2001), shown as time point 0 in each figure. Inoculum was then removed and replaced with 1mL fresh media. Infected wells were collected in triplicate at indicated time points and stored at $-80^{\circ}C$. To measure replication, samples were thawed and prepared as a 10-fold serial-dilution series in culture media, analyzed by $TCID_{50}$, then converted to PFU/ml. Error ranges were calculated by standard deviation.

Minimal synthetic circuit experiments

MIEPΔcrs-IE2-GFP was constructed by PCR cloning MIEPΔcrs from the CMV Δcrs IE2-YFP bacmid and inserted into MIEP-IE2-GFP. ARPE-19 cells were transduced

with the MIEP-IE2-GFP and MIEPΔ*crs*–IE2-GFP vectors and FACS sorted for GFP.

The transduced cell lines were allowed to recover for 24 hours before the percentage of

GFP-expressing cells for each cell line was quantified. Live cells were gated by forward

versus side scattering on a FacsCalibur cytometer. On the first day after recovery, 2,500

GFP events were recorded. Subsequently, at least 10,000 GFP events were recorded for

each experiment and analyzed using FlowJo™. For genomic PCR, genomic DNA was

purified using a NucleoSpin Tissue kit (Clontech).

Immunofluorescence

Cells were grown on cover slips (VWR) in 24-well plate culture wells (CoStar)

until ~60% confluency, then rinsed in cold PBS and fixed in 2% paraformaldehyde

(Fisher Scientific) for 10 minutes at $4°C$, blocked, and washed in PBS. IE2 protein was

detected using the IE2-specific monoclonal antibody MAB8140 (Millipore) at a 1:200

dilution in blocking buffer for one hour at room temperature. A secondary donkey anti-

mouse antibody conjugated to Texas Red (Santa Cruz Biotechnology, Inc.) was used at a

1:500 dilution in blocking buffer, for one hour at room temperature in the dark. Samples

were mounted in PBS and viewed with a 40X oil objective by confocal microscopy

(Olympus DSU, Olympus America, Inc.).

RESULTS

Transcriptional Acceleration-Without-Amplification in CMV

We examined MIE gene–expression levels after increasing MIEP activity using

transcriptional activators known to upregulate MIEP activity (Choi et al., 2005; Fan et al.,

2005; Hummel and Abecassis, 2002). These transcriptional activators, Valproic Acid (VPA), Trichostatin A (TSA), or Tumor Necrosis Factor Alpha (TNF-a), appear to accelerate IE2 expression but do not amplify IE2 protein levels, as measured by quantitative Western blot (Fig. 2.2, see also Appendix Fig. 2.1). To test whether IE2 was being accelerated (but not amplified) within single cells, quantitative live time-lapse microscopy was used to track single cells undergoing infection by a recombinant CMV encoding yellow fluorescent protein (YFP) fused to the IE2 open reading frame. This recombinant CMV IE2-YFP virus replicates with wild-type kinetics and IE2-YFP levels are equivalent to wild-type IE2 levels (Appendix Figs. 2.2-2.4). In agreement with previously reported IE2 fusion viruses, the IE2-YFP fusion protein correctly localizes to ND10 domains during infection (Sourvinos et al., 2007). Strikingly, increasing the activity of the MIEP by VPA pretreatment significantly accelerates IE2 expression in single cells but does not amplify steady-state IE2 levels in these single cells (Fig. 2.3)—a result also observed under TSA or TNF-a treatment (Appendix Figs. 2.5-2.7). Flow cytometry analysis (Appendix Fig. 2.8), confirms that acceleration without amplification is not an artifact of image processing.

To rule out the possibility that these results were caused by changes in cell physiology induced by pre-treatment with VPA (or TSA or TNF-a), we also generated an IE2-YFP virus that carried increased levels of the viral transactivator pp71 (Bresnahan and Shenk, 2000) and confirmed that this pp71+ virus, with high levels of packaged pp71 tegument factor, accelerates IE2 expression in the absence of pretreatment (Appendix Fig. 2.7). As an additional control, a generalized transcriptional activator that does not
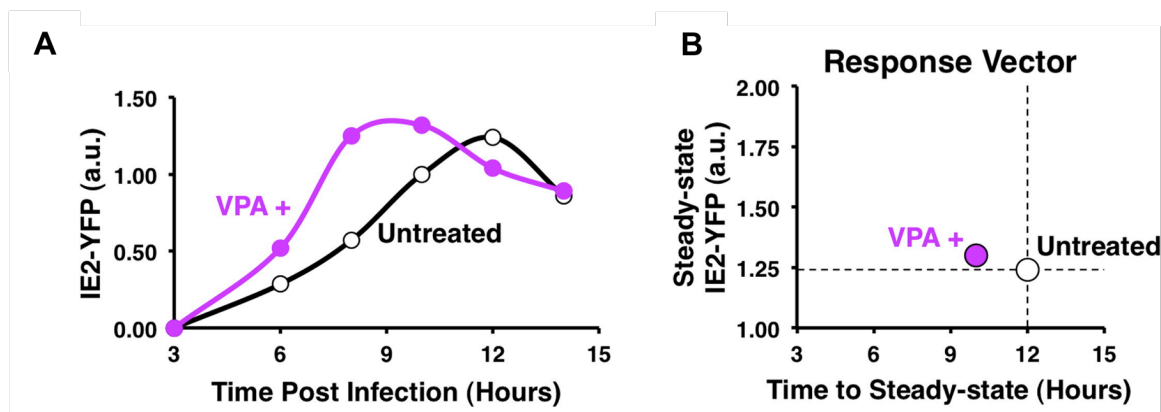
Figure 2.2: **Quantitative Western blot analysis shows that CMV encodes an endogenous accelerator of gene expression.** **A,** Quantitative Western-blot analysis of IE2 expression levels during CMV infection from 3 hours post-infection (h.p.i.), showing acceleration in presence of VPA (pink) but no amplification in IE2 levels compared to the untreated control (white). **B,** Response-vector map of Western blot data. VPA pre-treatment (pink) decreases time to steady-state without increasing steady-state IE2-YFP levels when compared to the untreated control (open circles). Error bars (gray) = ± one standard error. (Western blot data from Cynthia Bolovan-Fritts, and I performed Western blot quantification and data analysis.)
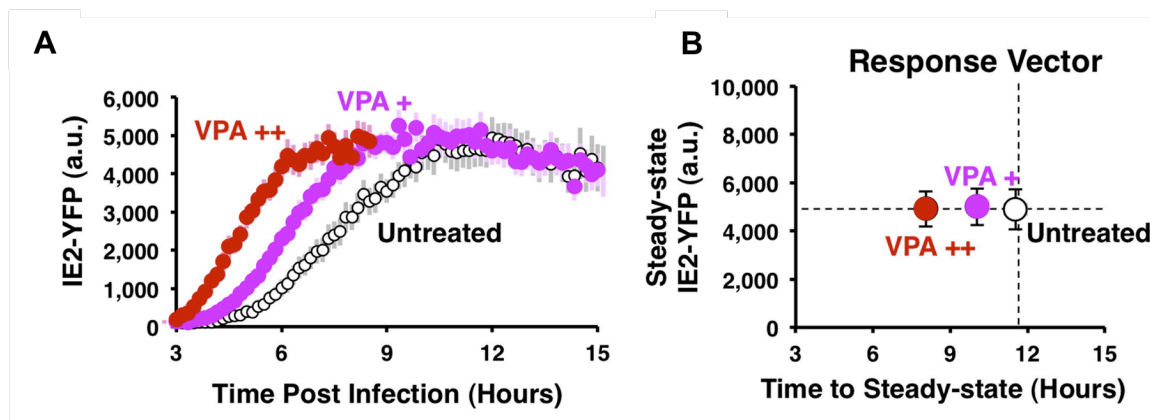
Figure 2.3: **Single-cell microscopy of IE2-YFP levels in cells infected with CMV shows that CMV encodes an endogenous accelerator of gene expression.** **A,** Single-cell time-lapse microscopy of IE2-YFP levels for an untreated infection (open circles) and infection in the presence of increasing exposure to the histone-deacetylase inhibitor VPA (72-hour VPA pre-treatment in red, 24-hour VPA pre-treatment in pink). Each trajectory is an average of 20 cells with ± one standard error in lighter background color. **B,** Response-vector map of single-cell microscopy data, showing that increasing VPA pre-treatment (pink, red) decreases time to steady-state without increasing steady-state IE2-YFP levels when compared to the untreated control (open circles). Error bars (gray) = ± one standard error.

specifically activate the MIE promoter during active infection was used, and it fails to accelerate IE2 expression in single cells (Appendix Fig. 2.7). These controls argue that accelerated rates of MIE expression result specifically from increased activation of the MIE promoter and not from generalized activation of the target cell. Thus, the MIE circuit appears to act as an 'accelerator' that allows only the rate of IE2 expression to change without allowing significant change in the steady-state levels of IE2.

Acceleration Provides a Fitness Advantage for the Virus

Previous studies in RNA viruses have noted that small increases in a single round of replication are sufficient to allow a viral strain to competitively exclude other 'less fit' strains in resource-limited environments; in other words, the strain with the highest basic reproductive number (R_0), which is measured during a single round of infection, wins and excludes all other competing strains, even if that strain's R_0 is only marginally greater than the closest competitor (Nowak and May, 2000).

To test if acceleration of IE2 expression provides any functional advantage for the virus, we analyzed viral replication kinetics after the first round of viral maturation (~96 hours) from cells infected with CMV IE2-YFP virus (Fig. 2.4). The results show that incremental increases in transcriptional activation, and the resulting acceleration in MIE kinetics, generate correlated increases in viral replication fitness with a 72-hour VPA pre-treatment, yielding an approximately five-fold increase in viral replication compared to the untreated control. IE2 acceleration and enhanced replication are also observed in the low-passage clinical CMV isolate TB40-E, which exhibits a nine-fold increase in titer (Appendix Figs. 2.9-2.10).
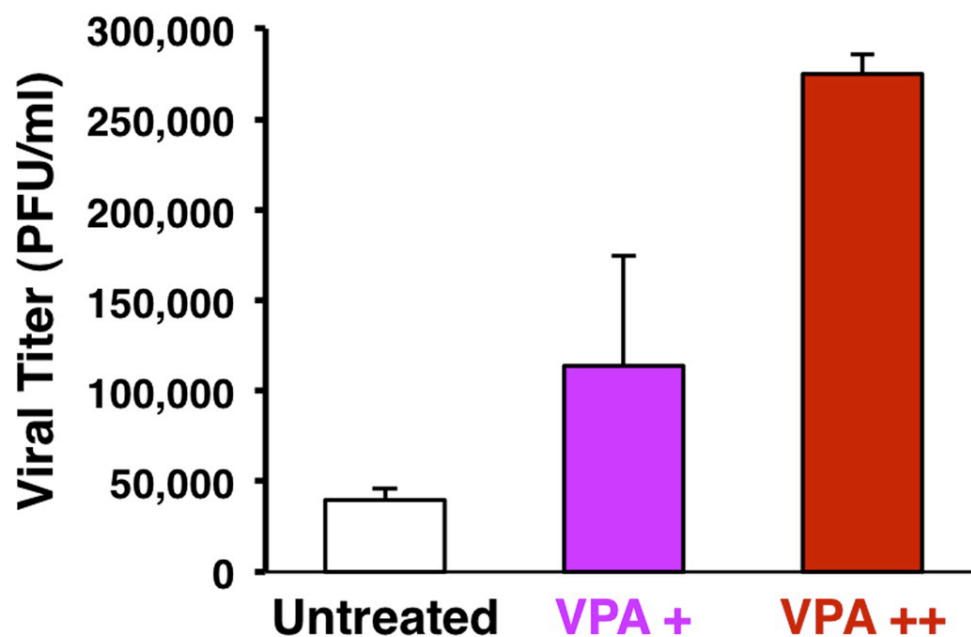
Figure 2.4: **IE2 acceleration provides a viral replication advantage**. Acceleration produces a significant fitness advantage for the virus as measured by CMV wild-type viral titers after a single round of infection (measured by plaque forming units, PFU/ml) on the peak day of viral production (day 4) after infection at MOI = 1. Average viral titers are shown in the absence of VPA (white) and for increasing VPA exposure (red, pink); Error bars = ± one standard deviation.treatment, yielding an approximately five-fold increase in viral replication compared to the untreated control. IE2 acceleration and enhanced replication are also observed in the low-passage clinical CMV isolate TB40-E, which exhibits a nine-fold increase in titer (Appendix Figs. 2.9-2.10). (Viral titers measured by Cynthia Bolovan-Fritts.)

Acceleration-Without-Amplification Requires Highly Self-Cooperative Negative

Feedback, and IE2 Exhibits a Hill Coefficient (H) of $H \approx 7$

   Next, we set out to identify the mechanisms driving acceleration in the CMV MIE

circuit. Based on previous studies showing that negative feedback speeds a circuit's

"response time", i.e., the time required for a circuit to approach to its respective steady-

state level (Black, 1999; Gardner et al., 2000; Kobayashi et al., 2004; Rosenfeld et al.,

2002; Savageau, 1976), we hypothesized that acceleration-without-amplification would

likely utilize negative feedback. By employing a rate-balance analysis, we find that

negative feedback encoding a high 'Hill' coefficient *(H)* is theoretically sufficient to

generate acceleration without amplification (Fig. 2.5), while alternate simple models

cannot generate acceleration without amplification (Appendix Figs. 2.11-2.13), in

agreement with previous studies (Black, 1999; Rosenfeld et al., 2002; Savageau, 1976).

Based on this analysis, we constructed a nonlinear ordinary differential equation (ODE)

model of the CMV MIE circuit (Appendix, Appendix Table 2.1) and performed nonlinear

least-squares regression of the model using the single-cell microscopy data to estimate

the H value of the IE2 negative feedback. $H \approx 7$ generates the best fit to the single-cell

time-lapse microscopy data (Fig. 2.6), and sensitivity analysis demonstrates that $H < 6$

and $H > 8$ cannot generate good fits to the data even when all other parameters are

allowed to vary across all physiological parameter space (Appendix Fig. 2.14). These

simulation results demonstrate that a negative-feedback model with a high H is sufficient

to generate acceleration without amplification and predict that the IE2 circuit requires

negative feedback with $H \gg 1$ in order to function as an accelerator.
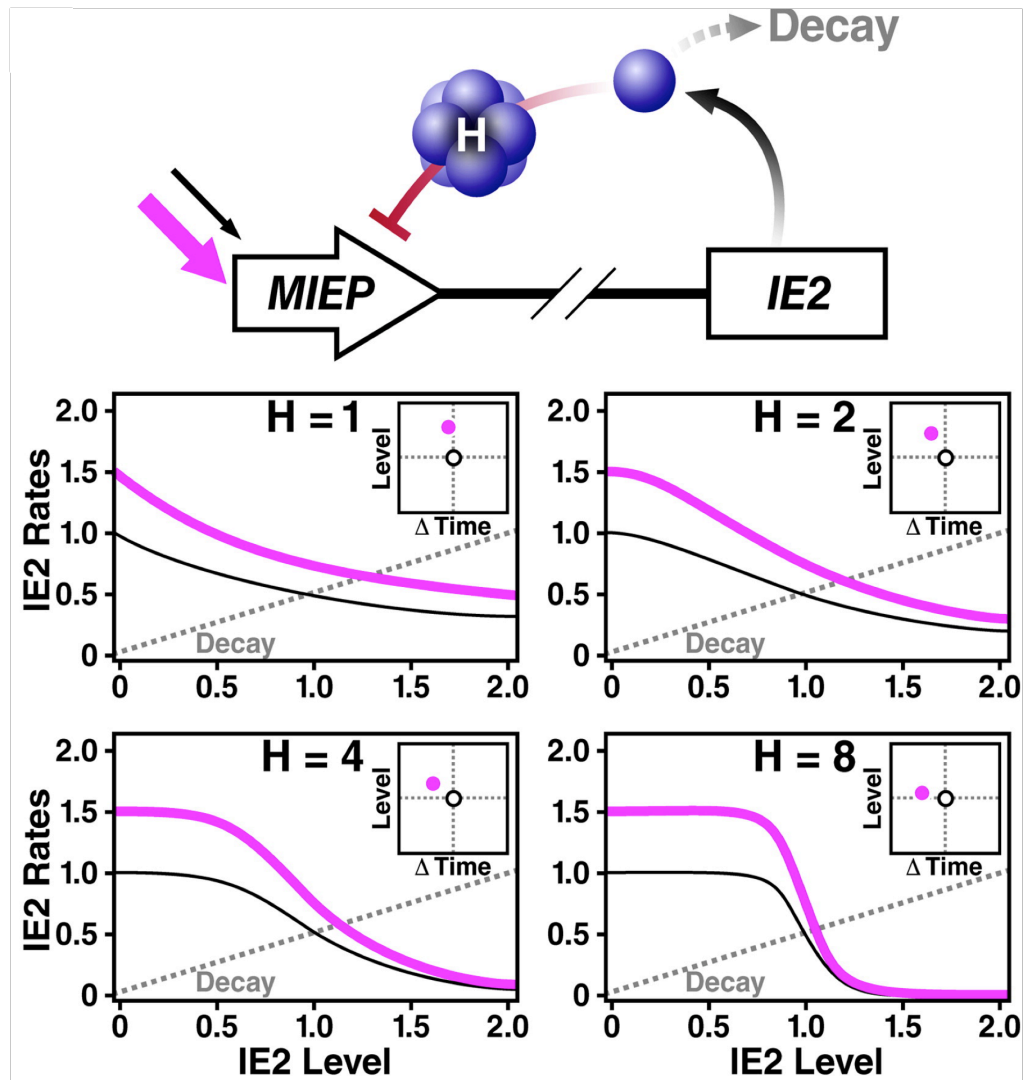
Figure 2.5: **Highly self-cooperative negative feedback is needed to generate an accelerator circuit.** **A,** Schematic and rate-balance analysis of a simplified negative-feedback model: $\dfrac{dx}{dt} = \dfrac{\beta}{(k^H + x^H)} - \delta \cdot x$ for different values of the Hill coefficient (H).

The dashed gray line represents the decay rate while solid lines (black and pink) represent synthesis rates for increasing values of β (1.0 and 1.5, respectively), which accounts for induction by a transcriptional activator that increases basal promoter activity by 1.5-fold. The points at which solid and dashed lines meet represents the steady-state and the distance separating the solid and dashed lines represents the rate of expression. Rate-balance analysis is shown for four values of H. High values of H allow expression rate to increase without amplification in the steady-state level. Insets: response vectors showing the change in steady-state level and the change in time to steady-state for each H value. (Mathematical modeling by Leor Weinberger.)
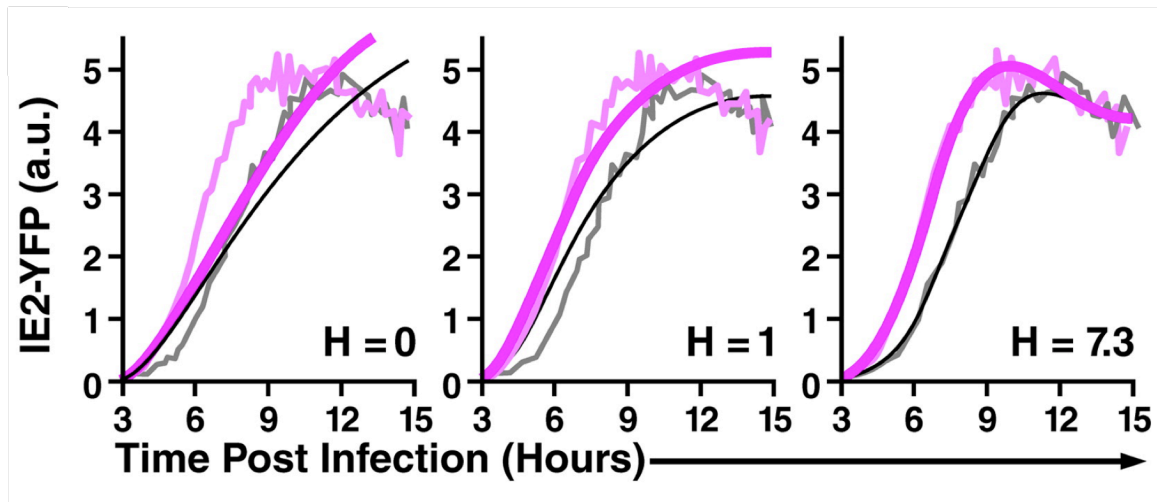
Figure 2.6: **A minimal model of the CMV MIE circuit with a high Hill coefficient best fits single-cell microscopy data of IE2-YFP in cells infected with CMV IE2-YFP virus.** Nonlinear least-squares regression of single-cell time-lapse microscopy data from Fig. 2.3 to a mathematical model of the CMV MIE circuit (Appendix) showing best-fit curve of $H = 7.3$ (right panel). Gray data points are untreated trajectories from Fig 2.3 while pink data points are VPA+ trajectories from Fig 2.3. Poor data fits are generated when H is fixed at $H = 1$ or $H = 0$ (no feedback) despite letting all other free parameters in the model vary (middle and left panels, respectively); sensitivity analysis shows that setting $H < 6$ or $H > 8$ generates poor fits to the data (Appendix Fig. 2.14).

H is traditionally measured by dose-response approaches, which are 'open-loop' (i.e., whereby feedback is removed from the system). However, for transactivators that are cytotoxic at high doses, such as IE2, the dose-response method destroys the cell before the response can be measured (data not shown). To circumvent this cytotoxicity problem, we developed a 'closed-loop' single-cell analysis method to analyze how a circuit's output (steady-state protein levels) saturates as a function of increasing promoter activation and varying *H* values (Fig. 2.7). This method essentially measures the change in steady-state levels as a function of increasing promoter strength.

To measure *H* via this closed-loop method, flow-cytometry measurements of steady-state GFP levels were collected for a minimal negative-feedback circuit encoding the full-length MIEP driving IE2 and GFP (MIEP-IE2-IRES-GFP), and compared to a minimal non-feedback circuit encoding the full-length MIEP driving GFP (MIEP-mCherry-IRES-GFP), which acts as the non-feedback control circuit. By increasing the MIEP activity using transcriptional activators (e.g. TSA or VPA) the response of each circuit can be measured (Fig. 2.7) and these responses can then be compared to theoretically predicted responses for varying *H* levels (Fig. 2.7). As expected for the non-feedback circuit, a linear increase in activator resulted in a linear increase in GFP steady-state levels (black). However, for the MIEP-IE2-IRES-GFP negative-feedback circuit (red), the equivalent linear increase in activator input results in a significant saturation in GFP steady state. This saturation in the GFP steady-state values is consistent with the regression analysis indicating $H \approx 7$ for IE2 negative feedback. These results indicate that IE2 negative feedback acts early during CMV infection (i.e., during the first 12 hours), which has not previously been reported. Taken together, the results
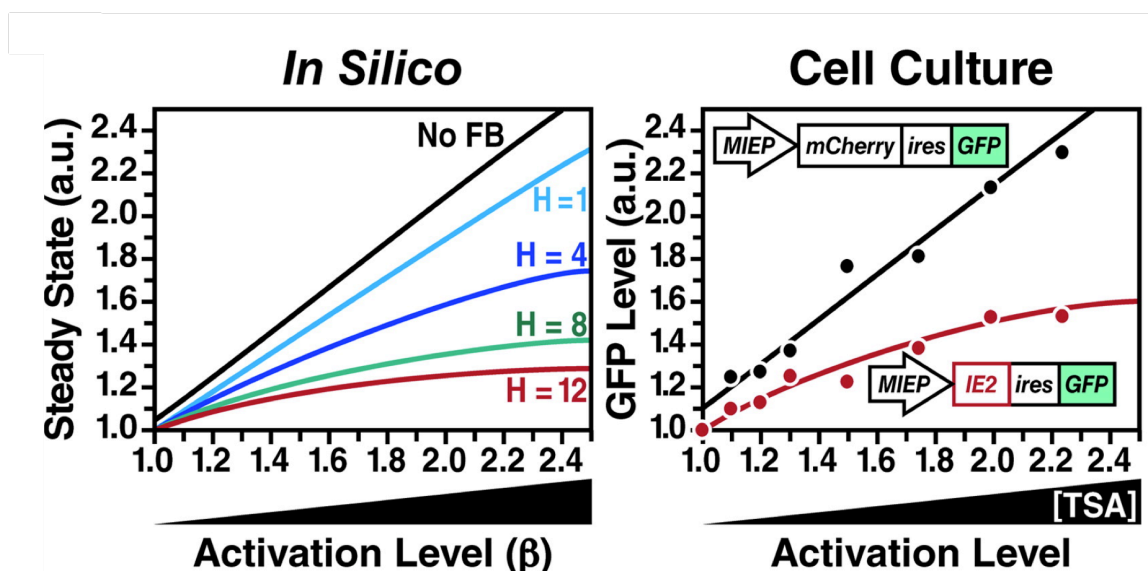
Figure 2.7: **Closed-loop dose-response analysis to measure *H* for the IE2 circuit.**
Left panel: steady-state solutions for the minimal negative-feedback ODE model (from
Figure 2.5) as a function of increasing basal promoter strength *β* for different *H* values.
Right panel: live-cell flow cytometry measurements of a non-feedback CMV MIEP-
mCherry-IRES-GFP control circuit (black) and a minimal negative-feedback CMV
MIEP-IE2-IRES-GFP circuit (red) induced to different levels of activation by TSA
treatment. CMV MIEP-mCherry-IRES-GFP shows a linear increase in final level while
CMV MIEP-IE2-IRES-GFP shows saturation in steady-state level consistent with $H \approx 7$.
(Mathematical modeling in left panel by Leor Weinberger, and I performed the dose-
response experiment.)

demonstrate that the IE2 circuit encodes a highly self-cooperative negative feedback with an H value sufficient to generate an accelerator that effectively abolishes IE2 amplification under different inputs.

Highly Self-Cooperative IE2 Feedback Results from IE2 Homo-Multimerization

We suspected that the high H value might be due to IE2 homo-multimerization, based on (i) *in vitro* biochemical studies reporting that IE2 peptide fragments can homo-multimerize when binding to DNA (Chiou et al., 1993; Waheed et al., 1998), and (ii) well-characterized mechanisms in other negative-regulation circuits encoding $H > 1$ (Chen et al., 1994; Hooshangi et al., 2005). To assay for IE2 homo-multimerization in real time during CMV infection, we utilized polarization anisotropy Förster Resonance Energy Transfer (FRET) imaging, which can differentiate between monomers and higher-order homo-multimers (Gautier et al., 2001). During the first 16 hours of infection, IE2-YFP exhibits a strong homo-FRET anisotropy (r) signal corresponding to high-order IE2 homo-multimerization (Fig. 2.8).

We next used an established theoretical model (Runnels and Scarlata, 1995) to estimate the number of individual IE2 monomers that might be interacting within an IE2 homo-multimer to generate the measured polarization anisotropy signal. While the model cannot precisely calculate the number of monomers making up the homo-multimer—since the distance between individual IE2 monomers is not known—a lower limit on the number of IE2 monomers within the homo-multimer can be estimated with confidence, under the most conservative assumption that the distance between each IE2-YFP monomer is the diameter of the YFP molecule (24 Å). Under this maximally
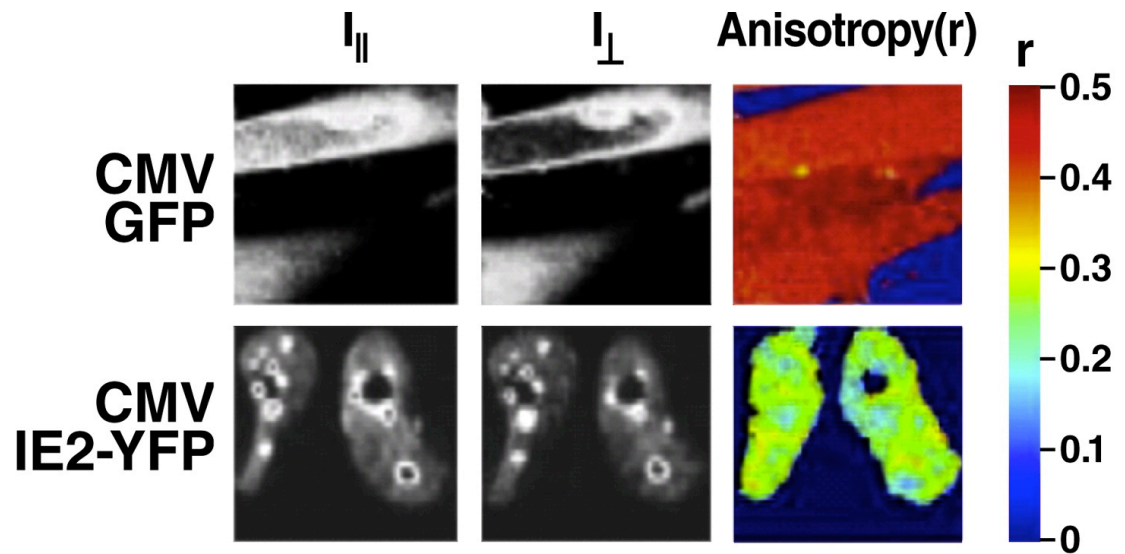
Figure 2.8: **Direct measurement of IE2 homo-multimerization by two-photon steady-state homo-FRET in live cells during CMV infection.** CMV IE2-YFP infected cells were imaged to determine fluorescence polarization anisotropy (*r*) at 15 hours post-infection and compared to cells infected with a control CMV GFP virus. An $r \approx 0.5$ represents no FRET exchange and is the two-photon theoretical maximum anisotropy for a GFP or YFP monomer. IE2-YFP exhibits significant homo-FRET exchange in the nucleus and especially at sub-nuclear foci, indicating the presence of a high-order IE2 homo-multimer. (Homo-FRET and figure by Leor Weinberger.)

conservative assumption, the measured anisotropy shift $(r \geq 0.5 \rightarrow r \approx 0.1)$ is consistent

with an IE2 homo-multimer composed of at least five to six IE2 monomers (Fig. 2.9).

Importantly, the IE2-YFP monomers are likely separated by > 24 Å, and the results of

Fig. 2.8 show that the measured anisotropy shift is well within the theoretical range of

IE2 forming a homo-heptamer or higher order homo-multimer at the ND10 foci.

Measurements of IE2 diffusion kinetics, from fluorescence recovery after

photobleaching (FRAP), support the assertion that IE2 aggregates at ND10 domains in

infected cells (Appendix Fig. 2.15). Despite these direct measurements of IE2 homo-

multimerization in live cells during active infection, structural studies would definitively

establish the presence of a high-order IE2 homo-multimer bound to DNA.

In summary, results from three independent measurements, namely (i) regression

fitting of a minimal ODE model to single-cell CMV IE2-YFP trajectories, (ii) the

'closed-loop' analysis of the isolated IE2 feedback circuit, and (iii) homo-FRET imaging

of IE2-YFP, all point toward the IE2 negative-feedback circuit as operating with a high

Hill coefficient ($H \approx 7$). These data argue that IE2 homo-multimerization is a core factor

in establishing the high Hill coefficient of this transcriptional negative-feedback circuit,

and that homo-multimerization underlies the circuit's ability to act as an accelerator.

A Minimal-Accelerator Circuit Provides a Fitness Advantage Outside the Infection Setting

To verify that highly self-cooperative negative feedback is sufficient to generate

an accelerator, we reconstructed a minimal IE2 feedback circuit lacking all other viral

elements and analyzed it completely outside the virus infection setting. The minimal IE2
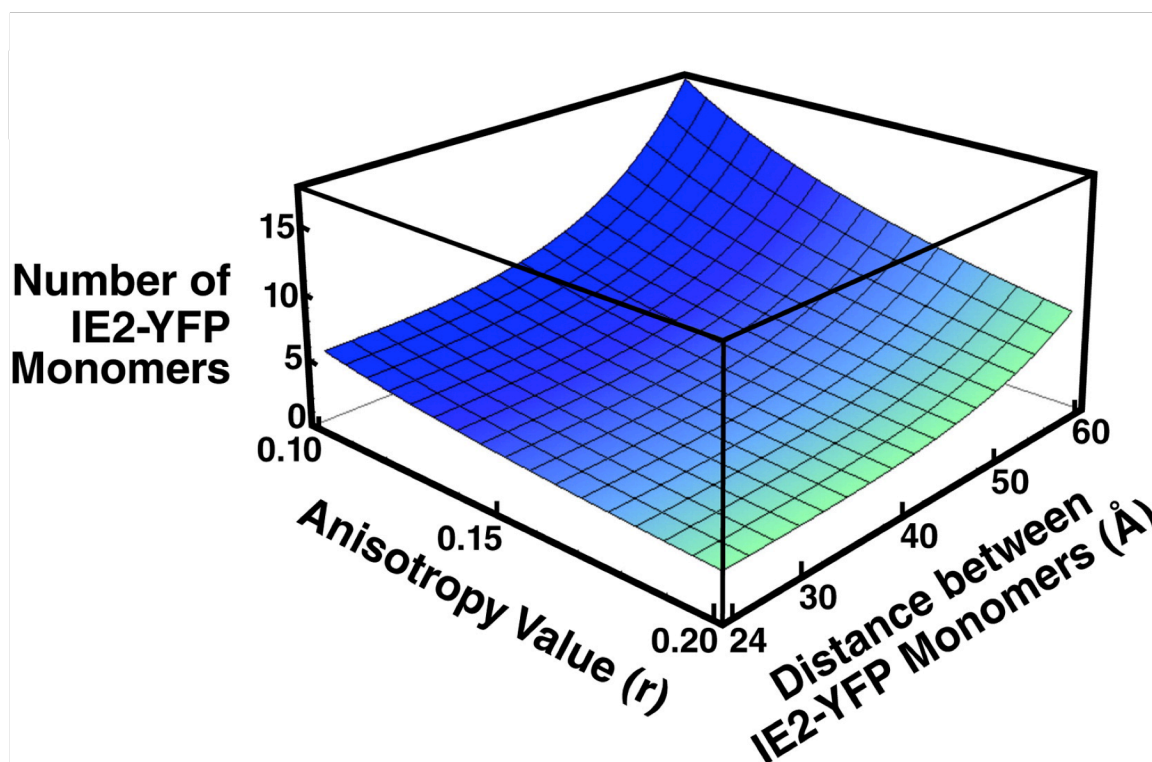
Figure 2.9: **IE2 forms a high-order homo-multimer that can account for a high *H* value**. The number of IE2 monomers present in the IE2 multimer were calculated based on measured anisotropy values. Plotted surface is the solution to the theoretical formula which accounts for the number of IE2-YFP monomers (*N*) in a complex participating in FRET exchange that could account for a given value of *r* based on the distance between each monomer (*R)*. The formula estimates a lower limit for YFP monomers in a homo-multimer that could generate a given *r*. Under the maximally-conservative assumption that all YFP monomers are as tightly packed as physically possible (*R* = 24 Å), the minimum number of IE2-YFP monomers participating in homo-FRET exchange that could generate an anisotropy value of *r* = 0.1 is approximately 6. (Analysis by Leor Weinberger.)

feedback circuit was constructed using a lentiviral vector expressing only IE2 and GFP from either the full-length wild-type MIEP or a mutant version of the MIEP where three nucleotides in the *crs* binding site are mutated to eliminate IE2 binding (Macias and Stinski, 1993) (Fig. 2.10). Both wild-type and mutant *Δcrs* lentiviral circuits were stably integrated into the cellular genome. The minimal wild-type circuit stably expresses IE2 (Appendix Fig. 2.16), and two-color imaging confirms that the MIEP exhibits comparable kinetics both within the context of the virus and stably integrated in host-genome DNA (Appendix Fig. 2.17). As predicted from the model, the minimal mutant circuit exhibits substantially increased mean GFP fluorescence intensity (Fig. 2.10, Appendix Fig. 2.18). The minimal mutant circuit fails to generate acceleration, instead acting as an amplifier (Fig. 2.11), while the wild-type feedback circuit generates acceleration (Appendix Fig. 2.19), even in the absence of all other viral elements. Cells carrying the wild-type accelerator circuit also exhibit a profound viability advantage over cells carrying mutant amplifier circuit (Fig. 2.12). Dramatically, cell populations carrying the minimal wild-type accelerator circuit maintain IE2 and GFP expression while cell populations carrying the minimal mutant circuit exhibit a rapid loss of IE2 and GFP expression that increases over time (Fig. 2.13, Appendix Fig. 2.20). Genomic PCR (Fig. 2.14) confirms that loss of IE2 and GFP expression is due to a loss of cells carrying the stably integrated mutant circuit, not from silencing of the integrated MIEP. These data argue that cells carrying the mutant circuit express higher IE2 levels and undergo increased cell death, leading to these cells being outcompeted from the population. Thus, a minimal IE2 accelerator circuit provides cells with a dramatic fitness advantage over a comparable IE2 amplifier circuit, even in the absence of all other viral factors.
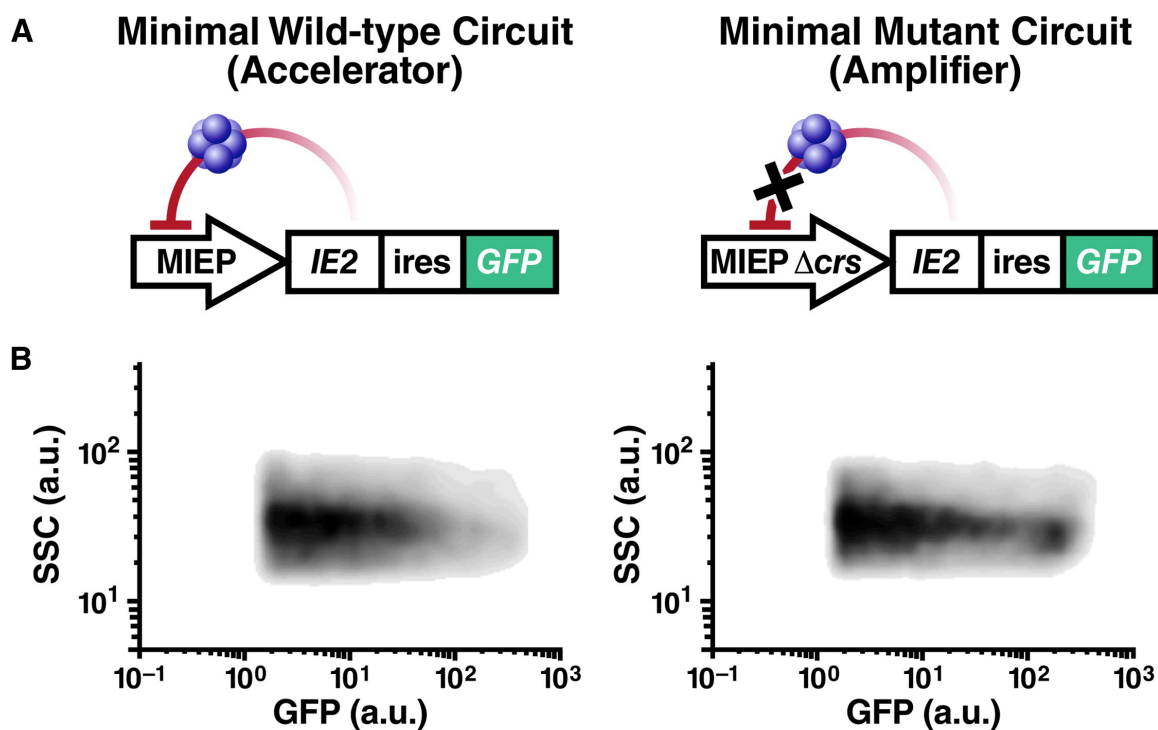
Figure 2.10: **Construction of a CMV MIE minimal wild-type accelerator circuit and a CMV MIE minimal mutant amplifier circuit.** **A,** Schematics of the minimal wild-type accelerator circuit MIEP-IE2-IRES-GFP (left) and minimal mutant amplifier circuit MIEP*Δcrs*-IE2-IRES-GFP (right). Both circuits are lentiviral vectors and encode an IRES element between IE2 and GFP. **B,** Flow cytometry density plot of cells stably expressing the wild-type accelerator (left) or the mutant amplifier (right) circuit that exhibits ~8-fold higher mean GFP.
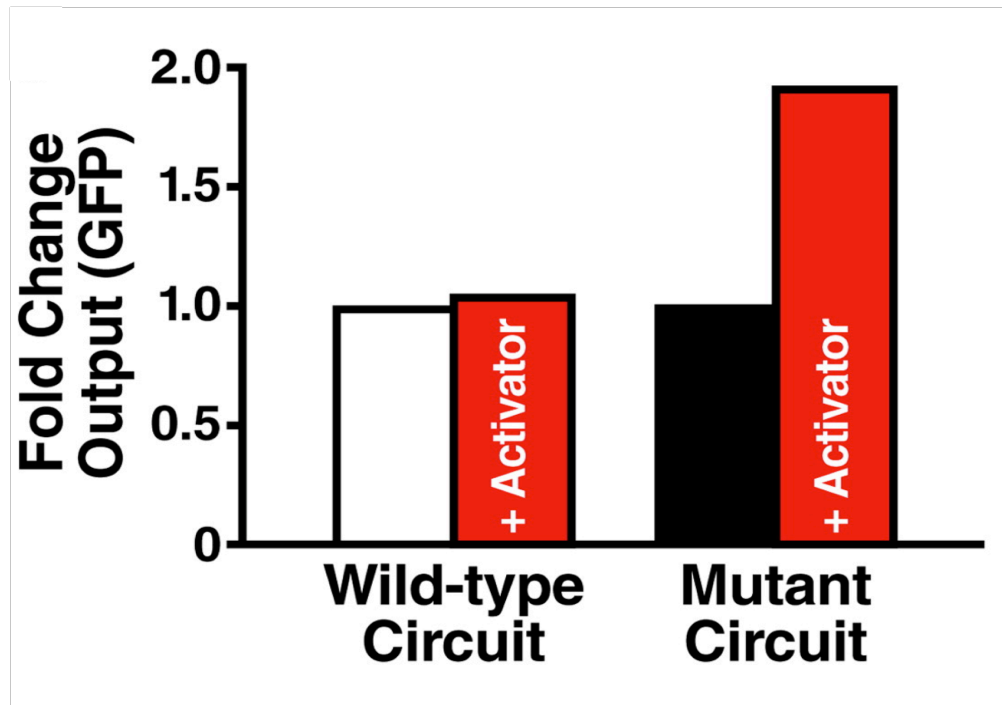
Figure 2.11: Fold increase in GFP for the wild-type accelerator and mutant amplifier circuits in the presence of a transcriptional activator. GFP expression was measured by flow cytometry for the wild-type acclerator and the mutant amplifier circuit in the absence (white, black) or presence (red) of TSA. The change in GFP for each circuit was normalized against each circuit's GFP expression in the absence of TSA.
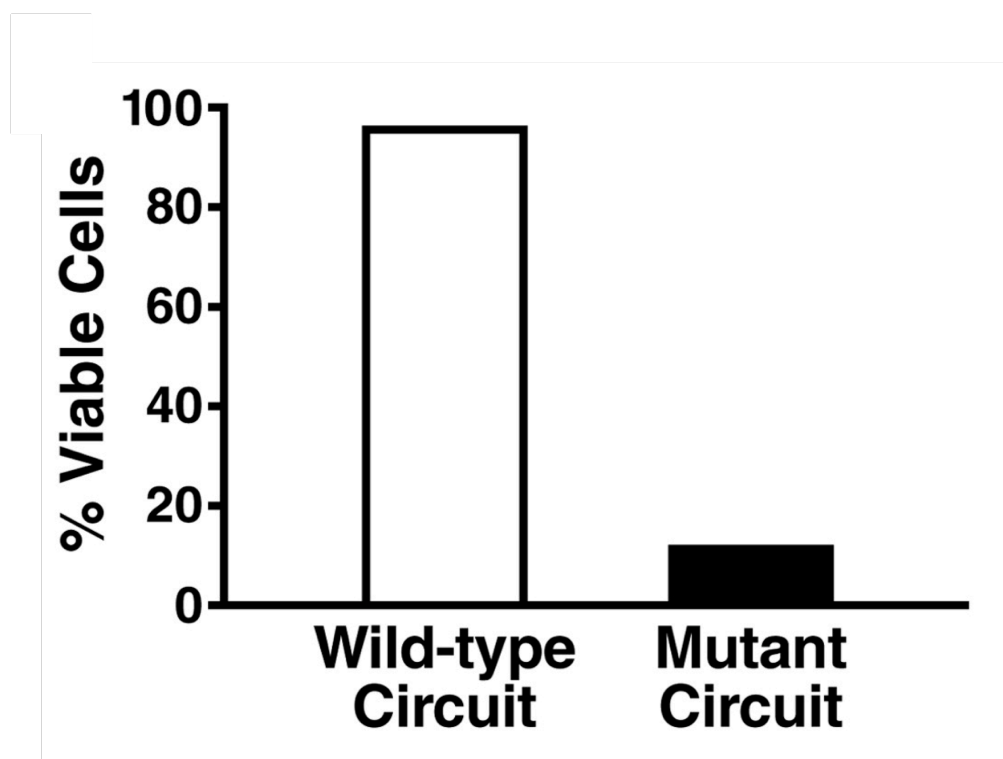
Figure 2.12: Percentage of live cells after 14 days of TSA treatment. TSA treatment has little effect on viability of cells expressing the wild-type accelerator circuit (white) but leads to significantly decreased viability in cells expressing the mutant amplifier cells (black). Percentage of live cells was measured by flow cytometry live/dead gating.
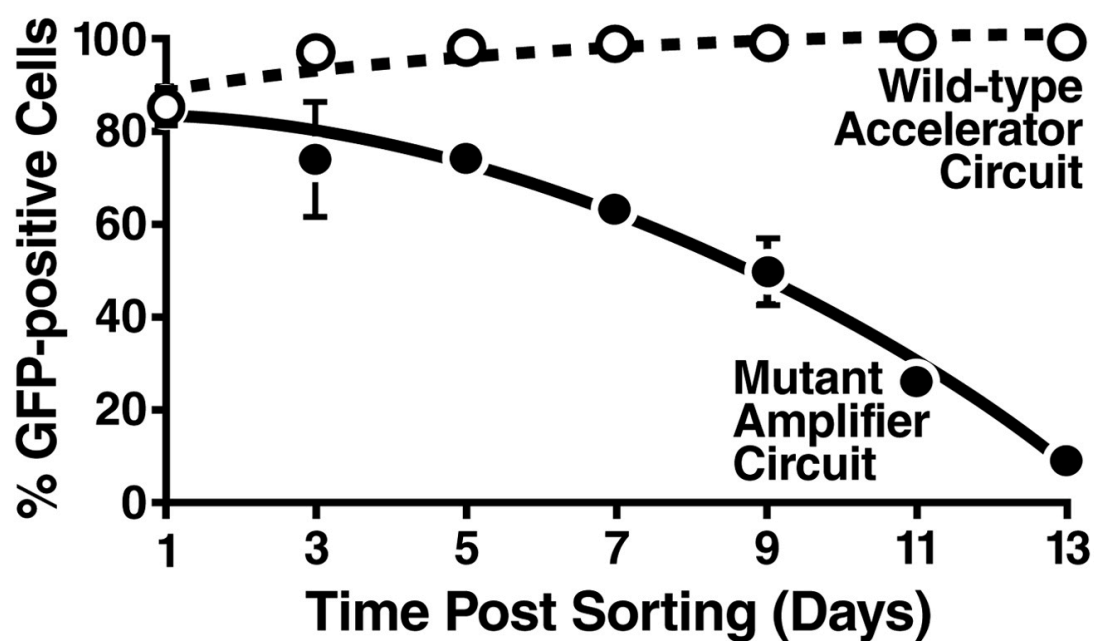
Figure 2.13: Flow cytometry time-course of the % of GFP expressing cells for the accelerator and amplifier circuits. GFP expression is lost from the cells transduced with the mutant amplifier circuit (black) but is maintained in cells transduced with wild-type accelerator circuit (white). Averages of 3 replicates are shown in bold with ± one standard deviation.

Figure 2.14: PCR amplification of the MIEP locus reveals loss of MIEP locus in cells transduced with the mutant amplifier circuit. PCR amplification of the MIEP locus from cellular genomic DNA of cells transduced with either wild-type accelerator circuit or mutant amplifier circuit on day 14 (lanes 1-2); plasmid DNA of wild-type accelerator or mutant amplifier lentiviral vector (lanes 3-4, positive PCR controls); and naïve non-transduced cells, negative control (lane 5) was performed. At day 14, the mutant amplifier circuit has been lost from the genomic DNA of the transduced population but the wild-type accelerator circuit remains present in the genomic DNA of the transduced population.

DISCUSSION

The unique architecture of IE2 negative feedback and the circuit's ability to act as an accelerator lies in the high Hill coefficient, $H \approx 7$, which to our knowledge is the highest value yet recorded for a transcriptional auto-regulatory circuit. While a number of mechanisms can generate high H values, including multiple binding sites for an auto-regulatory protein on the target DNA (Ozbudak et al., 2004) or sequential covalent modifications of an auto-regulator (Deshaies and Ferrell, 2001), in the case of IE2 the H value can be explained by formation of a homo-multimer, consisting of six to eight IE2 protein monomers that form at or around the 12 bp *crs* DNA–binding site for IE2. The formation of such a large homo-multimer leads to the question of how a 12 bp sequence of DNA (just over 40 Å in length) might have the steric space requirements to support binding of this homo-multimer complex, which is likely over half a MegaDalton with a diameter >120 Å, approximately three times as large as the DNA binding site itself. Notably, the eukaryotic transcription factor Sp1 is known to bind a 10 bp DNA sequence as a homo-tetramer (Haase, 2010) and many viral proteins cooperatively homo-multimerize to bind short palindromic DNA sequences, including the Rep 78/68 protein in adeno-associated virus, the SV40 large T antigen, and bovine papillomavirus type 1 E1 protein—all of which form homo-hexamers on short palindromic DNA sequences (Flint and American Society for Microbiology., 2009). Thus, homo-multimer formation appears to be a property shared among diverse proteins involved in viral replication as a way to bind short, palindromic DNA sequences. The high cooperativity of IE2 regulation may also be influenced by 'conditional cooperativity' (Garcia-Pino et al., 2010), since other host and viral factors, such as viral UL84, are known to functionally interact with

IE2 during the viral lifecycle (Gebert et al., 1997) and numerous covalent modifications of IE2 are reported to influence functionality (Barrasa et al., 2005; Hofmann et al., 2000). In general, highly self-cooperative negative feedback may provide a generic mechanism to optimize the rate-versus-level tradeoff.

The mechanics of the accelerator circuit in relation to other negative auto-regulatory circuits

Negative feedback has long been known to speed a circuit's response time (Black, 1999; Rosenfeld et al., 2002; Savageau, 1976), which is the time required for a circuit to reach its steady-state level or some fixed percentage of its steady-state level (e.g. 50%). Compared to non-feedback circuits, circuits encoding negative feedback (i.e. auto-regulation) approach a lower steady-state level but attain this relative steady-state level faster. However, a long-running biological counter-argument has been that transcriptional circuits must cross an absolute threshold (e.g. 10 molecules) and negative feedback necessarily slows (not speeds) this crossing. This incongruity, in which negative feedback speeds response time but slows threshold crossing, has led to a controversy regarding the kinetic role of negative feedback.

It has been argued that response time (i.e., 50% of some relative steady-state level) is a misleading measure and that negative feedback has no functional role in accelerating responses. The accelerator circuitry characterized here addresses this controversy because it acts as a hybrid between non-feedback and feedback circuits. Rate-balance analysis (Fig. 2.5) shows that as the self-cooperativity is increased, the accelerator circuit behaves more and more like a non-feedback circuit at low IE2

concentrations, allowing for faster crossing of an absolute molecular threshold. As IE2 levels approach the concentration threshold where self-cooperative negative feedback becomes active, feedback turns on very quickly (and at almost maximum strength) and sharply auto-represses the MIEP to keep the steady-state level from changing under different inputs. In the framework of electrical-circuit theory, the accelerator inverts the typical input/output transfer function and dynamically redistributes the 'gain-bandwidth' relationship (see Appendix). It is possible that diverse signaling pathways that employ negative feedback utilize this inversion of input/output as a means of signal discrimination or as a mechanism to approximate 'perfect adaptation' (Ma et al., 2009; Muzzey et al., 2009) in steady-state levels. The high cooperativity in negative feedback may also function to suppress stochastic fluctuations (i.e. noise) that influence the behavior of decision-making circuits (Cagatay et al., 2009).

ACKNOWLEDGEMENTS

the single-cell microscopy experiments. Andrew Womack and Thomas Shenk provided

reagents. Leor Weinberger directed all research.

APPENDIX

Theory

<u>Derivation of a Model for Rate Acceleration: Approach I (Graphical phase-plane argument)</u>

We consider one-dimensional ordinary differential equations of the general form:

$\dot{x}(t) = f(\beta, x) - \delta x(t)$ where f is an arbitrary function for "synthesis" which includes a basal "input" β that can be varied, δ is a fixed "decay" parameter, and t is time. To generate acceleration without amplification (i.e. rate acceleration) the function f must satisfy two criteria. First, the steady state of x must not vary significantly as β is increased—to limit any amplification—and second the rate of change of x (i.e. the right-hand side of the equation which is the difference between $f(\beta,x)$ and $\delta x(t)$) should be maximal for as long as possible—to generate the acceleration. A convenient way to examine these two criteria is to plot the synthesis function $f(\beta,x)$ and the decay function $\delta x(t)$ versus the value of x. The intersection of $f(\beta,x)$ and $\delta x(t)$ is the steady-state value—which we do not want to change significantly as β is increased—and the difference between $f(\beta,x)$ and $\delta x(t)$ is the rate—which we want to remain maximal for as long as possible.

There are two familiar classes of functions that have the potential to satisfy the criteria for rate acceleration: decaying exponentials and Hill functions:

$f(\beta,x) = \beta e^{-x(t)}$ or

where H and k are fixed parameters and β is the basal synthesis rate. Importantly, the exponential and Hill functions are not the only functions with the potential to satisfy the two criteria for acceleration, but it is helpful to consider these two familiar functions since they are illustrative of the points that must be considered.

For the Hill function, we plot the synthesis function $f(\beta,x)$ and the decay function δx versus the value of x for varying values of H (Appendix Fig. 2.11). At low values of H (i.e. $H = 0$ or 1) the steady state of x (the intersection of each curve with the diagonal) ends up shifting to a significantly higher x value as β is increased. However, for higher values of H ($H > 6$) the steady state of x (intersection of each curve with the diagonal) remains almost unchanged as β is increased, and the rate (the difference between the curves and the diagonal) remains large across a broad range of x values.

We construct similar plots the exponential function $f(\beta,x)=\beta\, e^{-k-x(t)}$ for varying values of k (Appendix Fig. 2.12). At higher values of k (i.e. $k = 2$) the change in the steady state of x appears to compress as β is increased (and below we explore this change in a more quantitative manner). However, the rate (the difference between the curves and the diagonal) does not appear to satisfy criterion 2 for acceleration since the difference between the synthesis and decay functions drops rather quickly for all values of k.

In summary, this graphical approach argues that a synthesis term that corresponds to the Hill functional form is able to satisfy both requirements for acceleration while a synthesis functional form that employs exponentially decaying synthesis does not appear to satisfy the conditions for acceleration. In the next section we present a slightly more mathematical and quantitative approach to exploring which functional forms can satisfy acceleration.

Derivation of a Model for Rate Acceleration: Approach II (Graphical-analytic argument)

An alternate approach is to consider that acceleration requires the function f to satisfy the following two criteria:

Criterion 1 (no amplification):

$$\frac{\partial}{\partial \beta} \bar{x} \rightarrow 0$$

where $\bar{x}$ is the steady-state solution (i.e. satisfies $\dot{x}(t) = 0$). Criterion 1 states that the steady state value changes very little as "input" β is changed.

Criterion 2 (acceleration):

To achieve acceleration the slope of $x(t)$ must be maximum at early times and must go to zero as the system approaches steady–state. So,

$$\frac{\partial}{\partial x} \dot{x}(t) \text{ must be maximum at } t{=}0 \text{ (arbitrarily defined)}$$

$$\Rightarrow \frac{\partial}{\partial x} f(\beta, x) \text{ must be maximum at } t{=}0 \text{ (arbitrarily defined)}.$$

There are two familiar classes of functions with the potential to satisfy criteria 1, decaying exponentials and Hill functions: $f(\beta, x) = \beta e^{-x(t)}$ or $f(\beta, x) = \dfrac{\beta}{k + x(t)^H}$ where H and k are fixed parameters and β is the basal synthesis rate.

Both the decaying exponential and the Hill function satisfy criterion 1. The

decaying exponential function $f(x(t)) = \beta e^{-x(t)}$ gives a steady-state $\delta\bar{x} = \beta e^{-\bar{x}}$ solution of

which is the Ω function (a.k.a. Product-Log function): $\bar{x} = \dfrac{ProductLog(\frac{\beta}{\delta})}{\beta}$ the slope of

which (with respect to β) does indeed get exceedingly small (Fig. S2). Similarly, the Hill

function $f(\beta,x) = \dfrac{\beta}{k + x(t)^H}$ gives a steady state (for $k=0$) of $\bar{x} = H-1\sqrt{\dfrac{\beta}{\delta}}$ the slope of

which (with respect to β) also becomes exceedingly small.

However, the decaying exponential $f\big(x(t)\big) = \beta e^{-x(t)}$ cannot satisfy criterion 2.

Since $\dfrac{\partial}{\partial x} f(\beta,x) = \dfrac{\partial}{\partial x}\beta e^{-x} = -\beta e^{-x}$ which has a *minimum* at $t=0$ (i.e. x = 0 since x[0] = 0)

and actually has its maximum at $t=\infty$ (Fig. S2). Importantly, the Hill function,

$f(\beta,x) = \dfrac{\beta}{k + x(t)^H}$ does satisfy criterion 2: $\dfrac{\partial}{\partial x} f(\beta,x) = \dfrac{\partial}{\partial x}\big(\dfrac{\beta}{k + x^H}\big) = -\dfrac{\beta H x^{H-1}}{(k + x^H)^2}$ which

does have its maximum at $t = 0$ (i.e. x = 0 since x[0] = 0).

While there are other potential functional forms that might satisfy criteria 1 & 2,

the Hill function is familiar and provides well-known physical intuition pointing towards

multimerization and self-cooperativity. For this reason, we focus on the models

employing the Hill function.

Derivation of a Model for Rate Acceleration: Approach III (Gain-bandwidth argument)

In electrical circuit theory, 'loop-transmission' analysis is used extensively to

determine stability, closed-loop response, transient response, and noise behavior of linear

feedback systems and has been successfully applied to the analysis of genetic circuits

(Austin et al., 2006; Cox et al., 2006; Simpson et al., 2003). The effect of negative

feedback is to couple two system parameters – gain and bandwidth (response time in the

time domain)—and thereby allow one to be traded for the other. To demonstrate, we

consider the step response ($u(t)$ is the unit step function) of an amplifier circuit. The

output, $O(t)$, is $O(t) = I\dfrac{A}{1-T}(1 - e^{\frac{-(1-T)t}{\tau}})$ where A is the open loop gain of the circuit;

I is the induction level; and we have assumed a single time constant (τ). In most genetic

circuits, τ would be determined by the protein half life and dilution rate (Austin et al.,

2006; Simpson et al., 2003). The loop transmission, T, is the transfer function around the

loop and may be thought of as a measure of the resistance of the feedback loop to

variation (Simpson et al., 2003). For the circuit considered here $T = -A\beta$.

If T is a constant, the steady-state value and the rate of increase in the output are

$O(t \rightarrow \infty) = I\dfrac{A}{1-T}$ and $\dfrac{dO(t)}{dt} = \dfrac{IA}{\tau}e^{\frac{-(1-T)t}{\tau}}$. Some authors have reported that negative

feedback speeds a circuit's response time, while others have reported the contrary result

that negative feedback slows response. In fact, both views are correct. One may say that

negative feedback speeds the response of the gene circuit because the circuit approaches

steady state (i.e. $\dfrac{dO(t)}{dt} \rightarrow 0$) at a rate of 1-T faster than the non-feedback circuit.

Alternatively, one may say that negative feedback slows response as it decreases the

absolute rate of increase ($\dfrac{dO_T = O(t > 0)}{dt} > \dfrac{dO_T < O(t > 0)}{dt}$). This dichotomy arises

because the decreased time to reach steady state is accompanied by a factor of 1-T

reduction in the steady-state level (i.e. product of the gain and bandwidth (GBW product)

of the circuit remains constant and the strength of the negative feedback controls the trade

of one for the other).

Is it possible to achieve the speedier arrival at steady state without sacrificing the

absolute rate of increase? The GBW product rule is in effect when T has a constant value

over all time. However, an examination of the equation above shows that the GBW

product relationship is established by repression that happens at two separate times: (1)

repression of the rate of increase that occurs during the transient; and (2) repression of the

steady-state level, which occurs at the end of the transient. A T that is variable such that

it is small during the first of these periods and becomes larger during the second period

provides both a speedier arrival to steady state and a fast rate of absolute increase during

the transient. This variable T is accomplished in the CMV circuit with a high hill

coefficient of the IE2 repression of the promoter, producing a T that increases

significantly as IE2 population grows. That is, for the Hill expression:

$$\frac{dIE2}{dt} = \frac{I}{1+(IE2/k_{IE2})^H} - \gamma IE2,$$ where γ represents the *IE2* decay/dilution rate and k_{IE2}

represents the IE2 population for 50% repression, there is almost no repression

(feedback) until $IE2 \rightarrow k_{IE2}$ for high values of n. Furthermore, regardless of the induction

level $IE2_{ss} \rightarrow k_{IE2}$, since repression increases sharply for $IE2 > k_{IE2}$. Until the circuit

approaches steady state, negative feedback is essentially disabled and the output grows at

nearly the maximum rate. Near the steady-state level T abruptly increases, the rate of IE2

increase is quickly extinguished, and the steady-state level is quickly established.

This negative-feedback circuit motif has several distinguishing characteristics that

may have biological significance. Foremost is that it produces an accelerator – larger

induction levels speed the rise to the steady-state, but only weakly influence steady-state level. Additionally, this circuit topology has interesting noise behavior. Due to weak feedback strength, this circuit would be sensitive to noise during its transient rise to steady-state. Conversely, the strong feedback strength at the approach to and during maintenance of steady state would both reduce noise magnitude and shift the remaining noise to higher frequencies where it may have little biological effect (Austin et al., 2006; Simpson et al., 2003).

Minimal Circuit Models & Closed-loop Analysis of Hill Coefficients

We used the analysis above to generate a standard two-dimensional model of gene expression (Alon, 2007b; Kaern et al., 2005) and we arrive at the following model:

$$\frac{d}{dt}mRNA(t) = \frac{\beta}{k^H + protein(t)^H} - \varepsilon \cdot mRNA(t)$$

$$\frac{d}{dt} = protein(t) = (1 - f)\varepsilon \cdot mRNA(t) - \delta \cdot protein(t)$$

Eqs. [1]

This two-dimensional model describes the time evolution of *mRNA* levels and *protein* levels in the cell, and *β* represents the basal rate of promoter activity, *k* is a Michaelis-Menten type constant describing the threshold level below which auto-repression does not act, *H* is the Hill coefficient describing the self-cooperativity in protein auto-repression of the basal promoter activity, *ε* is a lumped rate constant describing the per-capita rate of *mRNA* export from the nucleus and translation into protein, *f* is the fraction of *mRNA* that is lost to *mRNA* decay prior to being translated into

protein, and δ is the per-capita rate of protein decay (i.e. turnover). Since the *mRNA*

species acts an exponential delay term (Alon, 2007b; Murray, 2002; Savageau, 1976;

Weinberger and Shenk, 2007), such systems of ordinary differential equations (ODEs)

are commonly reduced and approximated by one-dimensional delay differential equations

such as:

$$\frac{d}{dt} protein(t) = \frac{\beta}{k^H + protein(t-\tau)^H} - \delta \cdot protein(t)$$

Eq. [2]

where τ acts as a fixed delay term. This simplified one-dimensional version of the model

was used for the rate-balance analysis in Fig. 2.5 and in the above sections (with $\tau = 0$

and $k=1$). For simulations lacking feedback, H was set equal to zero. δ, the per-capita

rate of protein decay (i.e. turnover), was set to 0.23 hour^{-1} the measured single-cell half-

life of IE2 (see Chapter 3, Appendix Fig. 3.6), which is in agreement with biochemical

data (Dwarakanath et al., 2001).

For closed-loop Hill coefficient analysis, (Fig. 2C) the steady-state for Eq. [2] was

numerically solved as β and H were varied, using a decay parameter value of $\delta = 0.23$

hour^{-1} and a k value determined by fitting to the data obtained for the non-feedback

circuit MIEP-mCherry-IRES-GFP.

Construction of the CMV MIE Circuit Model

The goal of generating a mathematical model of the CMV MIE circuit was only to

fit the single-cell CMV IE2-YFP data from Fig. 2.3 and the model is not intended to

represent a comprehensive mathematical description of all known MIEP interactions or

IE2 binding partners. Instead, our goal is utilitarian: to find the simplest model sufficient to fit the data in Fig. 2.3.

First, we expanded the minimal ODE model above to include IE1 protein, IE2 protein, and the MIE precursor mRNA. At the most fundamental level, the MIE locus is composed of the MIE promoter-enhancer (MIEP) driving two major alternative-splice variants which code for the 72-kDA IE1 protein and the 86-kDa IE2 protein, respectively (Stenberg, 1996). The MIEP is a relatively strong promoter (in transient transfection assays) and many cellular and viral activators including pp71, hDaxx, and NF-κB (Stinski and Isomura, 2008) are known to stimulate the MIEP. During CMV infection, the MIEP drives expression of a large 'pre-mRNA' transcript that includes MIE exons 1-5 and is spliced into either the IE1 mRNA transcript (exons 2-4) or the IE2 transcript (exons 2, 3, and 5) (Stenberg, 1996). Once translated, the IE1 and IE2 proteins regulate other viral and cellular promoters but also auto-regulate the MIEP (Meier and Stinski, 1996). IE2 is known to down-regulate the MIEP while IE1 has a very weak positive regulatory effect on the MIEP (Fields et al., 2007), which is typically ignored.

For tractability, the quasi-steady-state assumption was applied to nuclear and cytoplasmic IE1 and IE2 mRNA levels and a model utilizing three coupled ODEs describing MIE pre-mRNA, IE1 protein, and IE2 protein was developed.

$$\frac{d}{dt}MIE_{RNA} = (\beta + \frac{\alpha \cdot IE1^{H_1}}{k_1^{H_1} + IE1^{H_1}} \cdot \frac{1}{k_2^{H_2} + (\gamma \cdot IE2)^{H_2}}) - \delta \cdot MIE_{RNA} \qquad \text{Eq. [4]}$$

basal act. IE1 activation   IE2 repression   mRNA export/decay
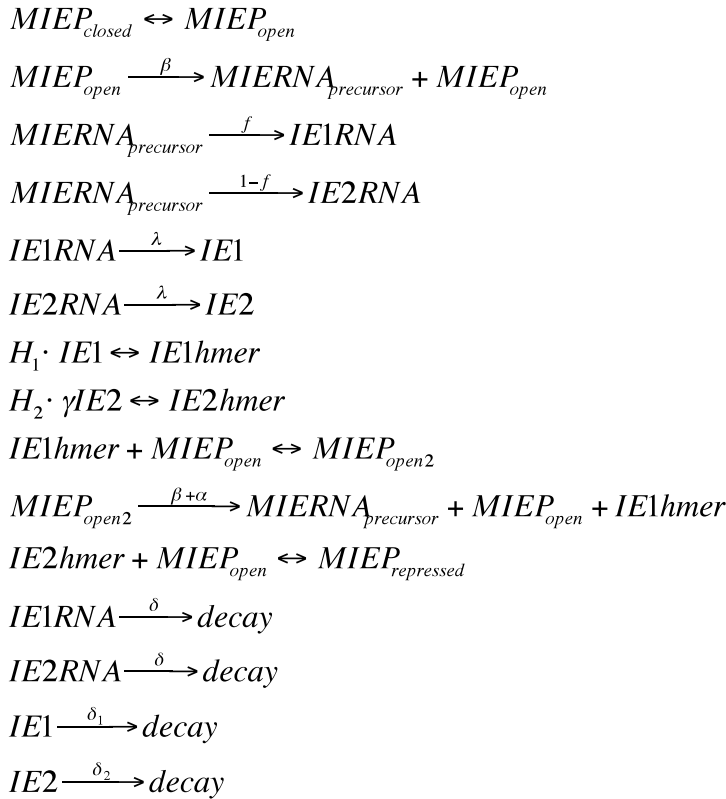
$$\frac{d}{dt}IE1 = f \cdot \lambda \cdot MIE_{RNA} - \delta_1 \cdot IE1 \qquad\qquad\qquad\qquad \text{Eq. [5]}$$

IE1 translation rate   IE1 protein decay

$$\frac{d}{dt}IE2 = (1-f) \cdot \lambda \cdot MIE_{RNA} - \delta_2 \cdot IE2 \qquad\qquad\qquad \text{Eq. [6]}$$

IE2 translation rate   IE2 protein decay

For tractability, the dimension of the left-hand side of each equation is only per hour (i.e. the state variables are dimensionless). Essentially this model considers the following biochemical 'reactions':

$$MIEP_{closed} \leftrightarrow MIEP_{open}$$

$$MIEP_{open} \xrightarrow{\beta} MIERNA_{precursor} + MIEP_{open}$$

$$MIERNA_{precursor} \xrightarrow{f} IE1RNA$$

$$MIERNA_{precursor} \xrightarrow{1-f} IE2RNA$$

$$IE1RNA \xrightarrow{\lambda} IE1$$

$$IE2RNA \xrightarrow{\lambda} IE2$$

$$H_1 \cdot IE1 \leftrightarrow IE1hmer$$

$$H_2 \cdot \gamma IE2 \leftrightarrow IE2hmer$$

$$IE1hmer + MIEP_{open} \leftrightarrow MIEP_{open2}$$

$$MIEP_{open2} \xrightarrow{\beta+\alpha} MIERNA_{precursor} + MIEP_{open} + IE1hmer$$

$$IE2hmer + MIEP_{open} \leftrightarrow MIEP_{repressed}$$

$$IE1RNA \xrightarrow{\delta} decay$$

$$IE2RNA \xrightarrow{\delta} decay$$

$$IE1 \xrightarrow{\delta_1} decay$$

$$IE2 \xrightarrow{\delta_2} decay$$

and this reaction-based model generates simulations which are qualitatively indistinguishable from the ODE model (data not shown), thus we concentrate on the ODE

model. Eqs. [4-6] describe MIE pre-processed mRNA transcripts, IE1 protein levels, and IE2 protein levels, respectively. β represents the MIEP basal promoter rate. The second term in Eq. [4] accounts for IE1 auto-activation, or positive feedback, on the MIE promoter and we assume that IE1 auto-activation on the MIE promoter saturates at some level (hence IE1 in both the numerator and the denominator to achieve an asymptotic function). Although IE1 transactivation is weak (Fields et al., 2007; Sambucetti et al., 1989), we included it in the model because we found it necessary for the model to fit the early-time concave-up curvature of the single-cell IE2-YFP trajectories during CMV IE2-YFP infection. α represents the rate of IE1 transactivation, and k_1 the Michaelis constant. Importantly, parameter-sensitivity studies (not shown) confirmed that the model is relatively insensitive to α and k_1 values and these parameter values can be varied over many orders of magnitude without altering the qualitative behavior of the system. The third term in Eq. [4] represents IE2 auto-repression on the MIEP with H being the Hill coefficient for IE2 that was varied for fitting to the data. k_2 represents the Michaelis constant but sensitivity analysis (not shown) showed that model behavior is not significantly affected by altering this value (while altering k_2 does change the absolute value of the IE2 response-time, peak height, and steady-state, the relative differences for differing β or H do not change significantly with different k_2 values, thus, the Michaelis parameters do not significantly affect the calculation of H). γ represents the strength of IE2 auto-repression. While the values are not known, it is clear that the IE2 repression rate and Michaelis constant should both be significantly smaller than those of IE1. This is because the strength of negative feedback is not strong enough to completely shut off the MIE promoter (Chiou et al., 1993; Macias and Stinski, 1993; Waheed et al., 1998)

and IE2 directly influences the MIE promoter, unlike IE1 (Sambucetti et al., 1989). δ is a lumped parameter that represents the decay of MIE pre-processed mRNA transcripts and can include splicing of the pre-processed mRNA into alternative splice variants and nuclear export. Eq. [5] and Eq. [6] are essentially 'housekeeping equations' that describe the production and turnover of IE1 and IE2, respectively. IE1 and IE2 are translated at a per capita rate λ and the fraction of MIE mRNA generating IE1 (*f)* versus IE2 (1-*f)* was calculated from published studies (Nevels et al., 2004). δ_1 represents the IE1 protein turnover rate and was calculated from previous studies (Stamminger et al., 1991) and single-cell experiments (data not shown) to be 0.032 hour^{-1} while δ_2 represents the IE2 protein turnover rate and was calculated from previous studies (Stamminger et al., 1991) and single-cell analysis to be 0.23 hour^{-1} (see Chapter 3, Appendix Fig. 3.6).

Upon increase of the MIE basal expression rate, β, the rate of IE2 expression is markedly accelerated when λ is sufficiently small and $f > 1/2$. When $f > 2 \times (1 - f)$ or $f > 2/3$, there is a significant acceleration in the response-time of IE2. This observation agrees with experimental data in the literature that reports IE1 being twice as abundant as IE2 (Nevels et al., 2004).

All parameters except the fraction of mRNA generating IE1 vs. IE2 (*f)* and the IE1 and IE2 protein turnover rates (δ_1 and δ_2) were derived by performing nonlinear least-squares regression curve fitting with IE2-YFP single-cell trajectories for untreated cells and VPA-treated cells (Fig. 2.3). Best-fit curves were generated by varying values for model parameters, while keeping δ_1 and δ_2 fixed. β was multiplied by 2 and 3 to fit IE2-YFP single-cell data under VPA 24 hour pre-treatment and VPA 72 hour pre-

treatment, respectively, as the initial slopes of these IE2-YFP trajectories were 2 and 3-fold greater than trajectories from untreated cells.

To model the MIE circuit with the MIEP *Δcrs* promoter, the IE2 repression term in Eq. [4] was set to zero.
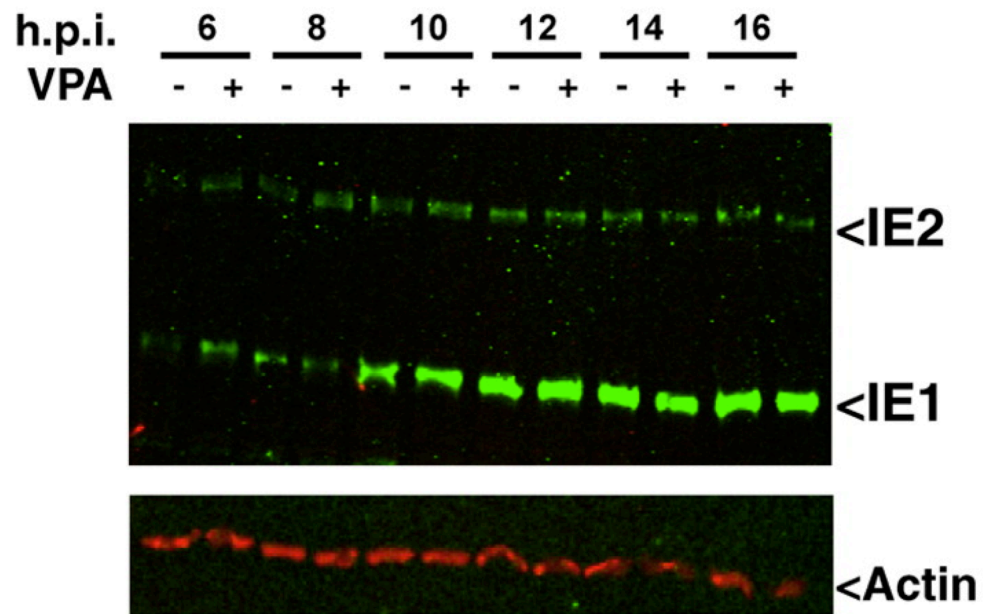
Appendix Figure 2.1: IE2-YFP protein levels, measured by Western blot in CMV IE2-YFP virus infection, accumulate at the same rate as IE2-YFP fluorescence levels, measured by single-cell microscopy. Western blot time-course of IE2-YFP and IE1 levels after infection with CMV IE2-YFP virus (strain AD169) at an MOI=1. VPA treatment accelerates both IE2 and IE1 protein expression, relative to an untreated control. Similar results were observed for TSA and TNF-α treatment (data not shown). These data further support that YFP fluorescence is a reliable reporter for IE2 protein levels. (Western blot by Cynthia-Bolovan-Fritts.)
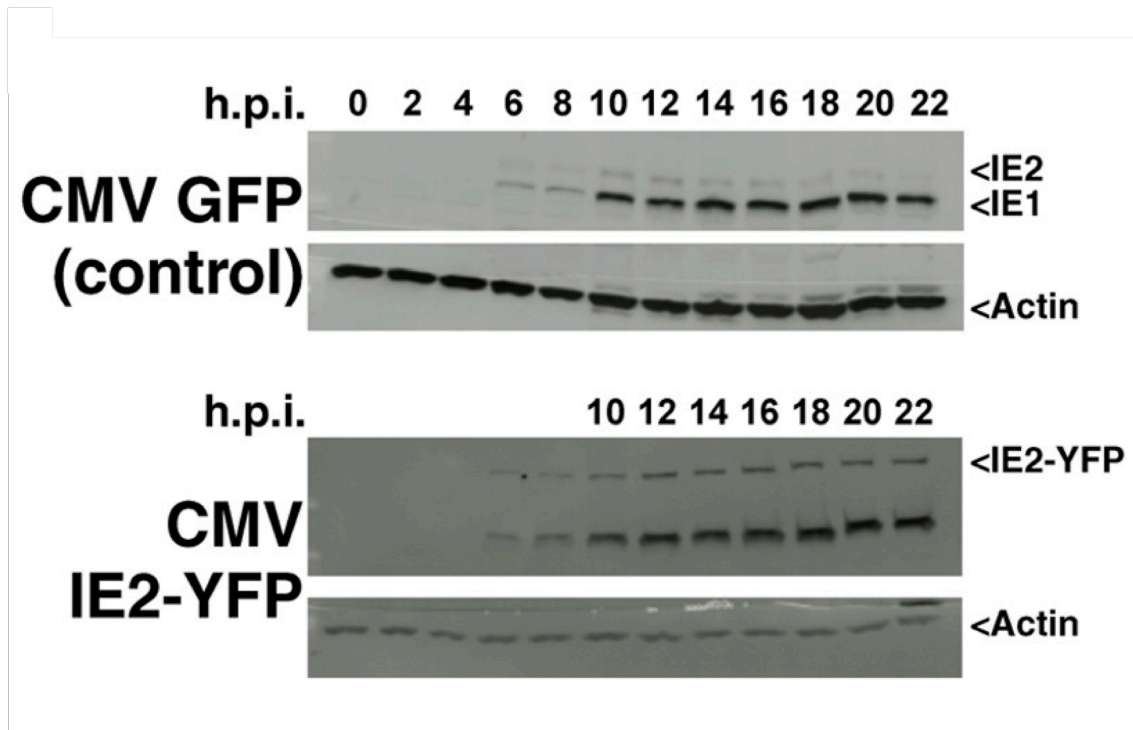
Appendix Figure 2.2: IE2 kinetics in CMV IE2-YFP virus are indistinguishable from IE2 kinetics in CMV GFP virus. Western blot time-course of IE2 levels after infection of cells with CMV IE2-YFP and CMV GFP viruses at MOI=1. (Western blot by Cynthia Bolovan-Fritts.)
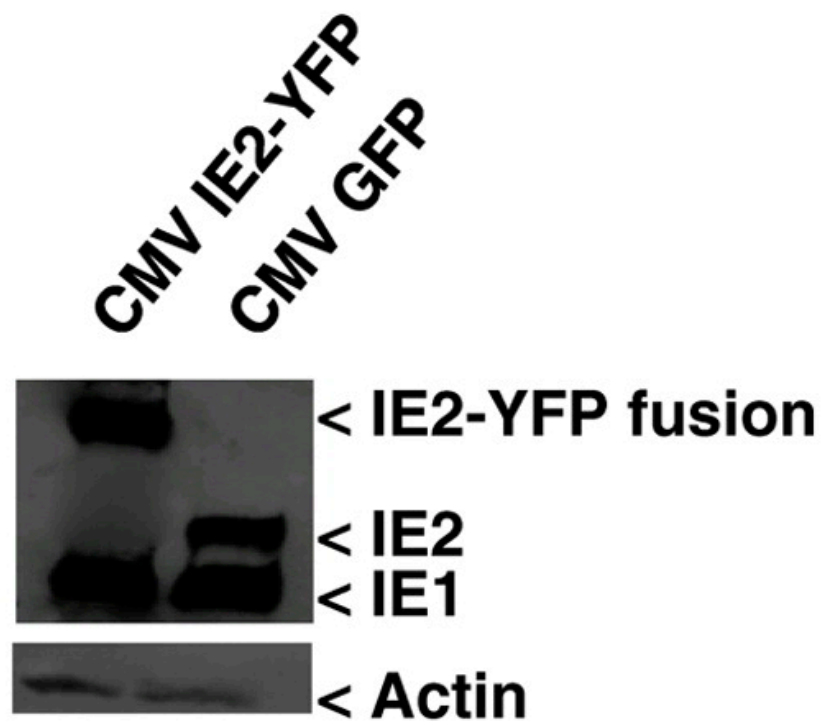
Appendix Figure 2.3: **CMV IE2-YFP and CMV GFP viruses generate roughly equivalent levels of IE1 and IE2, respectively, upon infection.** (Western blot by Cynthia Bolovan-Fritts.)
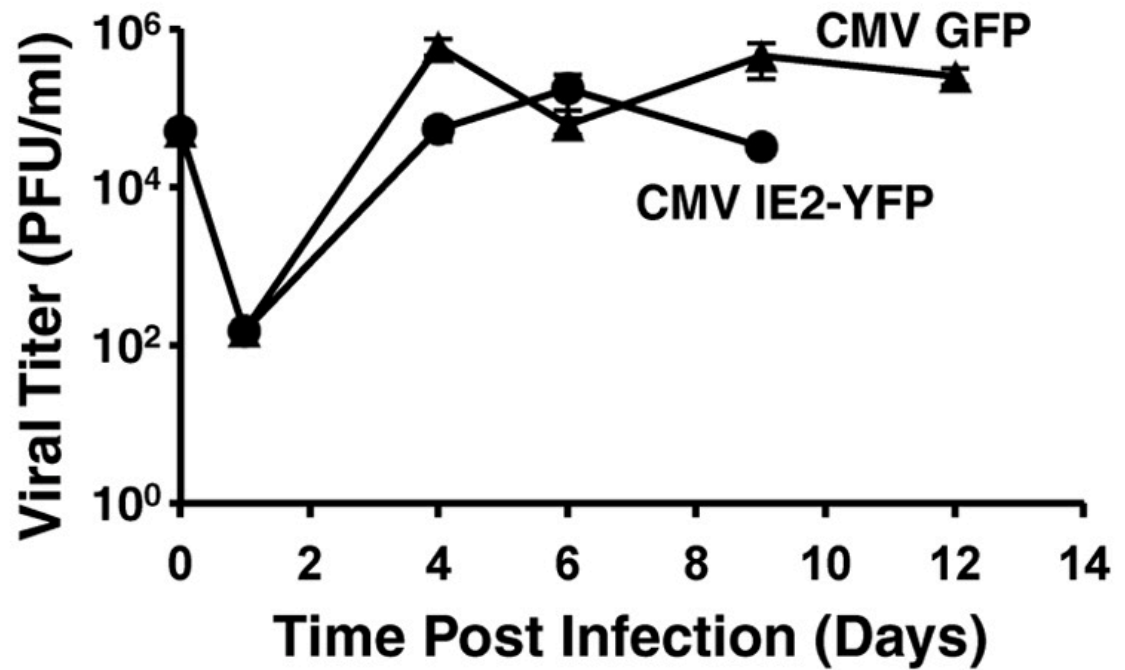
Appendix Figure 2.4: Fusion of YFP to IE2 does not significantly alter viral replication kinetics. Replication kinetics of CMV GFP virus (black triangles) and CMV IE2-YFP virus (black circles) at MOI=1. Error bars (gray) represent ±1 standard deviation. (Replication kinetics by Cynthia Bolovan-Fritts.)
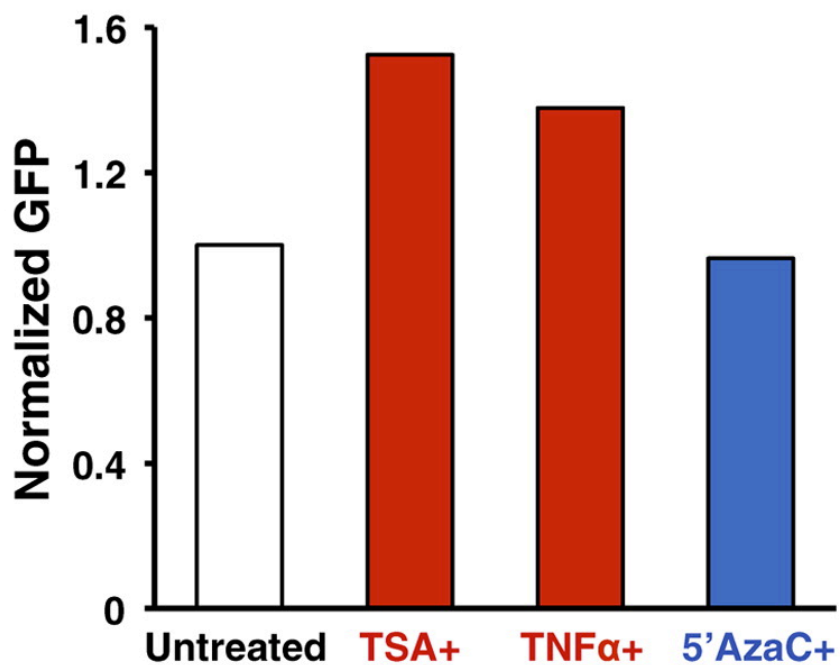
Appendix Figure 2.5: Specific activation of MIE promoter activity by TSA and TNF-α. Live-cell flow cytometry GFP measurements of MIEP-GFP transduced cells demonstrating activation of the MIEP in presence of TSA (red), TNF-α (red), 5'azacytidine (blue), compared to no drug (white).
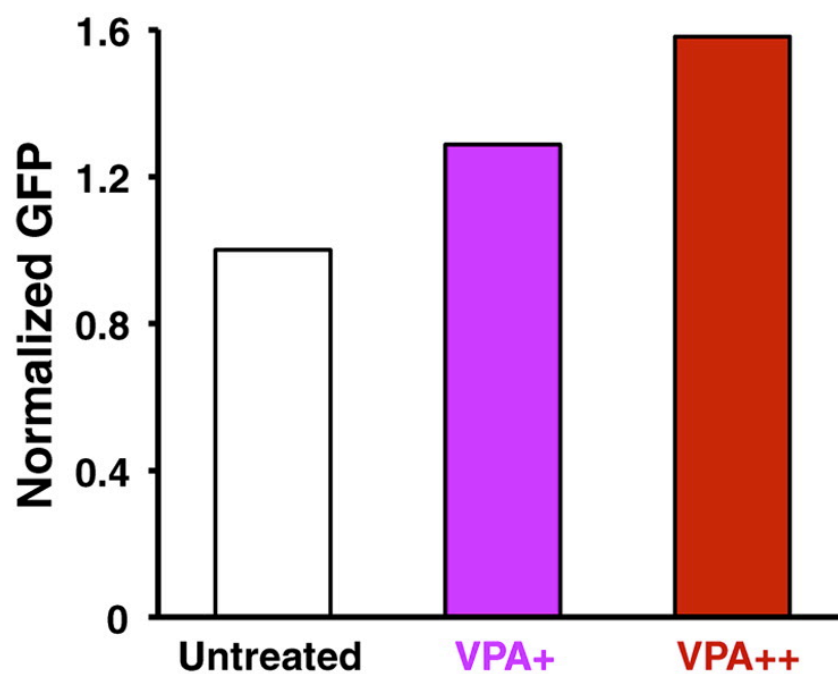
Appendix Figure 2.6: Activation of the MIEP with increasing VPA incubation times.
Live-cell flow cytometry GFP measurements of MIEP-GFP transduced cells in presence
of VPA at increasing incubation times (24 hours, pink; 72 hours, red) or absence of drug
(white), demonstrating increasing activation of the MIEP.
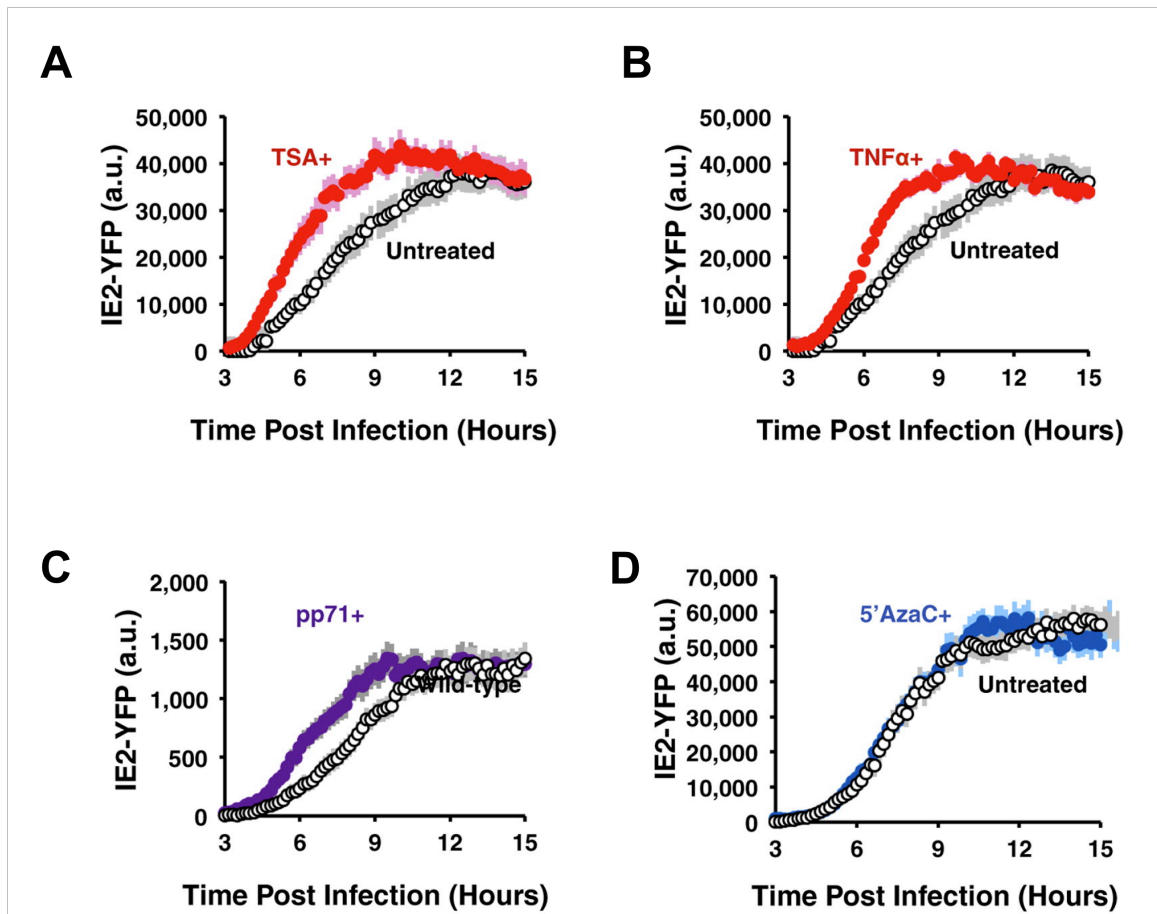
**Appendix Figure 2.7: Specific activation of MIE promoter activity is required for IE2 acceleration.** **A,** TSA activates the MIE promoter and accelerates IE2. Cells were infected in presence of TSA (red) or absence of drug (white). Error bars represent ± one standard error. **B,** TNF-α activates the MIE promoter and accelerates IE2. Cells were infected in presence of TNF-α (red) or absence of drug (white). Error bars represent ± one standard error. **C,** Viral pp71 activates the MIE promoter and accelerates IE2. An IE2-YFP virus carrying increased levels of the viral transactivator pp71 (purple), was generated and used to infect cells in parallel with IE2-YFP virus lacking extra pp71 (white). Error bars represent ±1 standard error. **D,** 5'Azacytidine (a generalized DNA methylation inhibitor) treatment does not activate the MIE promoter and does not generate IE2 rate acceleration. Despite 5'azaC's ability to act as a generalized transcriptional activator, it clearly does not enhance transcriptional activity from the CMV MIEP in contrast to TSA and TNF-α. Cells infected in presence of 5'azaC (blue) show no acceleration in IE2 expression as compared to infection in absence of 5'azaC (white). Error bars represent ± one standard error.
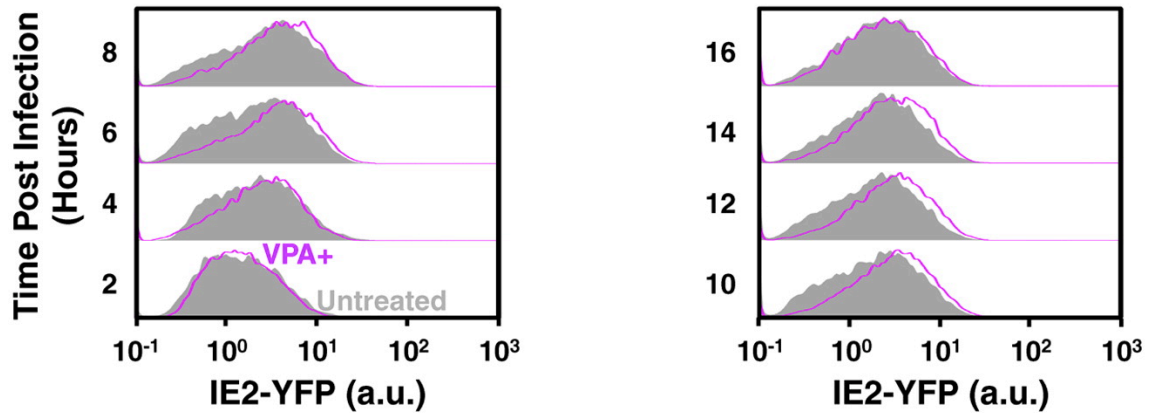
Appendix Figure 2.8: **Flow cytometry measurements of IE2 kinetics support Western blot and single-cell microscopy data.** Histograms are shown every 2 hours from 2 hours post infection (h.p.i.) to 16 h.p.i for cells infected with CMV IE2-YFP virus in the presence (pink) and absence (gray) of VPA. (Cells were infected and fixed by Cynthia Bolovan-Fritts, and I performed the flow cytometry experiment and data analysis.)
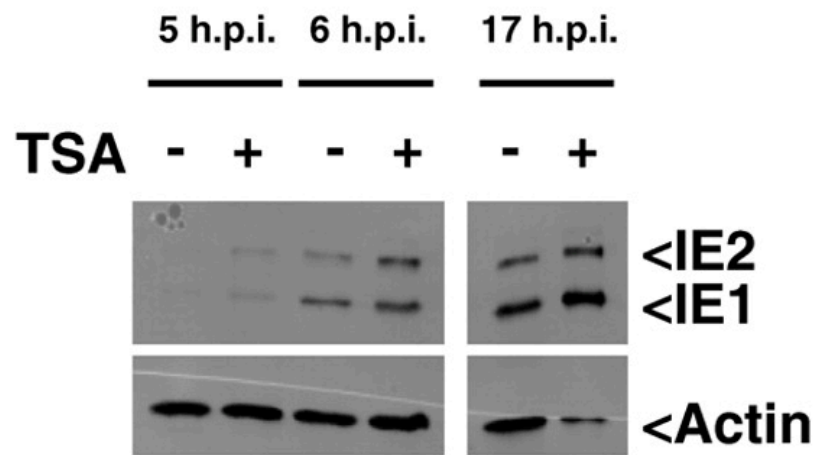
Appendix Figure 2.9: **Acceleration in the TB40-E clinical isolate of CMV.** Western blot time-course of IE2 and IE1 levels after infection with TB40-E at MOI=1. (Western blot by Cynthia Bolovan-Fritts.)
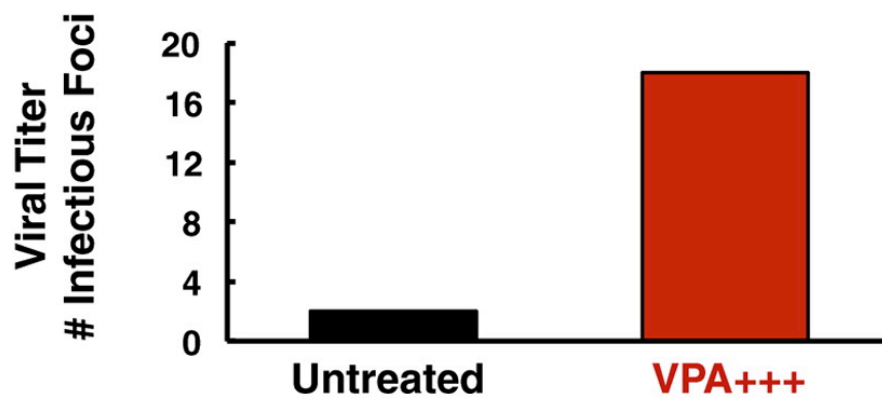
Appendix Figure 2.10: **Number of infectious foci/1000 cells after infection with TB40-E at MOI=1 with or without 7-day VPA pre-treatment.** (Viral kinetics measured by Cynthia Bolovan-Fritts.)

Appendix Figure 2.11: **Negative feedback with strong self-cooperativity generates acceleration without amplification.** The expression of a gene product (x) over time is described by an ordinary differential equation (ODE): $\dot{x}(t) = f(\beta, x) - \delta x(t)$, where f is an arbitrary function for synthesis, which includes a basal input β that can be varied, δ is a fixed decay parameter, and t is time. The synthesis term is a Hill function:

$$f(\beta, x) = \frac{\beta}{k^H + x(t)^H}$$ where H and k are fixed parameters. The plot shows a rate-balance

analysis where the synthesis rate $f(\beta,x)$ and the decay rate $\delta x(t)$ are plotted versus the value of x for varying increasing of H in each subplot. Each plot shows solutions with $\delta = 0.5$ (gray line) along with three values of $\beta = 1$ (black curve), $\beta = 1.5$ (pink curve), and $\beta = 2$ (red curve) where $k = 1$ for all plotted curves. (Mathematical modeling by Leor Weinberger.)
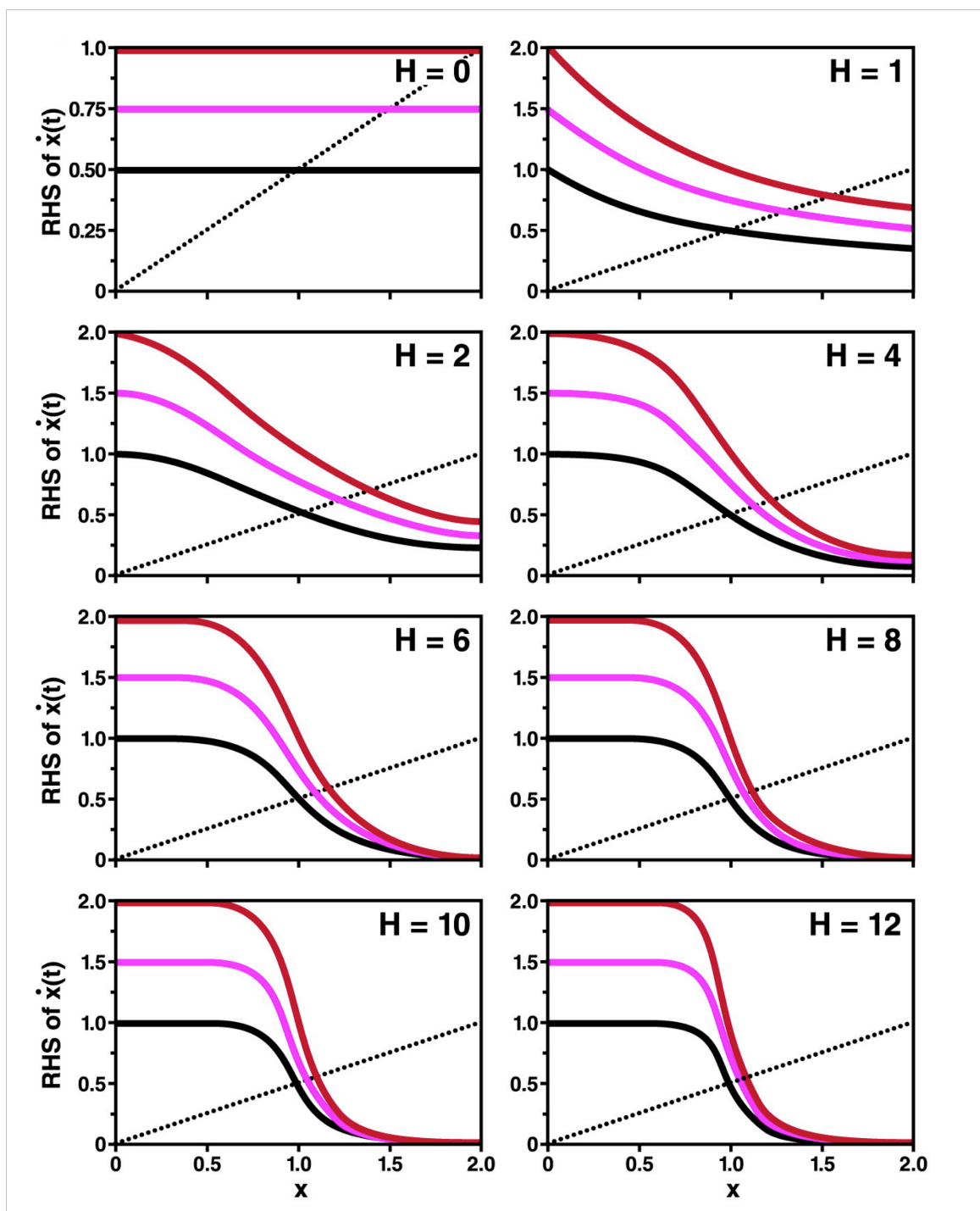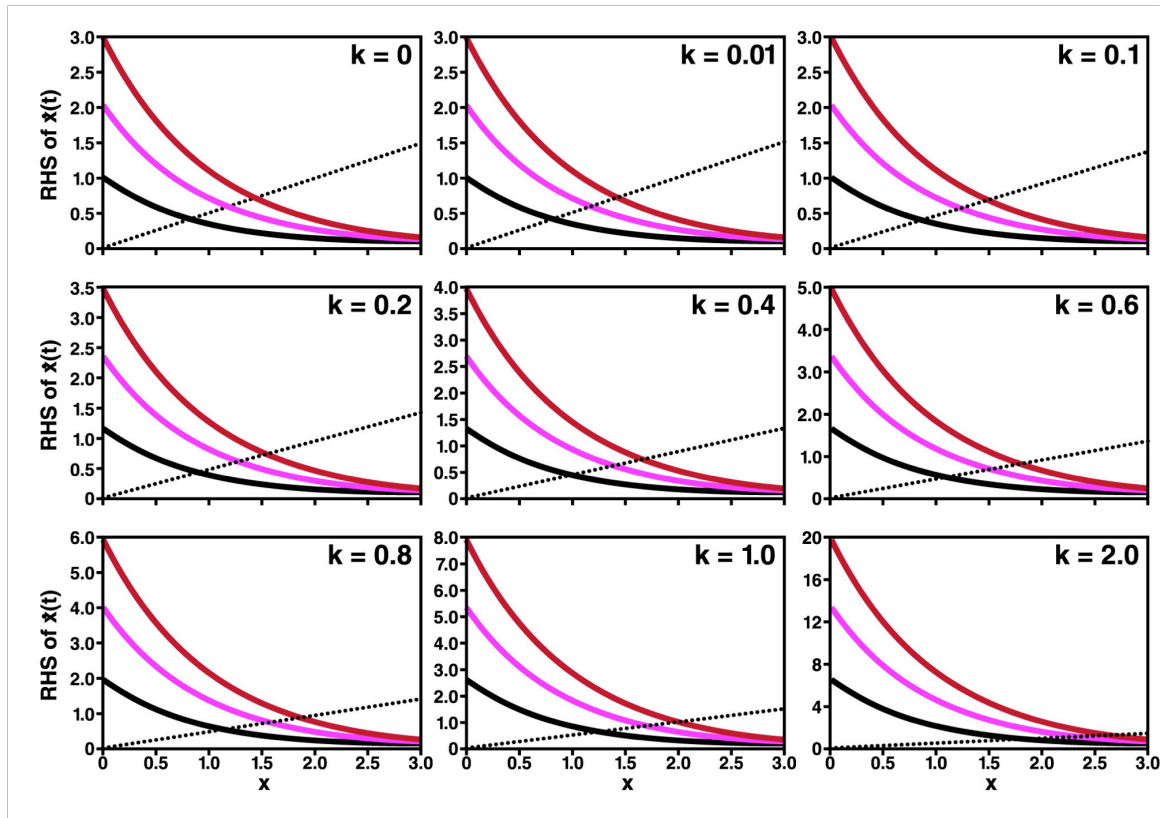
Appendix Figure 2.12: Gene expression as a decaying exponential function does not generate acceleration. Here, the synthesis term uses a decaying exponential function: $f(\beta, x) = \beta e^{k - x(t)}$. Each subplot shows rate-balance analysis with $\delta = 0.5$ (gray line) along with three values of $\beta = 1$ (black curve), $\beta = 1.5$ (pink curve), and $\beta = 2$ (red curve) for increasing k. (Mathematical modeling by Leor Weinberger.)
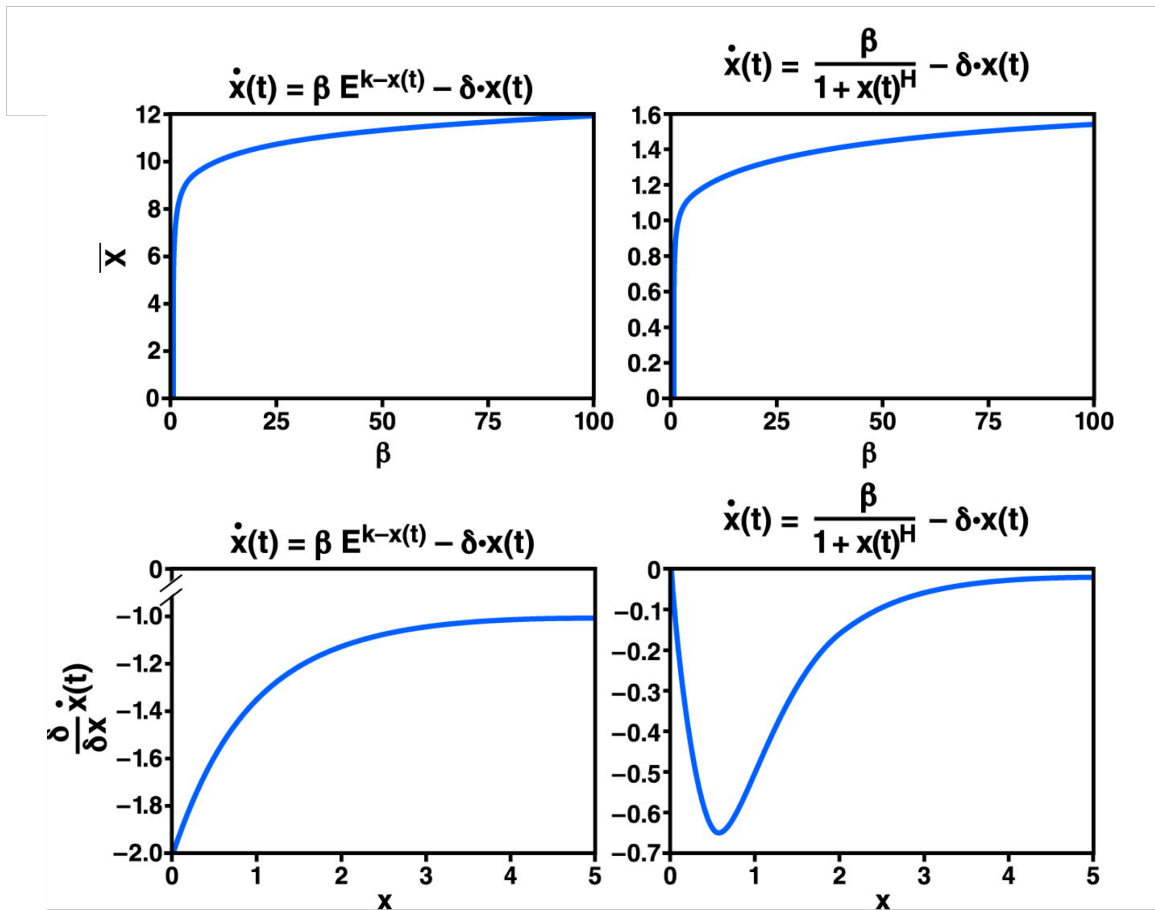
Appendix Figure 2.13: **The Hill function** $f(\beta, x) = \dfrac{\beta}{k^H + x(t)^H}$ **satisfies two criteria necessary for acceleration without amplification while the synthesis function described by the decaying exponential function** $f(\beta, x) = \beta e^{k-x(t)}$ **does not satisfy both criteria.** In the Hill function, k=1 for simplicity. Steady-state solutions of $\dot{x}(t) = f(\beta, x) - \delta x(t)$ show that both synthesis functions produce steady-state solutions ($\bar{x}$) that change very little as the basal input β increases. However, only the Hill function satisfies the criterion that the slope $\dfrac{\partial}{\partial x} \dot{x}(t)$ must be maximum at early times ($x(0) = 0$) and must go to zero as the system approaches steady state. (Mathematical modeling by Leor Weinberger.)
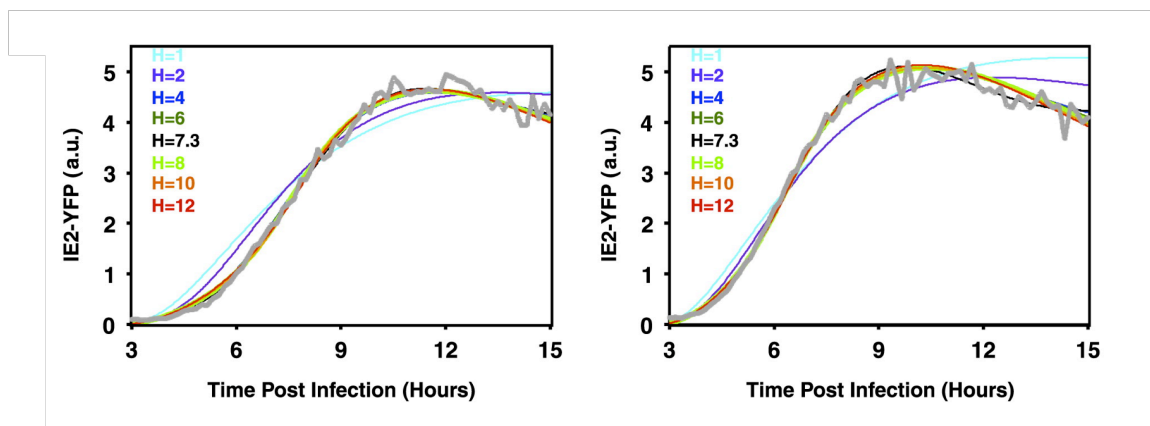
Appendix Figure 2.14: Sensitivity analysis of *H* for fits to single-cell data. Nonlinear least squares regression of single-cell time-lapse microscopy data from Fig. 2.3 (gray) to a mathematical model of the CMV MIE circuit (Table SI), showing best-fit curve of *H*=7.3 (black) along with best-fit curves for *H*=1 (cyan), *H=2* (purple), *H*=4 (blue), *H=6* (dark green), *H*=8 (light green), *H=10* (orange), and *H*=12 (red). The best-fit curves were generated by allowing all models parameters to vary, while keeping *H* fixed. The sensitivity analysis was preformed for both the untreated control cells (left) and cells pre-treated with VPA for 24 hours (right).
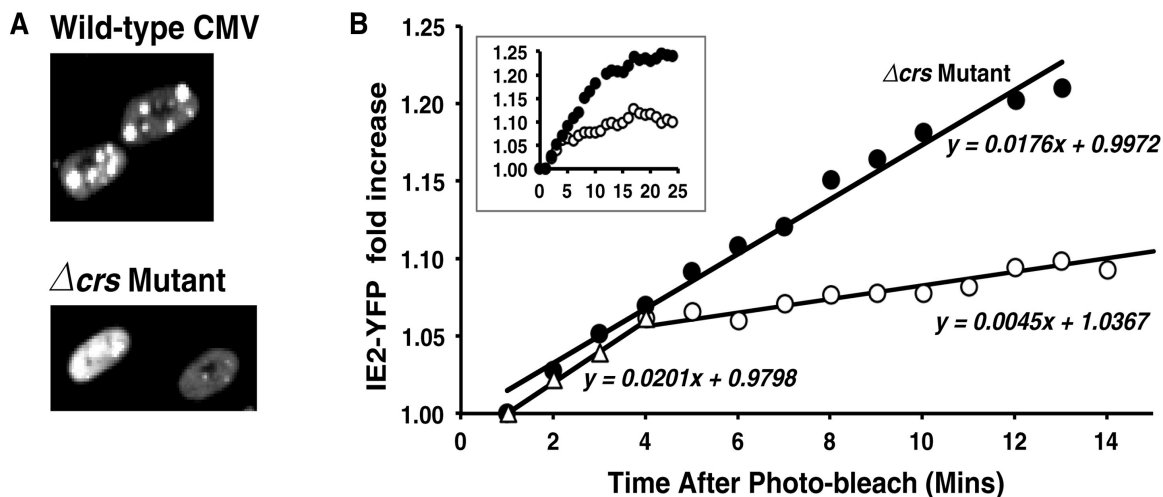
Appendix Figure 2.15: FRAP of IE2-YFP in single cells reveals two effective diffusion coefficients for IE2. A, Live-cell fluorescence micrographs of cells infected with CMV IE2-YFP virus or CMV *Δcrs* IE2-YFP virus. CMV IE2-YFP virus exhibits the previously reported nuclear foci of IE2-YFP accumulation, but foci are largely absent from *Δcrs* IE2-YFP virus. **B,** Quantification of FRAP of live cells infected with CMV IE2-YFP or mutant *Δcrs* IE2-YFP virus (i.e. lacking the IE2 DNA binding site). Cells were infected (at MOI=1) with either virus and when IE2 steady state reached, 12 hpi or 24 hpi, respectively, a pixel-area corresponding to ~1/4 to 1/3 of the nucleus was photobleached down to ~50% its original intensity. All data was normalized by dividing by the initial intensity at the first capture time-point directly after photo-bleaching. Little recovery is observed during the first 30 seconds (data not shown) which is consistent with IE2's numerous binding interactions with cellular proteins. During the first 4 minutes after bleaching, IE2-YFP in the bleached volume increases at the same rate for both parent and mutant. However, after 4 minutes the parent exhibits a second slope that is ~4-5 fold lower (corresponding to a ~4-5-fold slower diffusion coefficient) while the mutant continues to increase in YFP accumulation in the bleached volume. The slower effective diffusion rate in the parent is consistent with a model where photo-bleached IE2 is stably bound to the DNA and excludes new IE2-YFP molecules from efficiently residing in the bleached volume. Inset: Full recovery trajectories showing that FRAP of *Δcrs* IE2-YFP viruses exhibits far greater recovery of absolute fluorescence as compared to FRAP to CMV IE2-YFP virus. (FRAP experiment was performed by Leor Weinberger, and I completed the data analysis.)

| GFP | IE2 antibody | Merge |

Appendix Figure 2.16: Confirmation of stable IE2 expression. *Left:* GFP fluorescence of ARPE-19 cells expressing the lentiviral vector MIEP-IE2-IRES-GFP. *Center:* Immunofluorescent staining of same MIEP-IE2-GFP ARPE-19 cells with anti-IE2 antibody and Texas Red secondary antibody showing nuclear localization of IE2. *Right:* Overlay of GFP fluorescence and IE2 immunofluorescence. (Immunofluorescence was performed by Cynthia Bolovan-Fritts.)
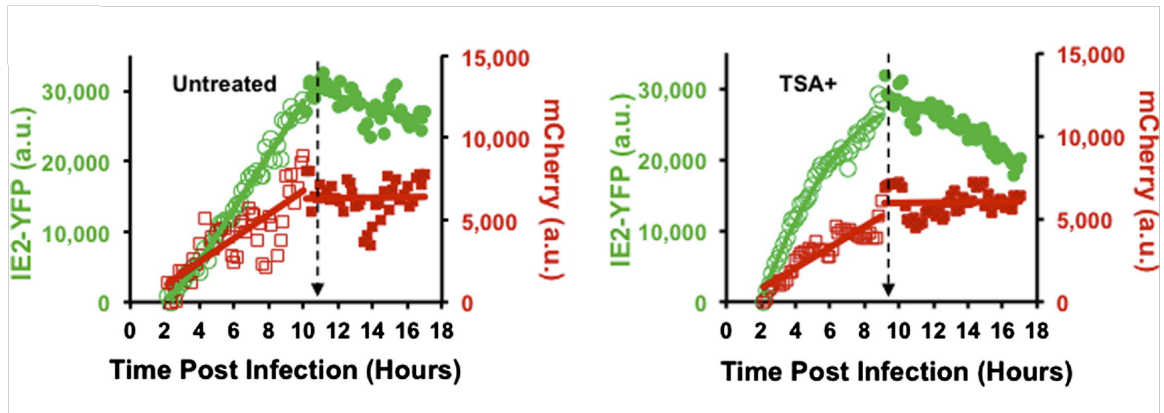
Appendix Figure 2.17: **MIE expression kinetics from integrated lentiviral vectors are highly correlated with CMV MIEP activity in CMV infected cells.** Human foreskin fibroblasts stably expressing a MIEP-mCherry lentiviral vector were infected with CMV IE2-YFP virus (MOI=1) in the presence (right) or absence (left) of TSA to generate two-color single-cell time-lapse microscopy trajectories (average of 20 cells) and track MIEP activity during CMV infection. The activity of the MIEP integrated within host genomic DNA (red) is highly correlated with CMV MIEP activity (green), the integrated MIEP exhibits negative auto-regulation (plateau in mCherry levels) that is correlated with the maximum in IE2-YFP levels, and the integrated MIEP exhibits an accelerated rate of MIEP shutdown in the presence of TSA. (Single-cell microscopy was performed by Leor Weinberger, and I performed the data analysis.)
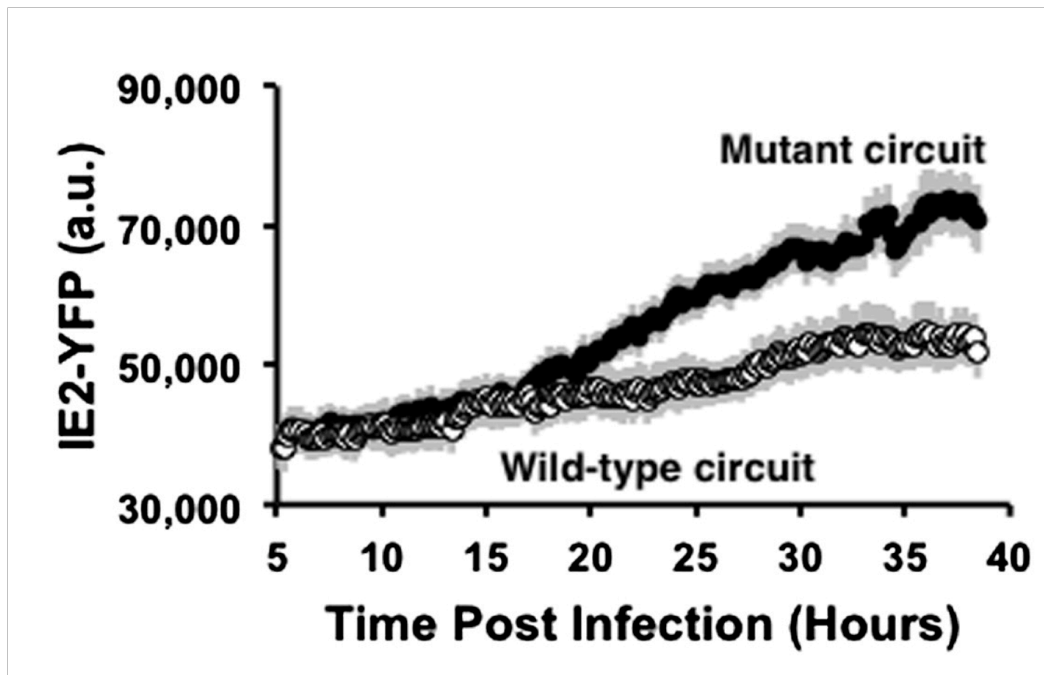
Appendix Figure 2.18: **Amplification of protein levels in a feedback-knockout mutant circuit.** Single-cell GFP levels (20 cells) were quantified in the negative-feedback MIEP-IE2-IRES-GFP circuit (white) and the feedback-knockout mutant MIEP*Δcrs*-IE2-IRES-GFP circuit (black) in presence of TSA. GFP levels are amplified in the mutant circuit compared to the wild-type circuit. Averages are shown in bold with ± one standard error shown gray.
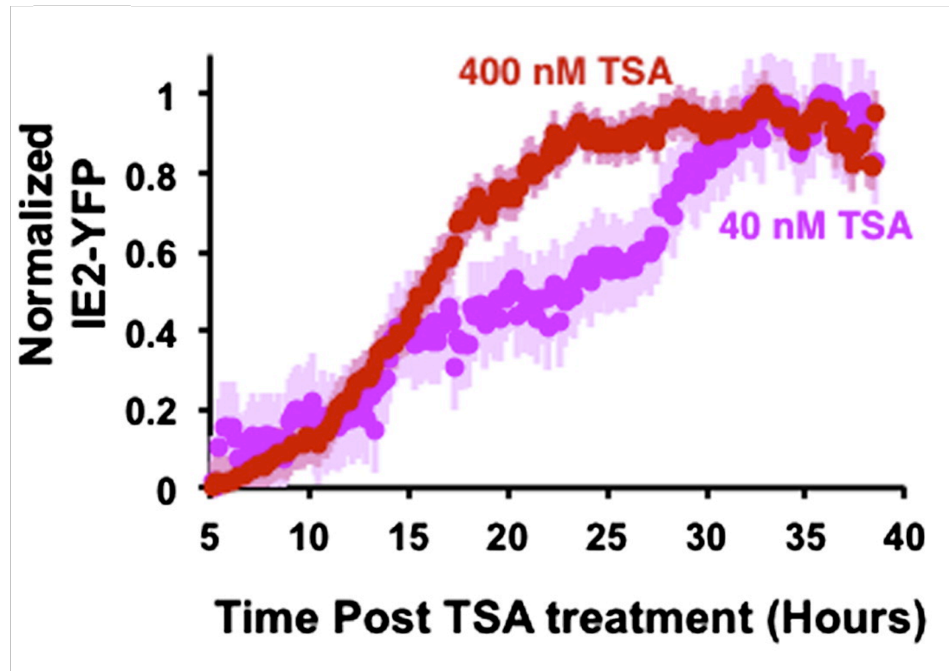
Appendix Figure 2.19: Fluorescence quantification of single-cell GFP levels in cells treated with increasing levels of TSA and stably expressing MIEP-IRES-IE2-GFP. Cells were treated with 400 nM (red) or 40 nM (pink) TSA. Averages are shown in bold with ± one standard error shown in light red (400 nM TSA) or light pink (40 nM TSA). IE2 expression accelerates with increasing levels of TSA.
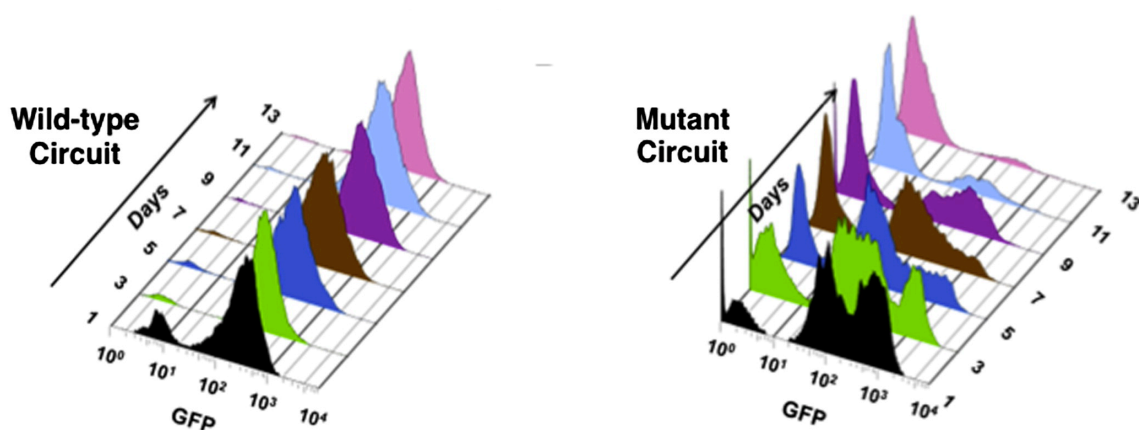
Appendix Figure 2.20: Live-cell flow cytometry time-courses of minimal circuits.
The flow cytometry histograms of GFP fluorescence for wild-type circuit (left) and
mutant circuit (right) used to construct Fig. 2.13 trajectories. The percentage of GFP
expressing cells for the wild-type circuit remains constant over time.. The percentage of
GFP expressing cells for the mutant circuit decreases over time. The relatively high
percentage of cells displaying low GFP fluorescence on day 1 in the wild-type circuit
may be due to sorting-induced cytotoxicity and the short recovery time for cells after
FACS sorting.

Appendix Table 2.1: Parameters for the CMV MIE model.

Symbol	Value	Description	Source
β	5.327	MIEP basal promoter rate	Parameter fit of model
α	12.398	IE1 transactivation rate	Parameter fit of model
k_1	0.984	IE1 Michaelis constant	Parameter fit of model
H_1	19.935	IE1 Hill coefficient	Parameter fit of model
γ	0.195	IE2 repression rate	Parameter fit of model
k_2	0.784	IE2 Michaelis constant	Parameter fit of model
H_2	7.295	IE2 Hill coefficient	Parameter fit of model
δ	0.394	MIE RNA decay rate	Parameter fit of model
f	0.67	Fraction of IE1 spliced transcripts	Literature (Nevels et al., 2004)
λ	0.025	Translation rate	Parameter fit of model
δ_1	0.032 hour^{-1}	IE1 protein decay rate	Literature (Stamminger et al., 1991)
δ_2	0.23 hour^{-1}	IE2 protein decay rate	Literature (Stamminger et al., 1991) and verified through single-cell microscopy

Chapter 3:

The CMV IE2 accelerator circuit provides a fitness advantage for the virus

ABSTRACT

In Chapter 2, I discussed the mapping of the CMV IE2-accelerator circuit to a highly-cooperative negative-feedback loop with a Hill coefficient of ~7. Here, we show that eliminating the IE2-accelerator circuit in CMV reduces transcriptional strength through mislocalization of incoming viral genomes away from PML bodies and carries a heavy fitness cost. CMV without the IE2 accelerator circuit is unable to outcompete CMV with an intact IE2-accelerator circuit in a fitness competition assay, despite having equivalent IE2 steady-state levels. Our results suggest that the IE2 expression rate is central to maintaining viral fitness in CMV.

MATERIALS AND METHODS

Cloning of recombinant viruses

The CMV *Δcrs* IE2-YFP virus was constructed by BAC 'recombineering' (Warming et al., 2005) of the CMV IE2-YFP virus as previously described (Cuevas-Bennett and Shenk, 2008). To propagate and purify virus, BAC DNA was electroporated (Yu et al., 2002) into MRC5 cells (American Type Culture Collection) using a GenePulser Xcell Electroporation System (Bio-Rad). Upon infection reaching 100% viral cytopathic effect or 100% GFP, the culture supernatant was collected and filtered with a 0.45 μm filter (Corning Inc.). For the CMV *Δcrs* IE2-YFP virus, low titers required concentration by ultracentrifugation: cells were disrupted by sonication to release virions, and supernatant was then filtered by a 0.45 μm filter and ultracentrifuged in a 'sorbitol cushion' (20% D-sorbitol, 50 mM Tris-HCl, pH 7.2, 1 mM $MgCl_2$ in dH_2O) in an SW 41 Ti rotor (Beckman Coulter, Inc.) at 25,000 rpm at 18ºC. Viral stocks were

titered by TCID$_{50}$ (Nevels et al., 2004). To verify the integrity of the CMV Δcrs IE2-YFP virus, a rescue virus, CMV $\Delta crsREVERT$ IE2-YFP, was constructed by homologous recombination, whereby CMV Δcrs IE2-YFP BAC DNA (20 µg) and a ~2.5 kb wild-type MIEP DNA fragment (2.5 µg) were co-transfected by electroporation into 10^6 MRC5 cells, and subjected to two rounds of plaque purification.

Cell-culture conditions and drug perturbations

MRC5 fibroblasts and life-extended human foreskin fibroblasts (HFFs) (Bresnahan and Shenk, 2000) were maintained in Dulbecco's Modified Eagle's Medium (DMEM) supplemented with 10% fetal bovine serum (FBS) and 50 U/ml penicillin-streptomycin at 37ºC and 5% CO_2 in a humidified incubator. Cells were pretreated in a final concentration of 1 mM VPA (Calbiochem).

Time-lapse fluorescence microscopy measurements

Cells were passed onto a 35 mm glass-bottom dish (MatTek Corp.) or a 96-well glass-bottom plate (Thermo Fisher Scientific) and grown to confluency for several days in order to hold cells in the G0 phase. Cells were synchronously infected on ice at 4ºC for 30 minutes or at room temperature for 30 minutes with virus at a MOI of 1. Live cells were imaged using a 20X oil objective on a spinning disk confocal microscope (Olympus DSU, Olympus America, Inc.) equipped with a 37°C, humidified, 5% CO_2 live-cell chamber. Image collection began when YFP signal was first detected and frames were subsequently captured every 10 minutes for 16-24 hours using an exposure time between 200 and 800 msec. For IE2 half-life measurements, cycloheximide was added to cells 15

hours after infection, and cells were imaged every 10 minutes for 12 hours. Images were acquired with Slidebook[TM] 4.2 software (Imaging Innovations, Inc.). Single-cell tracking and segmentation were performed with custom-written code in MatLab[TM] (Mathworks) as previously described (Weinberger et al., 2008). Code is available upon request.

Replication Kinetics

Confluent MRC5 monolayers at ~5 x 10^4 cells per well were infected at indicated MOIs using 0.45μm pre-filtered virus inoculum stocks diluted in culture media. Inoculums were calculated based on plaque-assay titrations (Bolovan-Fritts and Wiedeman, 2001), shown as time point 0 in each figure.   Inoculum was then removed and replaced with 1mL fresh media. Infected wells were collected in triplicate at indicated time points and stored at $-80^{°}C$. To measure replication, samples were thawed and prepared as a 10-fold serial-dilution series in culture media, analyzed by $TCID_{50}$, then converted to PFU/ml.   Error ranges were calculated by standard deviation.

Immunofluoresence and Brdu-labeled virus detection

Brdu-labeled virus was grown and detected by adapting a previously published method (Rosenke and Fortunato, 2004). Cells were grown on 16-well chamber slides (Lab-Tek) and infected with either CMV IE2-YFP or Δ*crs* IE2-YFP virus on ice and with 1% FCS media to synchronize infection. After 3 hours, cells were washed, fixed, and permeabilized (Rosenke and Fortunato, 2004). PML was detected by a polyclonal PML rabbit antibody (Santa Cruz) at a 1:500 dilution, with secondary goat anti-rabbit Alexa 488 antibody (Invitrogen) at 1:500. After PML detection, the cells were stained with

DAPI (Invitrogen) for 15 minutes before a second fixation with 3% formaldehyde. Brdu-labeled viral genomes were detected using a monoclonal rat Brdu antibody (Accurate Chemical Scientific Corp.) at 1:250, followed by secondary donkey anti-rat antibody conjugated with Alexa Fluor 568 (Invitrogen) at 1:500. Cells were mounted with ProLong Gold mounting media (Invitrogen) and a #1.5 cover slip (Nunc). Cover slips were imaged on a Zeiss Observer Z1 spinning-disk confocal microscope with a Plan-FLUAR 100X/1.45 oil objective. Co-localization analysis was performed in Slidebook^{TM} 5.0 (Imaging Innovations, Inc.).

RESULTS

Converting the Accelerator to an Amplifier Generates a Severe Fitness Cost for the Virus

To determine if negative feedback is necessary for the MIE circuit to act as an accelerator in the context of the virus, we constructed a Δ*crs* virus by BAC mutagenesis of the three nucleotides in the *crs* binding site (Fig. 3.1). In agreement with modeling predictions and the minimal circuit observations discussed in Chapter 2, this Δ*crs* mutant virus acts as an amplifier generating a ~1.5-fold amplification in single-cell expression levels in the presence of MIEP activators (Fig. 3.2 and Appendix Fig. 3.1) and exhibits virtually no acceleration (Fig. 3.3).

Strikingly, replication of this mutant amplifier virus is severely compromised in the presence of activators (Fig. 3.4 and Appendix Fig. 3.2). These data agree with the minimal-circuit data that amplification of IE2 levels is deleterious for the cell, leading to decreased viral output. Potential toxicity of VPA or TSA exposure alone cannot account
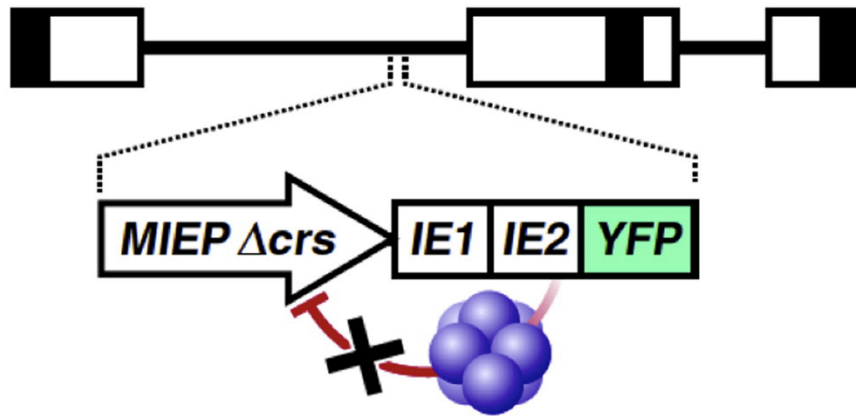
Figure 3.1: Schematic of the mutant CMV Δ*crs* mutant virus.
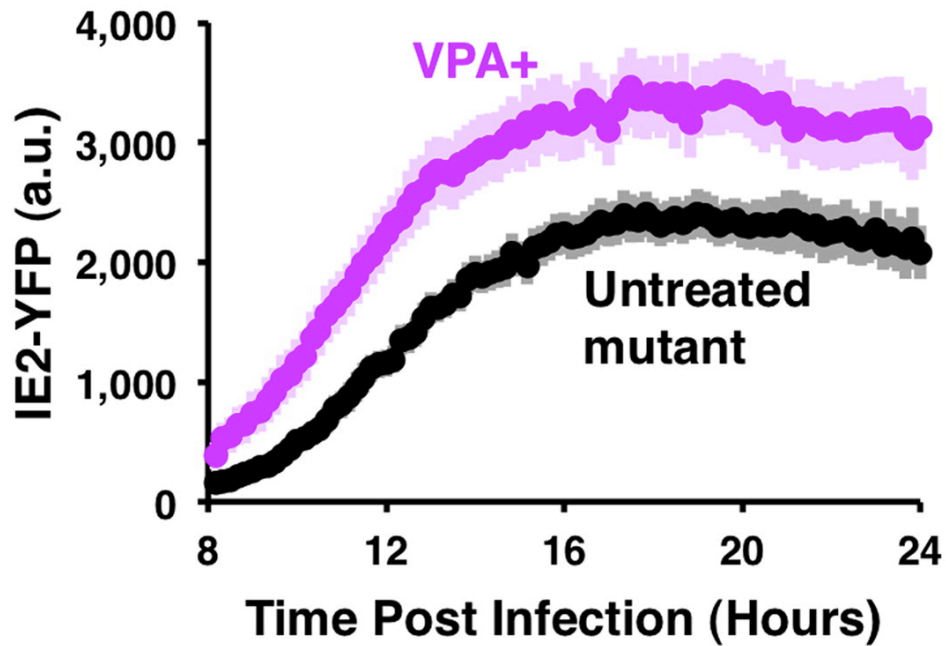
Figure 3.2: Abrogation of negative feedback in a CMV Δ*crs* mutant produces an amplification of IE2 levels in response to VPA. Single-cell time-lapse microscopy of cells undergoing infection with CMV Δ*crs* mutant in presence of 24-hour pre-treatment of VPA (pink) or absence of VPA (black). Trajectories are averages of 20 cells (bold) together with ± one standard deviation (lighter background). The CMV *Δcrs* mutant displays an ~1.5-fold amplification in IE2 levels in single cells in response to VPA.
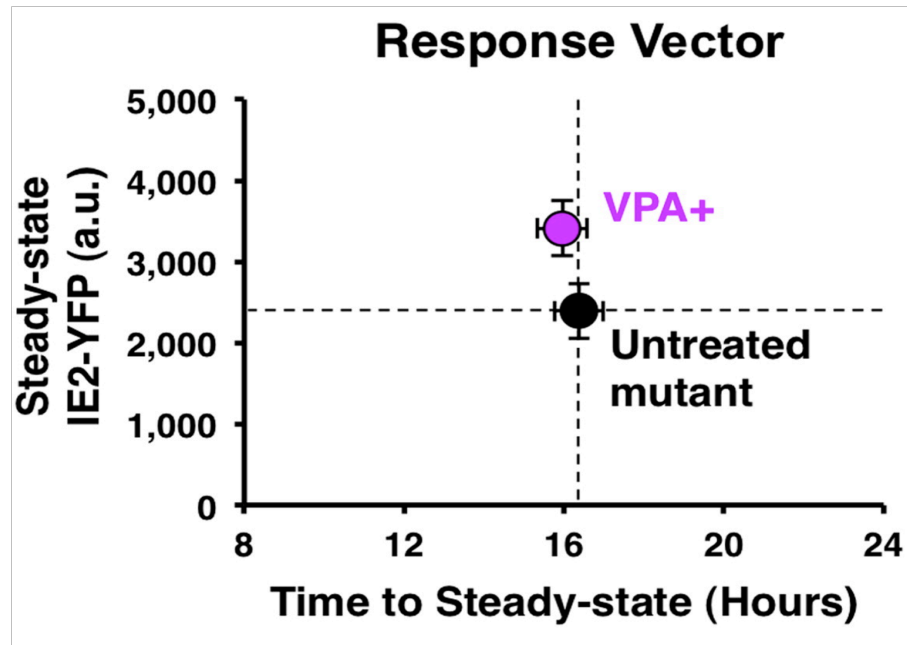
Figure 3.3: **Response-vector map of single-cell microscopy data showing that the *Δcrs* mutant virus amplifies steady-state IE2-YFP levels with VPA pre-treatment.** The untreated control (black) and the VPA pre-treated (pink) data are each averages of 20 cells. Error bars (gray) = ± one standard error.
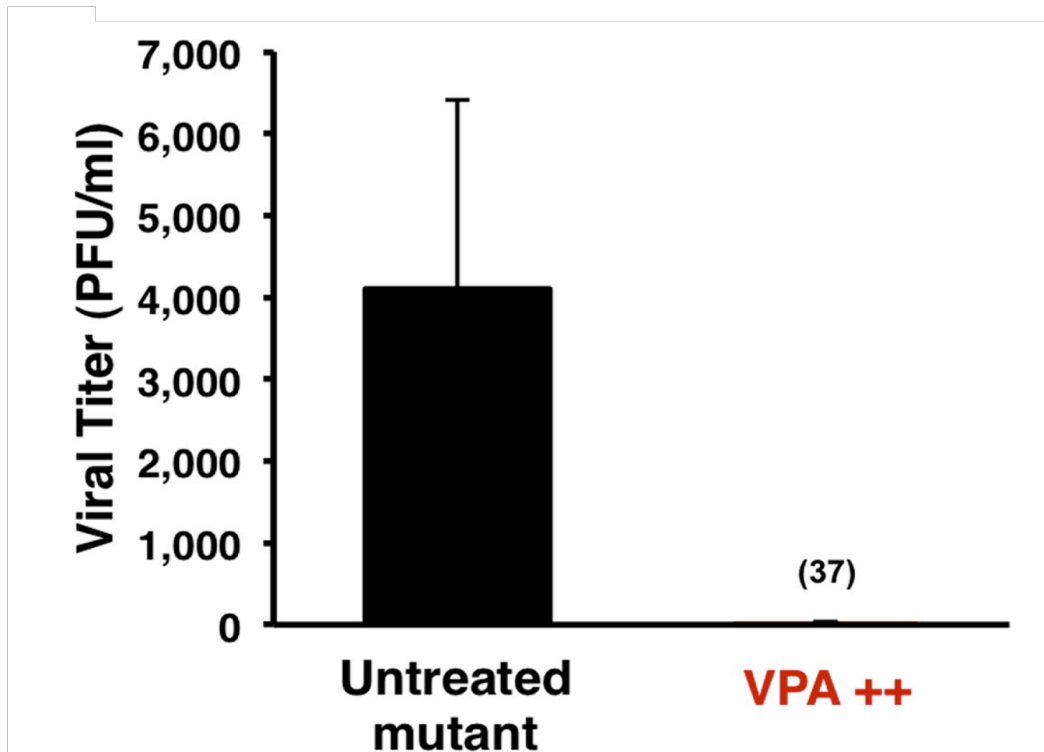
Figure 3.4: Converting the IE2 accelerator to an amplifier – by eliminating negative feedback – generates a severe fitness cost for the virus. Replicative fitness of the CMV *Δcrs* mutant in presence (red) and absence (black) of a 72-hour VPA treatment as measured by PFU/ml on the peak day of viral production (day 10) after infection at MOI=1. Averages are shown in bold gray with ± one standard deviation. (Replication kinetics by Cynthia Bolovan-Fritts.)

for reduced viral replication since neither activator reduces replication fitness of the parent virus (Appendix Fig. 3.2).

To rule out secondary mutations outside the *crs* region that could be responsible for amplification, these results were verified in two independently isolated BAC clones, and sequencing 1kb upstream and downstream of the *crs* verified the absence of secondary mutations (data not shown). The generation of a 'rescue' virus with wild-type IE2 expression kinetics (described below and in Fig. 3.9) independently verifies that secondary mutations do not account for the amplifier phenotype or reduced fitness. This absence of secondary mutations is not unexpected given the reported stability and specificity of BAC mutagenesis for CMV (Reddehase and Lemmermann, 2006).

The Loss of the Accelerator Circuit in the *Δcrs* Amplifier Mutant is Buffered by Reduced MIEP Activity through Mislocalization of Incoming Viral Genomes

While theory predicts that removal of negative feedback should increase IE2 steady-state levels (as in the minimal circuit), the biology of IE2 cytotoxicity and the presence of the accelerator circuit in the wild-type virus suggests that over the course of viral evolution, there is strong selection for mechanisms to maintain low IE2 levels. Therefore, to determine how the *Δcrs* amplifier mutant virus was able to maintain any viability even in the absence of activators (Fig. 3.4), we tested if IE2 steady-state levels were increased similar to the minimal virus setting or if the mutant virus employed compensatory mechanisms to keep IE2 levels low. Single-cell imaging and flow cytometry analysis reveal that IE2 steady-state levels in the *Δcrs* mutant amplifier virus (in the absence of activators) are essentially the same as IE2 levels in the wild-type virus

(Fig. 3.5 and Appendix Fig. 3.3) but the rate of IE2 expression is significantly slower in the mutant (Fig. 3.5). Based on literature indicating that sub-nuclear PML bodies facilitate transcription from the MIEP (Sourvinos et al., 2007), we tested if reduced IE2 levels were the result of decreased MIEP activity due to *Δcrs* mutation–induced mislocalization of incoming viral genomes away from PML bodies. While the wild-type virus exhibits IE2 localization to PML bodies, the *Δcrs* mutant virus displays virtually no IE2-positive foci during early infection (see Chapter 2, Appendix Fig. 2.15), and immunofluorescence analysis shows that *Δcrs* mutant viral genomes do not co-localize with PML bodies (Fig. 3.6). To confirm that PML-body mislocalization reduces IE2 levels, we infected a cell line lacking PML bodies (Everett and Chelbi-Alix, 2007) and observed significantly reduced steady-state IE2 levels (Fig. 3.7). In summary, the *Δcrs* mutant amplifier virus appears to compensate for the lack of accelerator circuitry by reducing MIEP transcriptional strength, through misdirecting incoming viral genomes away from sub-nuclear PML bodies.

The minimal circuit is integrated into the genome as a single-copy lentiviral provirus and MIEP does not appear to be influenced by PML body localization in this context.

Reduced MIEP Activity Decelerates IE2 Expression and Carries a Heavy Fitness Cost

Since the amplifier mutant and wild-type accelerator viruses exhibit equivalent IE2 steady-state levels but different rates of IE2 expression, we next tested if the mutant's reduced fitness could be rescued by acceleration. To do this, we provided the mutant
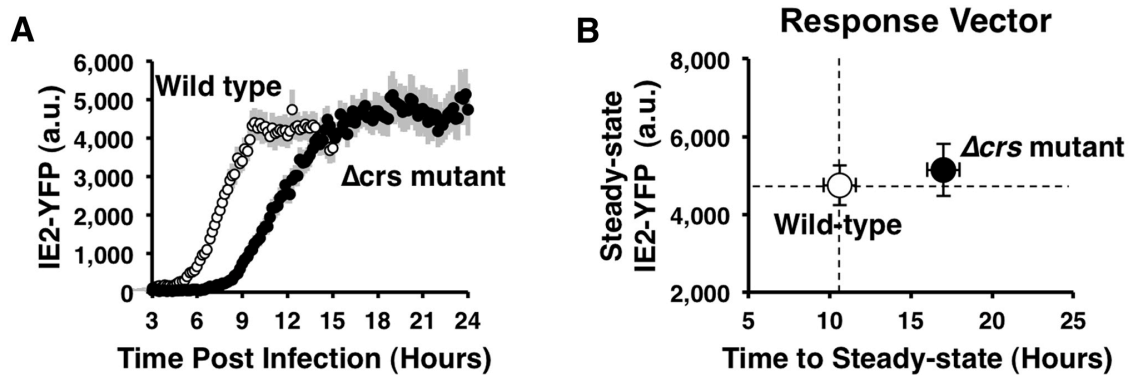
Figure 3.5: IE2-YFP levels are the same in the wild type and *Δcrs* mutant virus, but the *Δcrs* mutant virus has slower IE2-YFP kinetics. A, Single-cell time-lapse microscopy analysis comparing CMV IE2-YFP virus, referred to as "wild type" (white), to *Δcrs* amplifier mutant virus (black); infections imaged in parallel on the same day under the same conditions. Error bars (gray) = ± one standard error. **B,** Response-vector map showing that the *Δcrs* amplifier mutant virus (black) exhibits decelerated IE2 kinetics but no change in IE2 steady-state level compared to wild type (white).
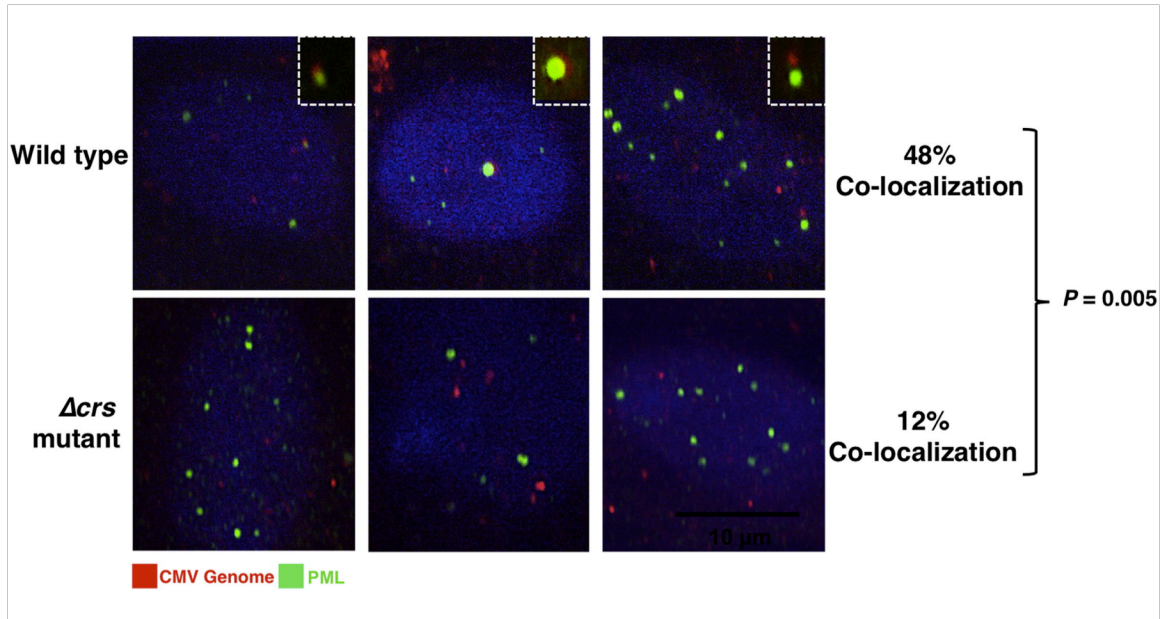
Figure 3.6: **Mutation of the *crs* in the CMV genome results in inefficient formation of IE transcriptional centers**. Immunofluorescence micrographs of cells infected with either wild-type CMV (top panels) or the *Δcrs* mutant virus (bottom panels) and stained for CMV genome (red), PML protein (green), and DNA (blue). CMV genomes and PML bodies appear to co-localize at a significantly higher frequency ($P < 0.01$) in cells infected with wild-type CMV virus compared to *Δcrs* amplifier mutant virus. Insets: representative co-localization of CMV genomes and PML bodies (Cynthia Bolovan-Fritts purified the Brdu-labeled virus, and I performed the immunofluorescence and image data analysis).
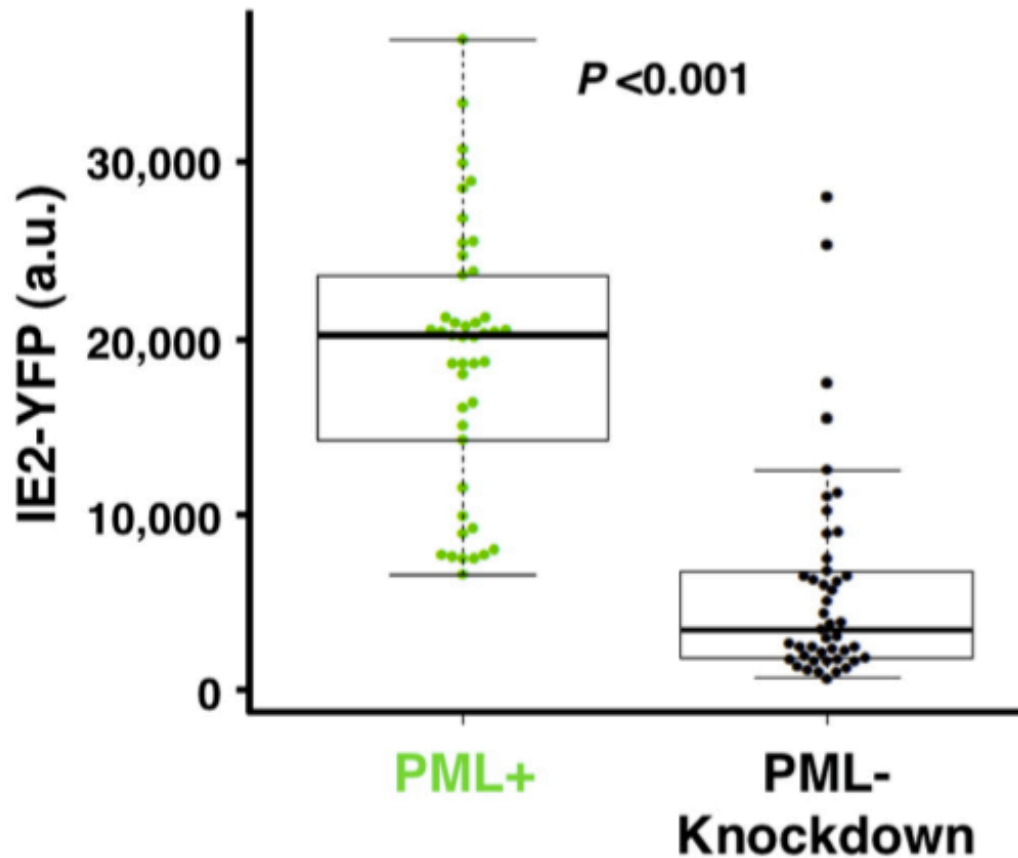
Figure 3.7: PML- knockdown in single cells infected with CMV IE2-YFP virus results in lower IE2-YFP steady-state levels. Steady-state IE2-YFP levels from single-cell microscopy in conventional PML+ cells (green) or PML- knockdown cells (black). Both cell types were infected with wild-type CMV IE2-YFP virus. Bold black lines in the box plot are the median IE2-YFP levels, boxes represent lower and upper quartile, and whiskers represent 1.5 interquartile range (IQR) of the lower and upper quartiles. PML knockdown significantly reduces IE2-YFP levels ($P < 0.001$).

virus with the opportunity to regain accelerator circuitry through homologous

recombination, by co-transfecting cells with the full *Δcrs* mutant virus genome together

with a short 1kb DNA fragment of the MIEP encoding the wild-type *crs* sequence. This

approach to generate recombinant "rescue" virus (Fig. 3.8) creates a "fitness

competition" since the mutant must compete with any rescue that arises within the

culture. After culturing the co-transfected cells for two weeks (the typical time for

growth of CMV IE2-YFP in culture), all observable CMV-positive plaques analyzed

were, rescue virus that exhibited accelerated expression kinetics (Fig. 3.9) and fitness that

was comparable to wild-type virus (Fig. 3.10). The fact that high-titer accelerator rescue

virus can be isolated from a background *Δcrs* infection, and that no detectable *Δcrs* virus

can be isolated from this background, indicates that viruses encoding the accelerator

circuit directly outcompete viruses encoding the mutant amplifier even in the absence of

transcriptional activator drugs. Sequencing results confirm that in the rescue virus the

Δ*crs* locus is restored to the wild-type sequence, and that the rescue virus exhibits a

complete recovery of the accelerator phenotype (Appendix Figs. 3.4-3.5). These results

show that a slower rate of IE2 expression is sufficient to generate a heavy fitness cost

even when IE2 levels are not elevated.

DISCUSSION

Chapter 2 showed that acceleration of transcriptional response time, without

modulation of steady-state levels, can confer a fitness advantage. The fitness advantage

is unlikely to result solely from faster IE2 expression but rather from IE2 driving
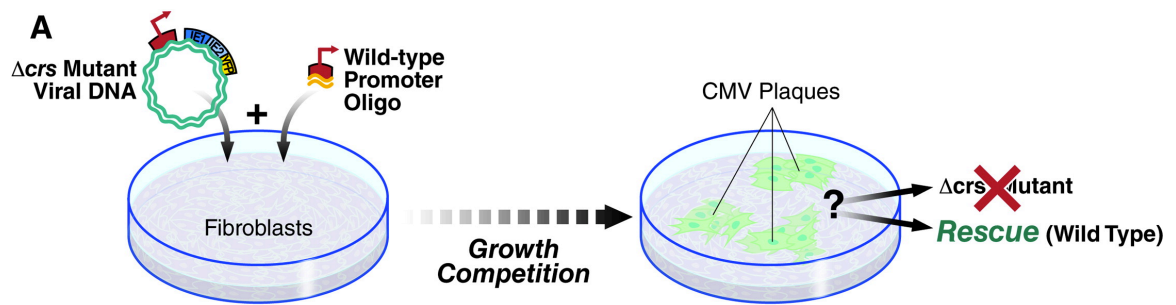
Figure 3.8: Schematic of 'rescue' experiment that represents a growth competition between the *Δcrs* amplifier mutant virus and 'wild-type' CMV IE2-YFP.
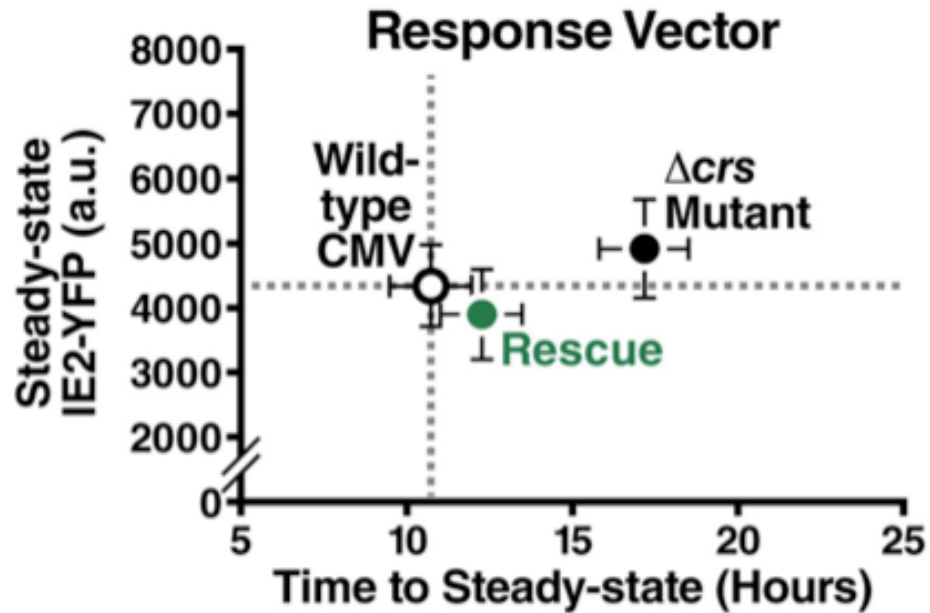
Figure 3.9: Response-vector map of single-cell microscopy showing that the rescue virus generated from the mutant amplifier virus, has regained the accelerated expression kinetics of the wild-type virus. The rescue virus (green), wild-type CMV (white) and Δ*crs* mutant virus (black) all exhibit equivalent IE2-YFP steady-state levels; all viruses (wild-type, mutant, and rescue) were imaged in parallel on the same day under the same conditions. Error bars (gray) = ± one standard error
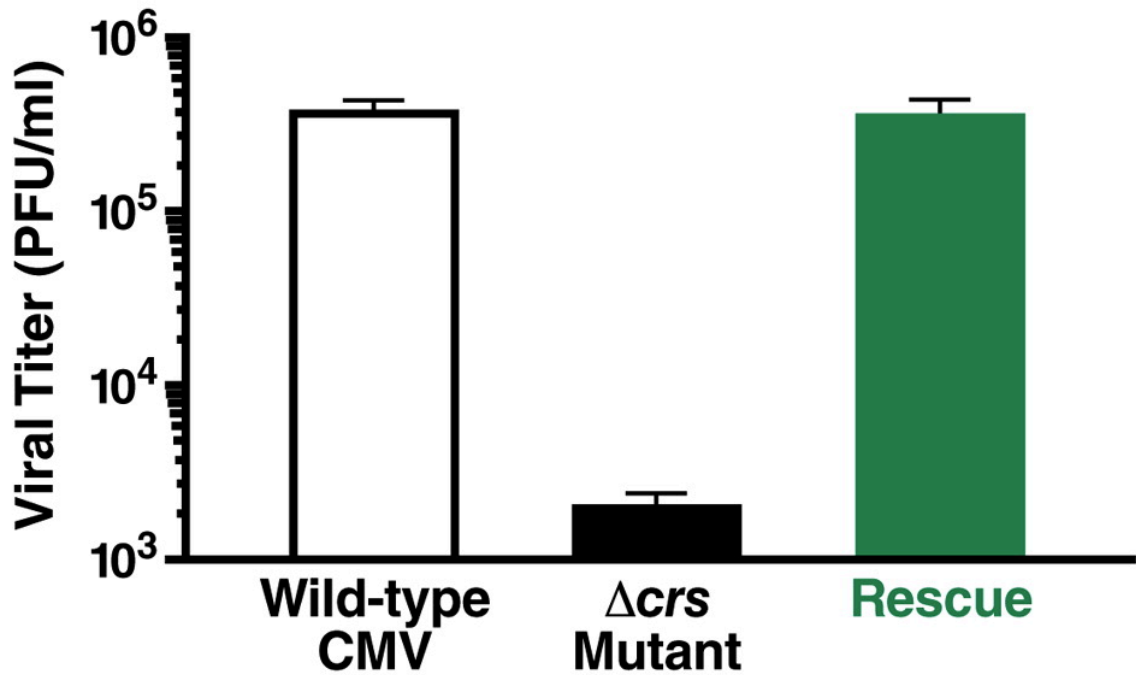
Figure 3.10: Loss of IE2 acceleration, despite equivalent IE2 levels, carries a heavy fitness cost. Viral replication titers for the rescue virus (green) compared to *Δcrs* amplifier mutant (black) and wild-type viruses (white) as measured by PFU/ml on the peak day of viral production in a multi-step assay (MOI=0.1). Despite all viruses exhibiting equivalent IE2-YFP steady-state levels, the rescue virus, which has reacquired the wild-type accelerator, replicates with the same high efficiency as wild-type virus while the *Δcrs* amplifier mutant virus exhibits a severe fitness disadvantage. Averages are shown in bold gray with ± one standard deviation. (Viral replication titers by Cynthia Bolovan-Fritts.)

acceleration of downstream viral expression, since viral c̲ytop̲athic e̲ffect (CPE) is observed earlier when IE2 kinetics are accelerated (data not shown), and other key steps in the viral life cycle are decelerated in Δ*crs* viruses (Isomura et al., 2008). Conversely, it is unlikely that the fitness advantage results from non-IE2-driven alternate pathways, since the same transcriptional activators that generate acceleration in the wild-type virus generate amplification with severe fitness loss in the Δ*crs* mutant amplifier virus and in minimal synthetic circuits where only the accelerator has been removed. The finding that a rescue virus (which only differs in rate of IE2 expression not level) outcompetes the Δ*crs* amplifier mutant, further argues that the expression rate drives the fitness advantage. These findings demonstrate a functional role for IE2 negative feedback in maintaining viral fitness.

Potential roles for the accelerator circuit in the evolution of virulence

Why might CMV have evolved the accelerator architecture over other potential mechanisms to maintain low levels of IE2? CMV's lifecycle *in vivo* involves replication in diverse cell types and host conditions and the strong, easily activated MIEP is well suited to activate under these diverse conditions. The MIEP's strength is due to numerous enhancer-binding sites that have the potential to generate large amplifications of input signal through combinatorial binding (Carey et al., 2009). Consequently, CMV's accelerator circuit may have evolved as a natural consequence of the strong MIEP to counteract and limit the inevitable amplification of signal from MIEP. An alternate mechanism would be to enhance the basal-expression strength of the MIEP while simultaneously increasing the decay (i.e. turnover) rate of IE2. This strategy would

difficult to achieve for CMV since the MIEP is one of the strongest known promoters and the IE2 half-life is ~2.5 hours (Appendix Fig. 3.6). Given this short half-life of IE2, coupled with the already exceptional strength of the MIEP, it may not be possible to further reduce IE2 half-life (while maintaining its essential functions) or increase the unstimulated MIEP activity level. However, this strategy may have been an evolutionary precursor to the accelerator circuit.

In settings where host defenses lead to high viral loss, faster expression and increased viral output in response to inflammatory or innate-defense factors may enable the virus to outpace host defenses. Thus, tuning of the expression rate may have evolved as a viral countermeasure to outpace the host cell's innate immune defenses. Since these considerations are not unique to CMV infection, accelerator circuitry may be a widespread architecture among gene-regulatory circuits.

Thomas Shenk provided reagents. Leor Weinberger conducted the IE2 decay rate experiment and directed all research.
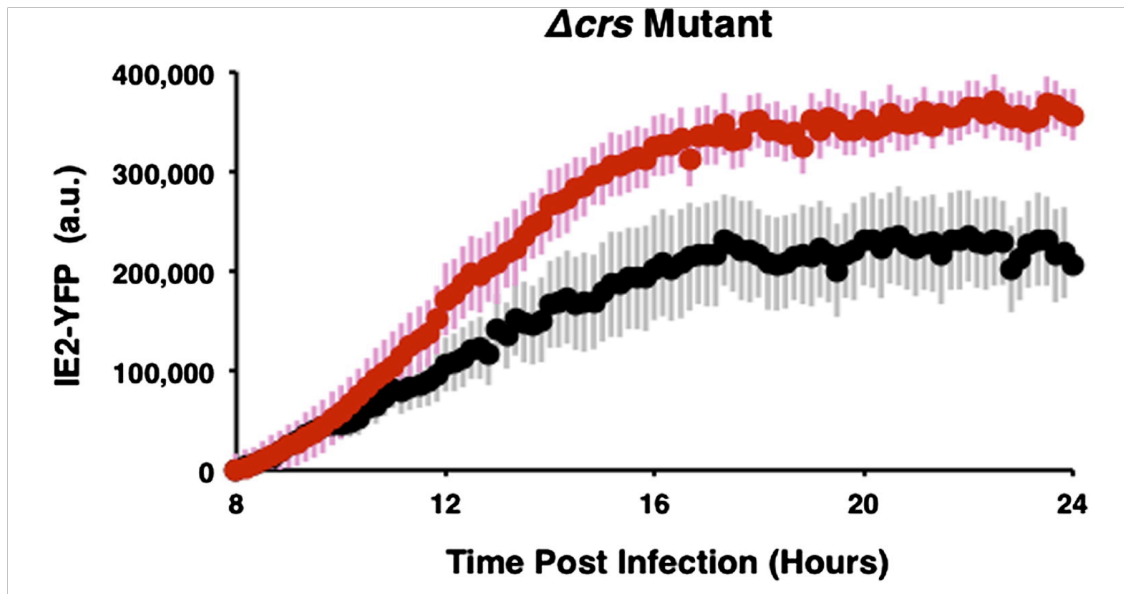
APPENDIX

Appendix Figure 3.1: **Eliminating IE2 negative feedback abrogates rate acceleration and generates level amplification.** Time-lapse microscopy results of cells undergoing infection with CMV *Δcrs* IE2-YFP mutant virus in presence of TSA (red) or absence of TSA (black). Trajectories are averages of 20 cells (bold) together with ± one standard error (lighter background).

Appendix Figure 3.2: Eliminating IE2 negative feedback produces a significant fitness cost for the virus. *Left:* Raw viral titers (measured by plaque forming units, PFU/mL) of cells infected with CMV *Δcrs* mutant virus in presence (red) and absence (black) of TSA. Averages are shown with ± one standard deviation in bold gray for day 9 post-infection. Decreased viral titer after TSA treatment is not due to TSA toxicity to cells at day 9 since cells treated with TSA and subsequently infected with CMV IE2-YFP virus do not exhibit a significant a drop in titer compared to untreated cells on day 10 (see panel C). *Right:* Raw viral titers (measured by plaque forming units, PFU/ml) of cells infected with CMV IE2-YFP virus at an MOI of 0.2 in presence (red) and absence (white) of TSA. Averages are shown with ± one standard deviation in bold gray for day 10 post infection. (Viral titers by Cynthia Bolovan-Fritts.)
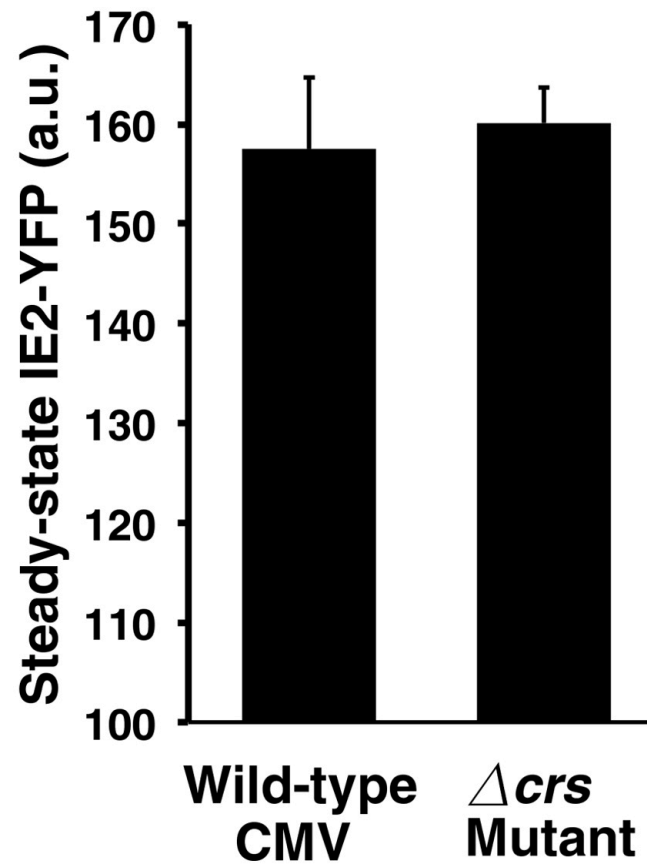
Appendix Figure 3.3: **Flow cytometry measurement of steady-state IE2-YFP levels of CMV IE2-YFP and CMV Δ*crs* IE2-YFP viruses measured agree with single-cell microscopy measurements.** Steady-state was measured at 15 h.p.i for CMV IE2-YFP and 24 h.p.i. for Δ*crs* IE2-YFP virus. Error bars in black are ± one standard deviation.
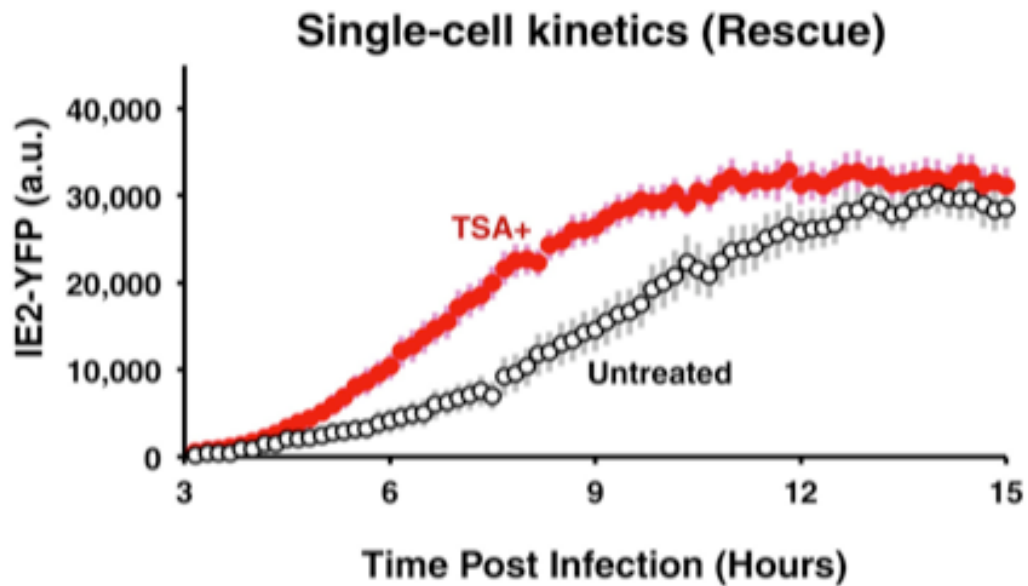
Appendix Figure 3.4: **Rescue of the *Δcrs* mutation to wild-type sequence results in recovery of rate acceleration.** Single-cell fluorescence microscopy trajectories of rescue virus IE2-YFP levels in presence (red) or absence (white) of TSA after an MOI=1 infection. Averages of 20 cells shown in bold with ± one standard error shown in pink (TSA) or gray (no drug).
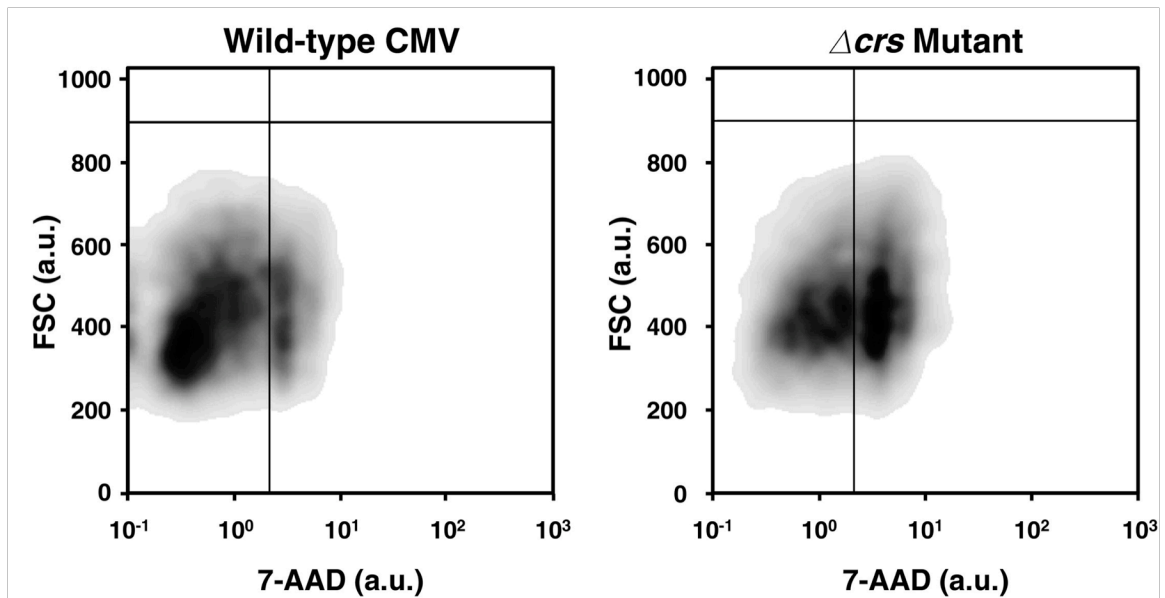
Appendix Figure 3.5: Accelerator circuitry provides a fitness advantage over amplifier circuitry by decreasing virus-induced cell death. Flow cytometry density plot of cells infected for 7 days with CMV IE2-YFP or CMV Δ*crs* mutant virus (at equal MOIs) and stained with 7-AAD to detect live and dead populations. Approximately half of the CMV Δ*crs* mutant population are positive for 7-AAD signal (right, bottom right quadrant) and are non-viable, while only 23% of the CMV IE2-YFP population (left, bottom right quadrant) are non-viable. (Cells were infected by Cynthia Bolovan-Fritts, and I performed the 7-AAD staining, flow cytometry, and data analysis.)
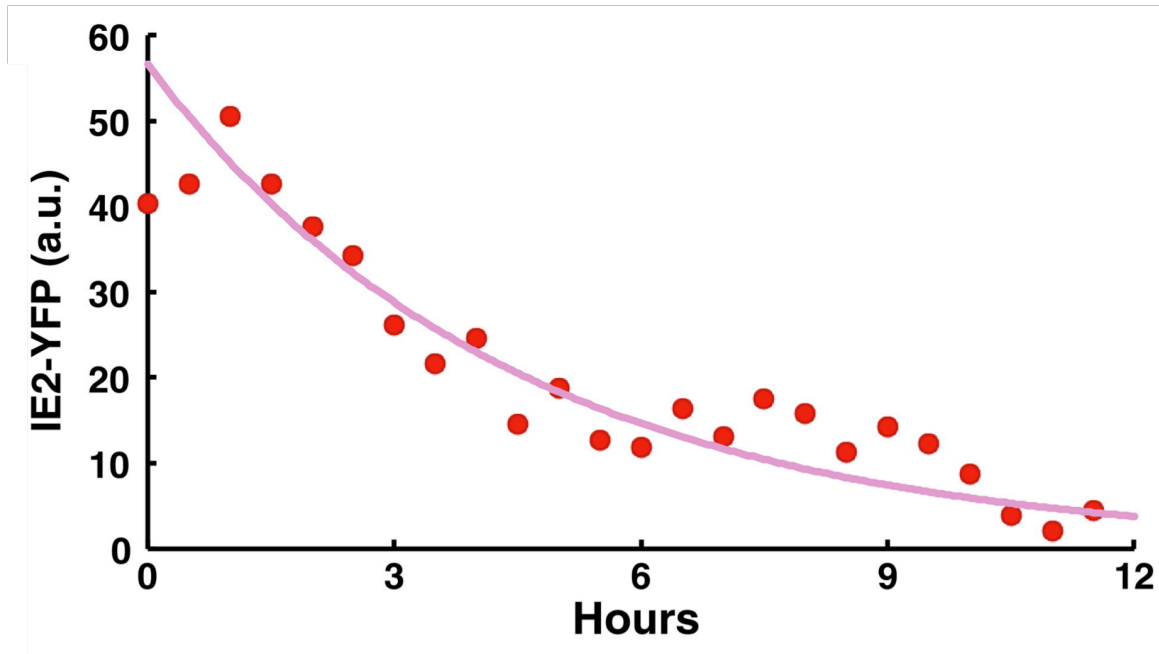
Appendix Figure 3.6: IE2 half-life calculated from single-cell microscopy is 0.23 hour^{-1}. IE2-YFP single-cell kinetics were measured after cycloheximide addition at 15 hours post infection. An average of 20 cells is shown (red), and the data was fit to a decaying exponential (pink). The exponential decay argues against non-linear decay models to explain the IE2 acceleration phenotype. (Single-cell microscopy by Leor Weinberger.)

Chapter 4:

The IE2:DNA complex is a ring-like structure with multiple IE2 subunits

ABSTRACT

The IE2 protein is the essential transcriptional activator in CMV and has long been a focal point of study. Previous attempts at studying the IE2 protein structure and its macromolecular structure in complex with DNA have largely proven challenging as the protein is prone to aggregation and is toxic to cells. Here, I discuss the purification of a C- terminal portion of the IE2 protein fused to maltose-binding protein (MBP). This portion of the IE2 protein contains the autoregulatory and dimerization domains, two domains important for IE2's ability to autoregulate its own expression and bind to the *cis-repression sequence (crs)* of the Major Immediate-Early promoter (MIEP). IE2 in complex with *crs* has been predicted to involve multiple subunits of IE2. Using electron microscopy, we have visualized these IE2-*crs* complexes, and we estimate that complexes with eight IE2 subunits are bound to the *crs* in a structure similar to DNA helicases.

INTRODUCTION

The major gene product of IE2 is an 86 kDa protein, sometimes referred to as IE2-86 (Stinski and Petrik, 2008). This protein contains 579 amino acids and several phosphorylation and sumoylation sites. IE2 has two activation domains that interact with viral promoters, two nuclear localization signal domains (Pizzorno et al., 1991), a serine domain (Barrasa et al., 2005), and a zinc-finger domain (Asmar et al., 2004) (Stinski and Petrik, 2008). Regions of IE2 containing mostly exon 5 have been mapped for its different functions: autoregulatory, dimerization, DNA binding, and transactivation (Fig. 4.1). The region between amino acids 450 and 552 has been designed as the core
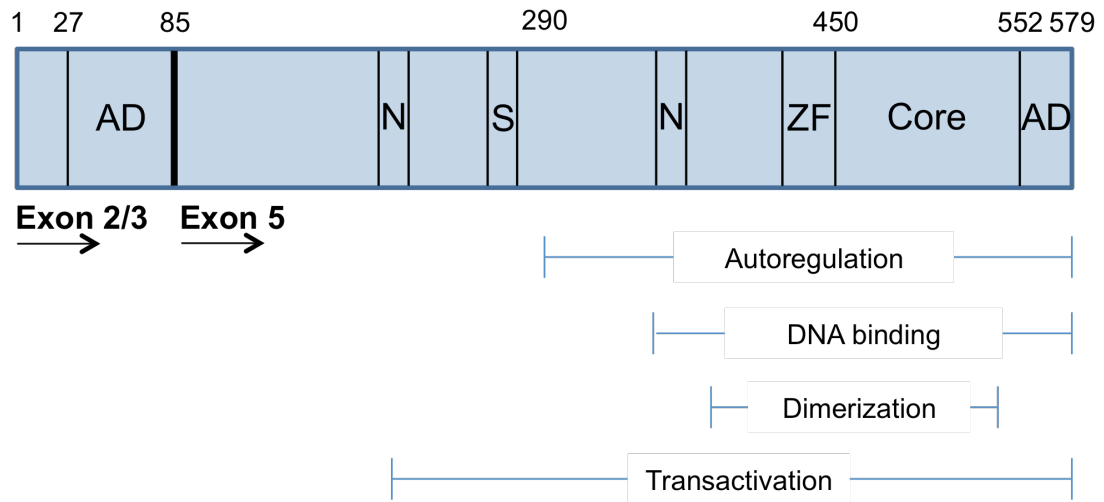
Figure 4.1: The IE2 functional domains. IE2 protein contains 579 amino acids and exons 2, 3, and 5 from the Immediate-early precursor mRNA. The core domain (amino acids 450-552) is necessary for IE2 autoregulation of the MIE promoter, early promoter transactivation, and cell cycle arrest. The domains responsible for autoregulation, DNA binding, dimerization, and transactivation span large regions of exon 5. AD: activation domain, N: nuclear localization domain, S: serine domain and ZF: Zinc finger domain.

domain. Mutation in this domain disrupts IE2's negative feedback activity, ability to arrest the cell cycle, and transactivation of CMV early promoters (Stinski and Petrik, 2008). Despite the overlap in regions affecting multiple IE2 functions, the IE2 autoregulation and IE2 transactivation mechanisms have been reported to be separate and distinct from one another (Petrik et al., 2007).

Despite the distinct functional domains that have been mapped, little is known about the tertiary IE2 protein structure. Few successful attempts to express and purify the protein have been reported in the literature. One of the first successful attempts to purify IE2 protein was described by Macias et al (Macias and Stinski, 1993).   A C-terminal region of IE2, including the dimerization and DNA-binding domains, was fused to a maltose-binding protein tag and expressed and purified from *E. coli*, to complete EMSA binding assays with the *cis-repression sequence (crs)*, the portion of the Major Immediate-early promoter (MIEP) to which IE2 binds to autoregulate its expression. Around the same time, purification of a His-tagged 86 kDa IE2 protein bound to the minor groove of the *crs* was reported by Lang et al (Lang and Stamminger, 1993, 1994).

Gary Hayward's lab, however, has provided the majority of the literature on expressing and purifying IE2 protein. Chiou et al. reported that their IE2 protein was produced via *in vitro* transcription followed by *in vitro* translation.   In solution, the purified IE2 protein dimerized alone but formed higher order multimers in complex with *crs* DNA (Chiou et al., 1993).   Subsequently, Hayward's group published another manuscript in which they discussed the expression and purification of IE2 protein fused to staphylococcal A protein or a GST tag (Waheed et al., 1998). They found that IE2 expressed and purified from bacteria, but not from mammalian cells, were able to bind

the *crs* and form higher order multimers. However, when bacterially expressed IE2 was phosphorylated, IE2 no longer bound to the *crs* in EMSA studies. Similarly, mammalian expressed IE2 that was dephosphorylated was able to bind the *crs* in EMSA studies. When IE2 protein with mutant DNA-binding domain was mixed in solution with IE2 protein with an intact DNA-binding domain, IE2 was unable to bind to the *crs*. This suggests that the ability to form higher order multimers is paramount to IE2's ability to bind to the *crs*.

Here, I discuss the expression and purification of the C-terminal portion of IE2 (rIE2) fused to maltose-binding protein (MBP), using the pMAL-xCS IE2 expression vector from Macias et al (Macias and Stinski, 1993). The protein was purified and analyzed by gel filtration chromatography. After sufficient purification, IE2 was bound in solution to the *crs* DNA sequence and subsequently imaged via electron microscopy (EM). The EM images support the literature from the Hayward lab and suggest that IE2 exists as a dimer in solution but forms a higher order multimer when in the presence of the *crs* sequence. The higher order multimer forms a ring-like structure in the presence of the *crs* and contains six or eight IE2 subunits.

MATERIALS AND METHODS

MBP-rIE2 expression

To express rIE2, E. coli were transformed with pMAL-xCS plasmid containing ampicillin resistance and maltose-binding protein (MBP) fused to the N-terminal end of rIE2 and grown in liquid culture with ampicillin at 37°C until they reached the logarithmic phase of growth (Macias and Stinski, 1993). MBP-rIE2 expression was

induced with IPTG (Sigma) and the induced E. coli were grown at 37°C for another 3-6 hours. The bacterial pellets were harvested and lysed. Protein expression was visualized by staining of an SDS-PAGE gel loaded and run with whole cell lysates.

rIE2 protein overexpression reached its maximum relative to endogenous protein expression 3 hours post induction by IPTG.

MBP-rIE2 protein purification

To purify MBP-rIE2 protein, cells overexpressing the protein were lysed with 1 mg/ml lysozyme at 4°C, with 1 mM PMSF (Sigma) and a complete Roche protease inhibitor tablet to prevent degradation. The lysate was sonicated (Fisher Scientific) at 40% amplitude for 10 second intervals with 30 seconds off for 6 cycles. DNase I (New England Biolabs) and $MgSo_4$ (Fisher Scientific) was added to the lysate and incubated on ice for 30 minutes before centrifugation at 9000 x g for 30 minutes in an Eppendorf tabletop centrifuge. The soluble fraction was collected, and pellets were discarded.

Batch affinity purification of MBP-rIE2 followed the protocol from the NEB pMAL-xCS purification kit. After purification, elution fractions were analyzed via protein gel electrophoresis, and the fractions with a single band of ~70 kDa were pooled and concentrated with an Amicon Ultra-15 filter unit (Millipore). Concentrated protein was filtered with an Ultrafree Durapore PVDF 0.22 μm filter (Millipore) before loading onto a gel filtration chromatography column for further purification.

Binding reactions and gel filtration analysis of IE2:DNA complex

Single-stranded wild-type or mutant crs DNA (sequences from Macias et al.) and their complements were annealed for 5 minutes at 95°C in a buffer solution of 10 mM Tris-HCl (pH=7.5-8.0), 50 mM NaCl, and 1mM EDTA. IE2 protein and wild-type or crs DNA were mixed in a 1:1.2 ratio in 25 mM Tris (pH=8.0), 100 mM NaCl, and 1 mM DTT (Bio-Rad). Reaction samples were incubated for 30 minutes at 25°C before use on EM grids or loading onto a Superose 6 GL (GE) column. For EM studies, the total MBP-rIE2 protein concentration was 100 μg/ml.

Electron microscopy

Glow-discharged copper grids were coated with carbon film for 30 seconds. A conventional negative stain with 0.75% uranyl acetate (Ohi et al) was performed on the grids prior to adsorption of 2.5 μl of the reaction sample. Imaging of grids was performed using a Tecnai T12 microscope (FEI company, Hillsboro, OR) with a LaB_6 filament. The images were collected using 120 kV accelerating voltage and at a 52,000X magnification with an UltraScan 4096 x 4096 CCD camera. Images were viewed using the WEB display program associated with the SPIDER software package as described (Racki et al., 2009).

RESULTS

MBP-rIE2 over-expression was tested for a range of conditions and optimized. The MBP-rIE2 protein migrated between protein standards of 70 and 80 kDa, as expected. The MBP-rIE2 protein was purified using affinity chromatography for MBP,

followed by gel filtration chromatography. MBP-rIE2 protein eluted from the gel filtration column less than a milliliter before the 158 kDa protein standard (Fig. 4.2). This is consistent with previous results that reported purified IE2 exists in dimers in solution (Chiou et al., 1993; Waheed et al., 1998).

Purified protein was bound to double-stranded DNA containing the *crs* or Δ*crs* sequence at various molar concentrations. Preious studies have shown that the MBP tag does not bind to the *crs* (Macias and Stinski, 1993). Following incubation, samples were immediately adsorbed to EM grids and examined under the electron microscope. For grids with MBP-rIE2:DNA at a 1:1.2 molar concentration, IE2 bound to the wild-type *crs* formed clusters of subunits, though the number of individual subunits involved in these clusters were not homogenous (Fig. 4.3). The clusters varied in size from only 4 subunits to larger aggregates of 20 or more subunits. MBP-rIE2 bound to the *crs* DNA did not form the same protein clusters and were typically seen as individual subunits or dimers, similar to what was seen for IE2 alone (Fig. 4.4). EM grids prepared with MBP-rIE2 protein alone did not reveal significant protein aggregation or subunit clusters (Fig. 4.5).

To obtain a more homogenous pool of protein species, purified MBP-rIE2 protein was bound to double-stranded wild-type *crs* DNA at a 1:1.2 molar concentration prior to loading on a gel filtration column. The DNA obscured the peak at which MBP-rIE2 dimers typically eluted from the column (Fig. 4.6). There was a broad shelf at the base of the DNA peak about 2.5 milliliters before the DNA peak. SDS-PAGE gel electrophoresis revealed that the corresponding fractions where the broad peak was
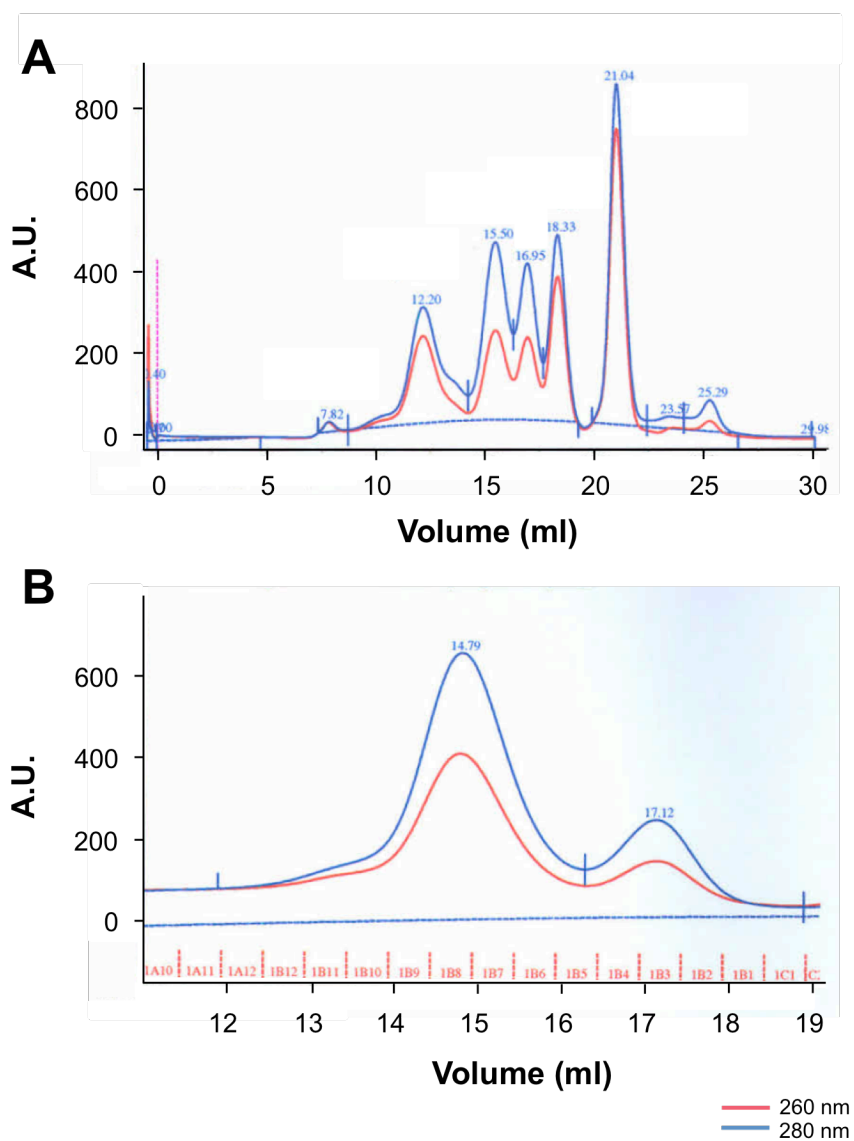
Figure 4.2: Gel filtration chromatography suggests IE2 is a dimer in solution without *crs* DNA. A, Gel filtration traces of a column loaded with various globular protein markers (7.82 – void, 12.20 – 670 kDa, 15.50 – 158 kDa, 16.95 – 44 kDa, 18.33 – 17 kDa 21.04 – 1.4 kDa). The absorbance was measured at 260 nm (pink) and 280 nm (blue). **B,** Gel filtration traces of a column loaded with MBP-rIE2 protein. The absorbance was measured at 260 nm (pink) and 280 nm (blue). MBP-rIE2 was purified prior to loading via affinity chromatography. The majority of the MBP-rIE2 protein eluted around the same time as a 158 kDa globular protein marker. These results confirm previous literature reports that IE2 exists as a dimer in solution. (I purified the MBP-rIE2 protein, and the gel filtration system run by JJ Miranda.)
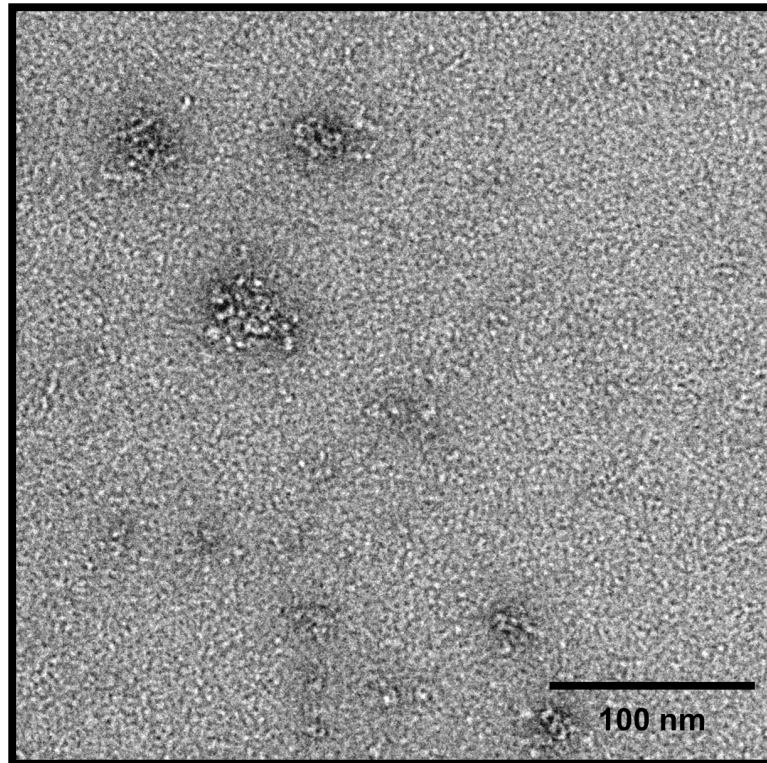
Figure 4.3: Electron micrograph of MBP-rIE2 mixed in solution with *crs* DNA.
MBP-IE2 and *crs* DNA were mixed at a 1:1.2 molar ratio with the *crs* DNA in excess.
MBP-rIE2 subunits are clustered together to form larger aggregates. (I prepared the
protein:DNA samples and the EM grids. Electron microscopy was performed by Na
(Maggie) Yang).
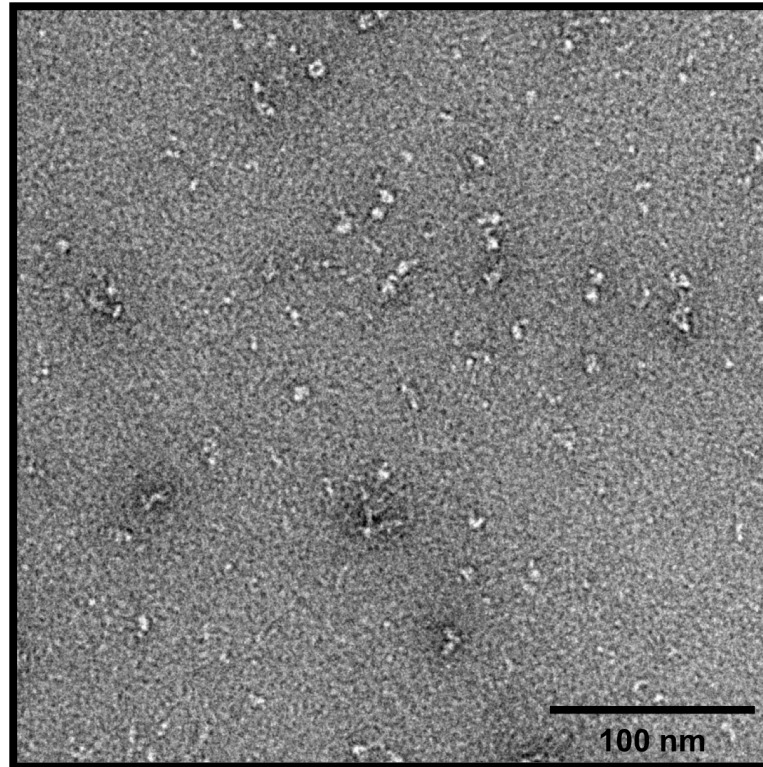
Figure 4.4: Electron micrograph of MBP-IE2 mixed in solution with Δ*crs* DNA.
MBP-IE2 and Δ*crs* DNA were mixed at a 1:1.2 molar ratio with the Δ*crs* DNA in excess. Higher order multimers of MBP-rIE2 are not seen with the Δ*crs* sequence. (I prepared the protein:DNA samples and the EM grids. Electron microscopy was performed by Na (Maggie) Yang.)
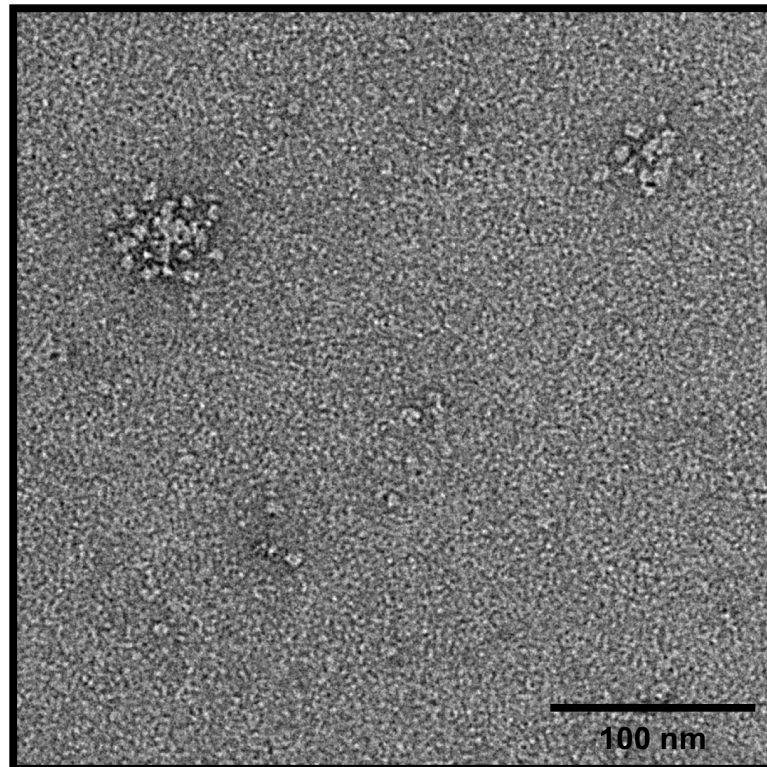
Figure 4.5: **Electron micrograph of MBP-IE2 protein alone.** MBP-rIE2 forms dimers in the absence of *crs* DNA. (I prepared protein:DNA samples and the EM grids. Electron microscopy was performed by Na (Maggie) Yang.)
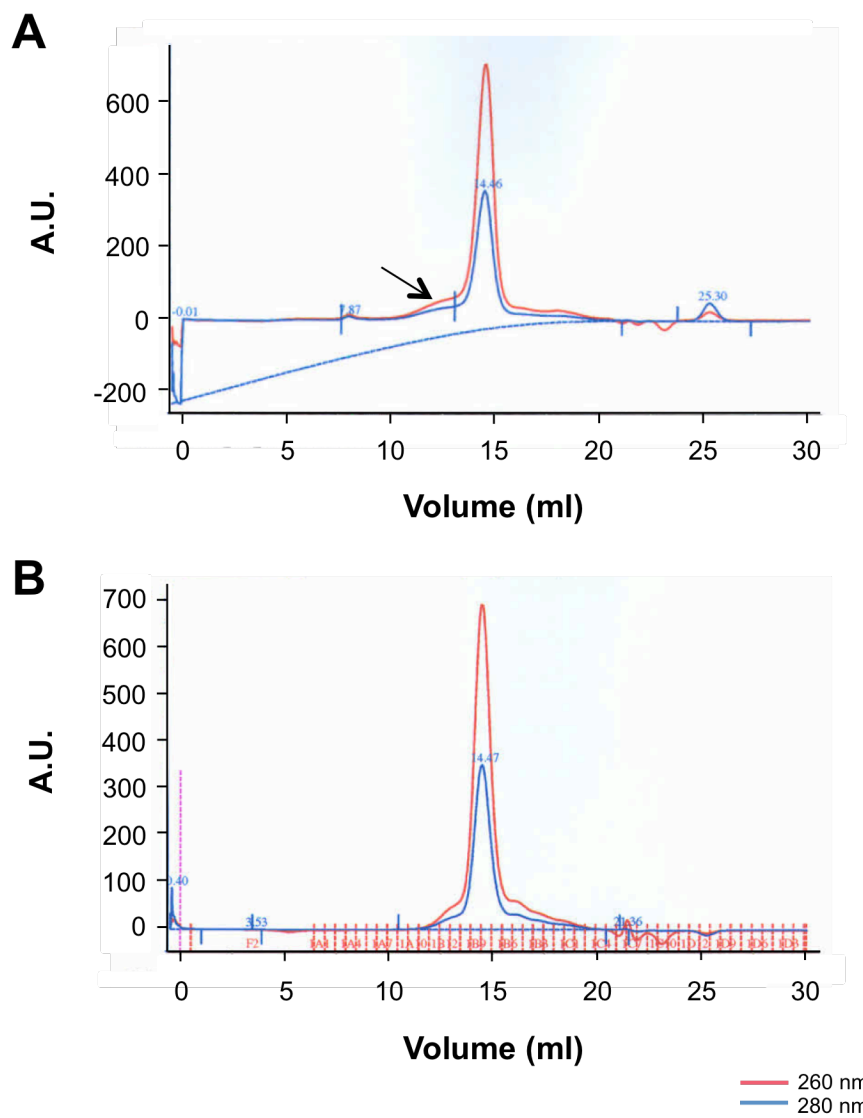
Figure 4.6: Gel filtration chromatography traces of *crs* DNA with or without IE2 protein. **A,** Gel filtration traces of a column loaded with MBP-IE2 protein bound in solution with *crs* DNA. MBP-IE2 was purified prior to loading via affinity chromatography and mixed in solution with the *crs* DNA in a 1:1.2 molar ratio, with the DNA in excess. Most of the DNA remained unbound and was visible as a strong signal at 260 nm.   The DNA signal obscured the MBP-IE2 signal at 280 nm. Some MBP-IE2 protein eluted around the same time as the 670 kDa globular protein marker and its presence was confirmed by SDS-PAGE gel electrophoresis. **B,** Gel filtration traces of a column loaded with *crs* DNA only. A strong signal at 260 nm was visible at the same elution volume where DNA signal was detected in Figure 4.2A. (I purified the MBP-rIE2 protein and performed binding assays, and the gel filtration system was run by JJ Miranda.)

located contained the highest concentration of MBP-rIE2 protein. The broad peak elution coincided with the 670 kDa protein standard, suggesting that the IE2 subunits form a multimer when bound to DNA. Very little protein eluted in the fractions where the MBP-rIE2 dimer typically elutes, suggesting that the majority of the protein formed multimers in the presence of the wild-type *crs* DNA. A negative control gel filtration experiment by my colleague Brian Linhares was performed with the mutant *crs* sequence and MBP-rIE2 protein eluted as a single dimer peak in the presence of the mutant DNA (data not shown).

Samples from gel filtration peak fractions of purified MBP-rIE2 protein mixed with *crs* DNA were collected and adsorbed on EM grids by my colleagues Cynthia Bolovan-Fritts, Jac Luna, Renee Ram, and JJ Miranda. The EM grids were imaged using an electron microscope by Sam Li (David Agard lab). Symmetrical MBP-rIE2 complexes with 6 or 8 subunits were observed under 52,000x magnification (Fig. 4.7). These complexes were all similar in geometry and shape, suggesting that IE2 forms a structured multimer in complex with the *crs* DNA. EM grids with MBP-rIE2 protein alone did not contain any organized multimeric protein structures. Most MBP-rIE2 subunits were seen in dimers, in agreement with the gel filtration analysis of MBP-rIE2 protein alone.

DISCUSSION

As predicted by our previously published manuscript (Teng et al., 2012), IE2 appears to form a hexamer or octamer in the presence of wild-type *crs* DNA. IE2
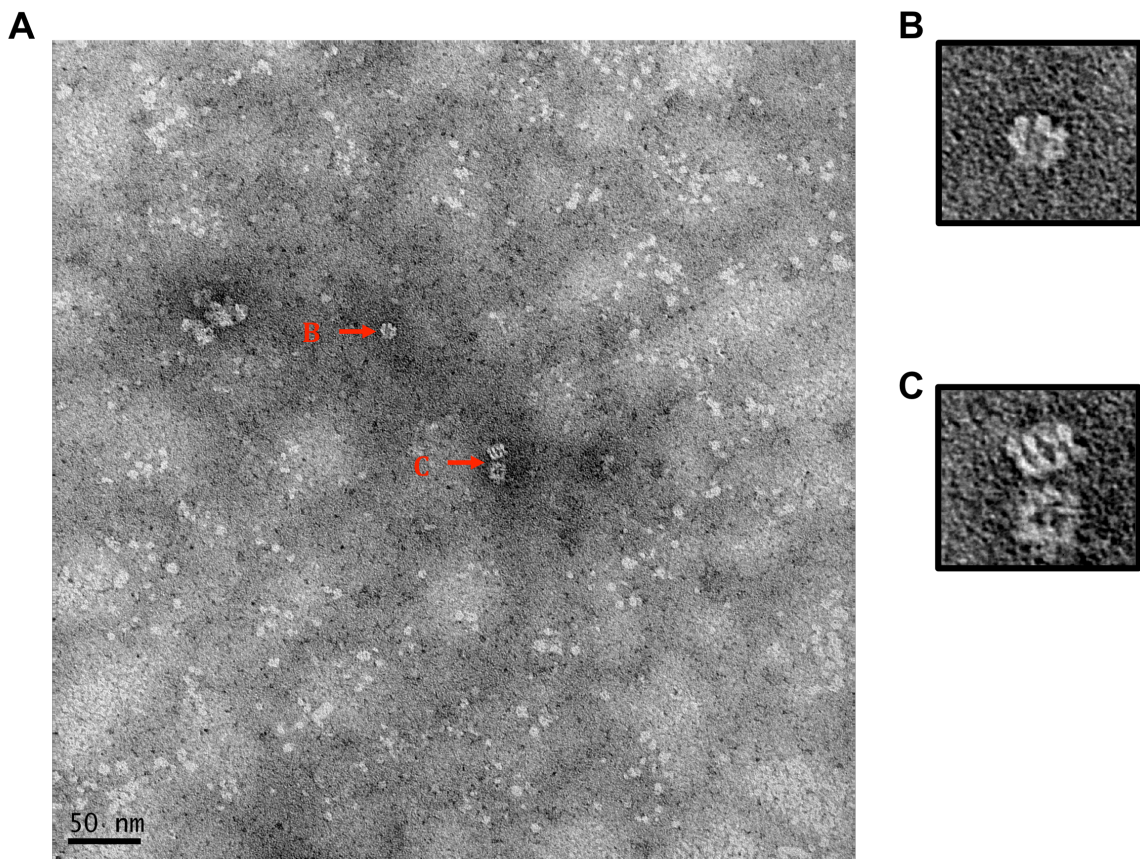
Figure 4.7: IE2 forms a ring-like structure in complex with *crs* DNA. A, Electron micrograph of MBP-IE2 hexamers and octamers. MBP-IE2 protein was bound to *crs* DNA in solution before loading on a gel filtration chromatography column. Fractions containing multimeric MBP-IE2 were collected and blotted on EM grids. **B,** View of an IE2 ring structure containing six or more IE2 subunits. The MBP-IE2 multimer appears to have six MBP-IE2 subunits in a ring with another possible subunit in the center. **C,** View of two IE2 ring structures containing eight IE2 subunits. The top structure is the clearest image. (Grid preparation was performed by Cynthia Bolovan-Fritts and Renee Ram, and electron microscopy imaging was performed by Sam Li. The MBP-rIE2:DNA complex was bound and purified by Jac Luna, Renee Ram and JJ Miranda.)

multimerization is likely responsible for the high Hill coefficient that is necessary for IE2 acceleration without amplification in the MIE circuit. Our gel filtration results, combined with the Hayward group's published observations, suggest that IE2 multimerization forms a distinct and particular higher order multimer. EMSA results from Hayward's group revealed a sharp super shifted IE2 band in the presence of wild-type *crs* DNA. However, mixing with smaller heterodimers (IE2 proteins with different affinity tags) resulted in intermediately mobilized protein complexes, confirming that IE2 binds DNA as a higher order multimer.

Likewise, our gel filtration experiments resulted in a shifted IE2 concentration peak when IE2 was run through the column in the presence of wild-type *crs* DNA, in agreement with the results reported on IE2 multimerization in EMSA assays from Hayward's group (Chiou et al., 1993; Waheed et al., 1998). Further follow-up experiments should include gel filtration analysis of the mutant Δ*crs* sequence in solution with IE2 protein to confirm that IE2 multimerization is dependent on the *crs* sequence as reported by the literature (Chiou et al., 1993; Waheed et al., 1998). Similarly, EM visualization of IE2 mixed with the Δ*crs* sequence should be completed in order to rule out non-specific IE2 self-binding resulting from the presence of non-specific DNA.

Higher order multimerization in quartenary ring structures, similar to the structures we report, have been documented in eukaryotic systems and are particularly common among enzymes involved in DNA and RNA metabolism and regulation (Karow et al., 1999; VanLoock et al., 2001; Yu and Egelman, 1997). Most notably, several eukaryotic helicases have been reported to form a hexameric ring structure. These hexameric structures are necessary for helicases to unwind DNA. It is unclear if there are

any other functions for IE2 ring formation besides cooperative autoregulation, but it is interesting to note that there could be undiscovered additional functions of IE2 multimerization.

IE2 transactivation of homologous and heterologous promoters has been documented to require the IE2 dimerization domain (Asmar et al., 2004). IE2 transactivation can occur through protein-protein interactions as well as protein-DNA interactions. IE2 has been known to associate with transcriptional activators such as CREB, Sp-1, TBP, and TAF-like proteins. IE2 has also been shown to directly bind to and transactivate the UL112/113 promoter. Because IE2's dimerization domain overlaps significantly with IE2's DNA binding and autoregulation domains, it is possible that IE2 multimerization may play a role in IE2 transactivation.

Chapter 5:

Discussion

Using a combination of mathematical modeling and biological experimentation, we have revealed a novel gene circuitry in which increasing input results in acceleration, without amplification, of output protein levels (Chapter 2). This circuit has been previously theoretically described in the literature but has not been found in an endogenous system until now. In CMV, the accelerator circuit operates through IE2, a protein that autoregulates its own expression and is also the major transcriptional activator of all downstream viral gene expression. Highly cooperative autoregulation is sufficient to drive IE2 acceleration without amplification, and our data suggests that IE2 homo-multimerization is the mechanism through which IE2 cooperative negative feedback occurs (Chapters 2 and 4).

As is common with many proteins expressed by pathogens, IE2 is highly cytotoxic and regulation of its expression is paramount to CMV's ability to replicate in the host cell. It is likely that the accelerator circuit exists in other systems where regulation of protein levels and response rate is important. However, the signature characteristics of an accelerator circuit may be difficult to observe unless a single-cell methodology is used. When conducting experiments with pooled populations of cells, the effects of averaging can mask an accelerated response rate, especially when cells are not synchronized. Single-cell technologies will be able to shed light on whether accelerator circuits exist elsewhere in nature. Notably, negative feedback is employed by herpes simplex virus-1 (HSV-1) early on in infection via ICP4, an immediate-early viral protein. There is evidence that the ICP4 protein forms a dimer, similar to IE2 (Godowski and Knipe, 1986) and thus may be driving acceleration without amplification in a similar manner as IE2.

In CMV, it is clear that the accelerator circuit is necessary for optimal viral replication for the virus (Chapter 3). The function of IE2 negative feedback so early in the viral lifecycle has largely remained a mystery until now. Why would the virus want to inhibit expression of its essential viral transactivator, IE2? Our data reveal that disruption of IE2 negative feedback results in a fitness loss, and viral replication is severely impaired. In fact, when IE2 steady-state levels are equivalent between wild-type CMV and a negative-feedback impaired CMV mutant, the wild-type CMV is superior in replicative fitness and is able to outcompete the mutant CMV in a fitness competition assay (Chapter 3). IE2 autoregulation functions to keep IE2 levels from amplifying above the cytotoxic threshold while producing IE2 quickly enough to jumpstart viral gene expression and outpace cellular defenses.

Much is unclear about the exact interaction between the IE proteins and cellular defense proteins such as PML and ND10. Our data suggests that PML and the presence of the *crs* are necessary for efficient transcription of the IE genes. It appears that the *crs* is necessary to recruit IE2 to transcription centers based on our observance of the reduction in IE2 punctate dot formation when the *crs* is mutated (Chapter 3). Previous literature reports have debated whether the interaction between CMV and PML bodies fosters or antagonizes IE gene expression (Maul, 1998). Our data (Chapter 3) support previous claims that ND10 domains provide an environment conducive to CMV IE transcription. In PML knockdown cells infected with CMV IE2-YFP virus, we have observed a reduction in IE2-YFP steady-state levels compared to cells with intact PML expression (Figure 5.1). PML knockdown cells pre-treated with transcriptional activator
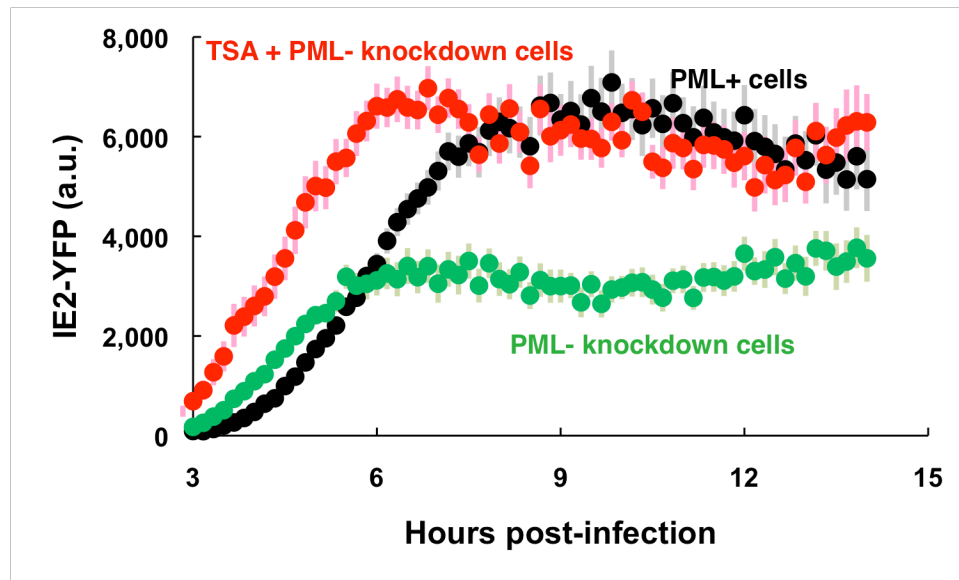
Figure 5.1: **Knockdown of PML in cells infected with CMV IE2-YFP virus eliminates IE2 acceleration and produces an IE2 amplifier.** Single-cell time-lapse microscopy of cells undergoing infection with CMV IE2-YFP virus in presence of 24 hr pretreatment of TSA (red) or absence of VPA (PML+cells: black, PML- knockdown cells: green). Trajectories are averages of 15 or more cells (bold) together with ±1 SE (lighter background). Pretreatment of TSA in PML- knockdown cells produces an IE2 amplifier. IE2-YFP expression in PML- knockdown cells is accelerated.

(TSA) produce an amplification of IE2-YFP levels compared to untreated PML

knockdown cells, similarly to the Δ*crs* IE2-YFP virus in cells with intact PML expression

(Chapter 3). Initial IE2-YFP expression in both the TSA-treated and untreated PML

knockdown cells appears accelerated compared to control cells with intact PML

expression. It is possible that the *crs* sequence could be responsible for recruiting IE2 to

the PML-associated CMV transcription centers. However, in an environment with no

PML protein, the *crs* sequence may not be able to efficiently recruit IE2 to transcription

centers, thus breaking negative feedback. The accelerated, yet lower IE2-YFP expression

in untreated PML knockdown cells suggests that PML both activates and represses CMV

IE viral gene expression. Future directions include examining whether the addition of

extra *crs* sequences in the CMV genome can increase the number of CMV transcription

centers at PML bodies or increase recruitment of IE2 to PML bodies.

The tertiary structure of the IE2 protein and the structure of the macromolecular

complex of IE2 multimerization on the *crs* sequence are unknown, despite attempts by

several labs to crystallize the IE2 protein and its self-binding interactions with and

without *crs* DNA. Most of the IE2 sequence does not contain any homologous domains

to existing eukaryotic proteins. Previous literature reports have revealed IE2 to exist as a

dimer in solution. EMSA and gel filtration studies of IE2 in complex with *crs* DNA have

suggested that IE2 homo-multimerizes in the presence of the *crs* sequence (Hayward),

but exact quantification of IE2 subunits and the macromolecular structure have not been

explored. Our initial electron microscopy experiments provide the first visualization of

the IE2-*crs* macromolecular structure. We have observed IE2 in the presence of *crs*

DNA as involving 6 or 8 IE2 subunits in the formation of a ring-like structure. It is

likely that this ring-like structure is forming around the *crs* sequence, similar to

eukaryotic helicase multimerization around DNA (Karow et al., 1999; Yu and Egelman,

1997). Our preliminary results suggest that multimerization does not occur in the

presence of *crs* DNA, and this structure is specific to the *crs* sequence. Future directions

include visualizing the IE2-*crs* complex with cryo-EM in order to determine the exact

number of subunits centered on the DNA and to obtain a clearer image of the 3D

structure. Efforts to crystallize IE2 are also underway.

REFERENCES

Ahn, J.H., Jang, W.J., and Hayward, G.S. (1999). The human cytomegalovirus IE2 and UL112-113 proteins accumulate in viral DNA replication compartments that initiate from the periphery of promyelocytic leukemia protein-associated nuclear bodies (PODs or ND10). J Virol *73*, 10458-10471.

Alon, U. (2007a). An introduction to systems biology : design principles of biological circuits (Boca Raton, FL, Chapman & Hall/CRC).

Alon, U. (2007b). An introduction to systems biology : design principles of biological circuits (Boca Raton, FL, Chapman & Hall/CRC).

Asmar, J., Wiebusch, L., Truss, M., and Hagemeier, C. (2004). The putative zinc finger of the human cytomegalovirus IE2 86-kilodalton protein is dispensable for DNA binding and autorepression, thereby demarcating a concise core domain in the C terminus of the protein. J Virol *78*, 11853-11864.

Austin, D.W., Allen, M.S., McCollum, J.M., Dar, R.D., Wilgus, J.R., Sayler, G.S., Samatova, N.F., Cox, C.D., and Simpson, M.L. (2006). Gene network shaping of inherent noise spectra. Nature *439*, 608-611.

Barrasa, M.I., Harel, N.Y., and Alwine, J.C. (2005). The phosphorylation status of the serine-rich region of the human cytomegalovirus 86-kilodalton major immediate-early protein IE2/IEP86 affects temporal viral gene expression. J Virol *79*, 1428-1437.

Bodaghi, B., Slobbe-van Drunen, M.E., Topilko, A., Perret, E., Vossen, R.C., van Dam-Mieras, M.C., Zipeto, D., Virelizier, J.L., LeHoang, P., Bruggeman, C.A.*, et al.* (1999). Entry of human cytomegalovirus into retinal pigment epithelial and endothelial cells by endocytosis. Invest Ophthalmol Vis Sci *40*, 2598-2607.

Bolovan-Fritts, C., and Wiedeman, J.A. (2001). Human cytomegalovirus strain Toledo lacks a virus-encoded tropism factor required for infection of aortic endothelial cells. J Infect Dis *184*, 1252-1261.

Bresnahan, W.A., and Shenk, T.E. (2000). UL82 virion protein activates expression of immediate early viral genes in human cytomegalovirus-infected cells. Proc Natl Acad Sci U S A *97*, 14506-14511.

Britt, W. (2008). Manifestations of human cytomegalovirus infection: proposed mechanisms of acute and chronic disease. Curr Top Microbiol Immunol *325*, 417-470.

Cagatay, T., Turcotte, M., Elowitz, M.B., Garcia-Ojalvo, J., and Suel, G.M. (2009). Architecture-dependent noise discriminates functionally analogous differentiation circuits. Cell *139*, 512-522.

Carey, M., Peterson, C.L., and Smale, S.T. (2009). Transcriptional regulation in eukaryotes : concepts, strategies, and techniques, 2nd edn (Cold Spring Harbor, N.Y., Cold Spring Harbor Laboratory Press).

Chen, D.H., Jiang, H., Lee, M., Liu, F., and Zhou, Z.H. (1999). Three-dimensional visualization of tegument/capsid interactions in the intact human cytomegalovirus. Virology *260*, 10-16.

Chiou, C.J., Zong, J., Waheed, I., and Hayward, G.S. (1993). Identification and mapping of dimerization and DNA-binding domains in the C terminus of the IE2 regulatory protein of human cytomegalovirus. J Virol *67*, 6201-6214.

Cuevas-Bennett, C., and Shenk, T. (2008). Dynamic histone H3 acetylation and methylation at human cytomegalovirus promoters during replication in fibroblasts. J Virol *82*, 9525-9536.

Everett, R.D., and Chelbi-Alix, M.K. (2007). PML and PML nuclear bodies: implications in antiviral defence. Biochimie *89*, 819-830.

Fields, B.N., Knipe, D.M., and Howley, P.M. (2007). Fields virology, 5th edn (Philadelphia, Wolters Kluwer Health/Lippincott Williams & Wilkins).

Gerna, G., Percivalle, E., Sarasini, A., Baldanti, F., Campanini, G., and Revello, M.G. (2003). Rescue of human cytomegalovirus strain AD169 tropism for both leukocytes and human endothelial cells. J Gen Virol *84*, 1431-1436.

Ishov, A.M., Stenberg, R.M., and Maul, G.G. (1997). Human cytomegalovirus immediate early interaction with host nuclear structures: definition of an immediate transcript environment. J Cell Biol *138*, 5-16.

Isomura, H., Stinski, M.F., Kudoh, A., Nakayama, S., Murata, T., Sato, Y., Iwahori, S., and Tsurumi, T. (2008). A cis element between the TATA Box and the transcription start site of the major immediate-early promoter of human cytomegalovirus determines efficiency of viral replication. J Virol *82*, 849-858.

Kaern, M., Elston, T.C., Blake, W.J., and Collins, J.J. (2005). Stochasticity in gene expression: from theories to phenotypes. Nat Rev Genet *6*, 451-464.

Karow, J.K., Newman, R.H., Freemont, P.S., and Hickson, I.D. (1999). Oligomeric ring structure of the Bloom's syndrome helicase. Curr Biol *9*, 597-600.

Lang, D., and Stamminger, T. (1993). The 86-kilodalton IE-2 protein of human cytomegalovirus is a sequence-specific DNA-binding protein that interacts directly with the negative autoregulatory response element located near the cap site of the IE-1/2 enhancer-promoter. J Virol *67*, 323-331.

Lang, D., and Stamminger, T. (1994). Minor groove contacts are essential for an interaction of the human cytomegalovirus IE2 protein with its DNA target. Nucleic Acids Res *22*, 3331-3338.

Macias, M.P., and Stinski, M.F. (1993). An in vitro system for human cytomegalovirus immediate early 2 protein (IE2)-mediated site-dependent repression of transcription and direct binding of IE2 to the major immediate early promoter. Proc Natl Acad Sci U S A *90*, 707-711.

Maul, G.G. (1998). Nuclear domain 10, the site of DNA virus transcription and replication. Bioessays *20*, 660-667.

Milo, R., Shen-Orr, S., Itzkovitz, S., Kashtan, N., Chklovskii, D., and Alon, U. (2002). Network motifs: simple building blocks of complex networks. Science *298*, 824-827.

Murphy, E., and Shenk, T. (2008). Human cytomegalovirus genome. Curr Top Microbiol Immunol *325*, 1-19.

Murray, J.D. (2002). Mathematical biology, 3rd edn (New York, Springer).

Nevels, M., Brune, W., and Shenk, T. (2004). SUMOylation of the human cytomegalovirus 72-kilodalton IE1 protein facilitates expression of the 86-kilodalton IE2 protein and promotes viral replication. J Virol *78*, 7803-7812.

Petrik, D.T., Schmitt, K.P., and Stinski, M.F. (2007). The autoregulatory and transactivating functions of the human cytomegalovirus IE86 protein use independent mechanisms for promoter binding. J Virol *81*, 5807-5818.

Pizzorno, M.C., Mullen, M.A., Chang, Y.N., and Hayward, G.S. (1991). The functionally active IE2 immediate-early regulatory protein of human cytomegalovirus is an 80-kilodalton polypeptide that contains two distinct activator domains and a duplicated nuclear localization signal. J Virol *65*, 3839-3852.

Racki, L.R., Yang, J.G., Naber, N., Partensky, P.D., Acevedo, A., Purcell, T.J., Cooke, R., Cheng, Y., and Narlikar, G.J. (2009). The chromatin remodeller ACF acts as a dimeric motor to space nucleosomes. Nature *462*, 1016-1021.

Reddehase, M.J., and Lemmermann, N. (2006). Cytomegaloviruses : molecular biology and immunology (Wymondham, Caister Academic Press).

Rosenfeld, N., Elowitz, M.B., and Alon, U. (2002). Negative autoregulation speeds the response times of transcription networks. J Mol Biol *323*, 785-793.

Rosenke, K., and Fortunato, E.A. (2004). Bromodeoxyuridine-labeled viral particles as a tool for visualization of the immediate-early events of human cytomegalovirus infection. J Virol *78*, 7818-7822.

Ryckman, B.J., Jarvis, M.A., Drummond, D.D., Nelson, J.A., and Johnson, D.C. (2006). Human cytomegalovirus entry into epithelial and endothelial cells depends on genes UL128 to UL150 and occurs by endocytosis and low-pH fusion. J Virol *80*, 710-722.

Savageau, M.A. (1970). Biochemical systems analysis. 3. Dynamic solutions using a power-law approximation. J Theor Biol *26*, 215-226.

Savageau, M.A. (1974). Comparison of classical and autogenous systems of regulation in inducible operons. Nature *252*, 546-549.

Savageau, M.A. (1975). Significance of autogenously regulated and constitutive synthesis of regulatory proteins in repressible biosynthetic systems. Nature *258*, 208-214.

Savageau, M.A. (1976). Biochemical systems analysis : a study of function and design in molecular biology (Reading, Mass., Addison-Wesley Pub. Co., Advanced Book Program).

Shen-Orr, S.S., Milo, R., Mangan, S., and Alon, U. (2002). Network motifs in the transcriptional regulation network of Escherichia coli. Nat Genet *31*, 64-68.

Shenk, T., and Stinski, M. (2008). Human cytomegalovirus (Berlin, Springer).

Simpson, M.L., Cox, C.D., and Sayler, G.S. (2003). Frequency domain analysis of noise in autoregulated gene circuits. Proc Natl Acad Sci U S A *100*, 4551-4556.

Sinzger, C., Hahn, G., Digel, M., Katona, R., Sampaio, K.L., Messerle, M., Hengel, H., Koszinowski, U., Brune, W., and Adler, B. (2008). Cloning and sequencing of a highly productive, endotheliotropic virus strain derived from human cytomegalovirus TB40/E. J Gen Virol *89*, 359-368.

Sourvinos, G., Tavalai, N., Berndt, A., Spandidos, D.A., and Stamminger, T. (2007). Recruitment of human cytomegalovirus immediate-early 2 protein onto parental viral genomes in association with ND10 in live-infected cells. J Virol *81*, 10123-10136.

Stamminger, T., Puchtler, E., and Fleckenstein, B. (1991). Discordant expression of the immediate-early 1 and 2 gene regions of human cytomegalovirus at early times after infection involves posttranscriptional processing events. J Virol *65*, 2273-2282.

Stenberg, R.M. (1996). The human cytomegalovirus major immediate-early gene. Intervirology *39*, 343-349.

Stinski, M.F., and Isomura, H. (2008). Role of the cytomegalovirus major immediate early enhancer in acute infection and reactivation from latency. Med Microbiol Immunol *197*, 223-231.

Stinski, M.F., and Petrik, D.T. (2008). Functional roles of the human cytomegalovirus essential IE86 protein. Curr Top Microbiol Immunol *325*, 133-152.

Teng, M.W., Bolovan-Fritts, C., Dar, R.D., Womack, A., Simpson, M.L., Shenk, T., and Weinberger, L.S. (2012). An endogenous accelerator for viral gene expression confers a fitness advantage. Cell *151*, 1569-1580.

VanLoock, M.S., Yu, X., Kasai, M., and Egelman, E.H. (2001). Electron microscopic studies of the translin octameric ring. J Struct Biol *135*, 58-66.

Waheed, I., Chiou, C.J., Ahn, J.H., and Hayward, G.S. (1998). Binding of the human cytomegalovirus 80-kDa immediate-early protein (IE2) to minor groove A/T-rich sequences bounded by CG dinucleotides is regulated by protein oligomerization and phosphorylation. Virology *252*, 235-257.

Wang, D., and Shenk, T. (2005a). Human cytomegalovirus UL131 open reading frame is required for epithelial cell tropism. J Virol *79*, 10330-10338.

Wang, D., and Shenk, T. (2005b). Human cytomegalovirus virion protein complex required for epithelial and endothelial cell tropism. Proc Natl Acad Sci U S A *102*, 18153-18158.

Warming, S., Costantino, N., Court, D.L., Jenkins, N.A., and Copeland, N.G. (2005). Simple and highly efficient BAC recombineering using galK selection. Nucleic Acids Res *33*, e36.

Weinberger, L.S., Dar, R.D., and Simpson, M.L. (2008). Transient-mediated fate determination in a transcriptional circuit of HIV. Nat Genet *40*, 466-470.

Weinberger, L.S., and Shenk, T. (2007). An HIV feedback resistor: auto-regulatory circuit deactivator and noise buffer. PLoS Biol *5*, e9.

Xu, Y., Cei, S.A., Rodriguez Huete, A., Colletti, K.S., and Pari, G.S. (2004). Human cytomegalovirus DNA replication requires transcriptional activation via an IE2- and UL84-responsive bidirectional promoter element within oriLyt. J Virol *78*, 11664-11677.

Yu, D., Silva, M.C., and Shenk, T. (2003). Functional map of human cytomegalovirus AD169 defined by global mutational analysis. Proc Natl Acad Sci U S A *100*, 12396-12401.

Yu, D., Smith, G.A., Enquist, L.W., and Shenk, T. (2002). Construction of a self-excisable bacterial artificial chromosome containing the human cytomegalovirus genome and mutagenesis of the diploid TRL/IRL13 gene. J Virol *76*, 2316-2328.

Yu, X., and Egelman, E.H. (1997). The RecA hexamer is a structural homologue of ring helicases. Nat Struct Biol *4*, 101-104.